NASA CR-72599
AEROJET 3788

ANALYSIS OF FILAMENT-WOUND DOME AND POLAR BOSS OF METAL-LINED GLASS-FILAMENT-WOUND PRESSURE VESSELS

by

R.E. Landes and E.E. Morris

AEROJET-GENERAL CORPORATION

prepared for

NATIONAL AERONAUTICS AND SPACE ADMINISTRATION

NASA Lewis Research Center
Contract NAS 3-10289
James R. Barber, Project Manager

Requests for copies of this report should be referred to

National Aeronautics and Space Administration
Scientific and Technical Information Facility
P. O. Box 33
College Park, Md. 20740

NASA CR-72599
AEROJET 3788

TOPICAL REPORT

ANALYSIS OF FILAMENT-WOUND DOME AND POLAR BOSS OF METAL-LINED GLASS-FILAMENT-WOUND PRESSURE VESSELS

by

R. E. Landes and E. E. Morris

AEROJET-GENERAL CORPORATION
Structural Composites Department
Mechanical Systems Operations
Azusa, California

prepared for

NATIONAL AERONAUTICS AND SPACE ADMINISTRATION

January 1970

CONTRACT NAS 3-10289

NASA Lewis Research Center
Cleveland, Ohio
James R. Barber, Project Manager
Liquid Rocket Technology Branch

FOREWORD

This report was prepared by the Structural Composites Department of Aerojet-General Corporation under National Aeronautics and Space Administration Contract NAS 3-10289 ("Cryogenic Filament-Wound Tank Evaluation"). This topical report covers analysis of the filament-wound dome and polar boss of metal-lined glass-filament-wound pressure vessels, as well as complete vessel designs developed under the contract. The work is under the direction of the NASA, Lewis Research Center, Liquid Rocket Technology Branch; James R. Barber is the Project Manager.

Approved by:

D.E. Deutsch, Manager
Structural Composites Department
Mechanical Systems Operations

ABSTRACT

ANALYSIS OF FILAMENT-WOUND DOME AND POLAR BOSS OF METAL-LINED GLASS-FILAMENT-WOUND PRESSURE VESSELS

by

R. E. Landes and E. E. Morris

Structural analysis of an aluminum-lined glass-filament-wound pressure vessel was conducted. Pressure-vessel design criteria were reviewed, and filament strength levels and the vessel configuration were established using netting analysis of the membrane, discontinuity analysis of the dome-to-cylinder junctions, and wrap-pattern calculations. The vessel's dome was characterized and a discontinuity analysis of the polar boss region was completed. Axial polar-boss design concepts were reviewed, and detailed structural analyses of two configurations were carried out. Then the polar-boss designs were incorporated in the membrane analysis.

TABLE OF CONTENTS

TABLE OF CONTENTS (cont.)

I. SUMMARY

Structural analysis was conducted of an aluminum-lined glass-filament-wound pressure vessel which included a conventional membrane analysis, a discontinuity analysis of the dome-to-cylinder juncture, and a special analysis of the domed ends of the pressure vessel in the vicinity of the axially located polar boss. Pressure-vessel design criteria were reviewed, filament design strength levels established, and the vessel configuration was established from netting analysis of the membrane (which included provision for the metal liner), discontinuity analysis of the dome-to-cylinder juncture, and wrap pattern calculations. The dome was characterized using both netting analysis and orthotropic analysis, to establish its elastic properties, deflections, rotations, and strains when subjected to internal pressure and boss reaction loads. A discontinuity analysis of the vessel dome at the polar boss was conducted by considering the filament-wound composite in this region as a ring plate. Axial polar-boss design concepts were reviewed, and detailed structural analyses of two selected configurations are presented. The polar-boss designs were then incorporated into the membrane-analysis pressure-vessel designs.

II. INTRODUCTION

Much work has been conducted by NASA to develop and evaluate metal-lined glass-filament-wound vessels for cryogenic operation in propulsion and spacecraft systems. The objective of Contract NAS 3-10289 ("Cryogenic Filament-Wound Tank Evaluation") is to demonstrate the feasibility of producing closed-end, cylindrical, glass-filament-wound pressure vessels with thin aluminum liners for operation in the +75 to -423°F range. Designs for metal-lined glass-filament-wound vessels 12 in. in diameter and 18 in. long, with a burst pressure of 3000 psi at 75°F, are being developed, as well as processes for fabricating thin (0.010-in.-thick) aluminum liners, for providing joints in the liner having the necessary properties, and for providing a bond between the liner and the filament-wound composite. The effectiveness of the designs and processes will be demonstrated and evaluated by fabricating and testing vessels at +75, -320, and -423°F.

The pressure-vessel membrane design method being used for the aluminum-lined glass-filament-wound tanks was developed by Aerojet under a previous NASA program (ref. 1-3). This method analyzes all portions of the vessel except areas of discontinuity (e.g., cylinder-to-dome juncture) and the immediate vicinity of the axially located port on the vessel dome, where the analysis "blows up" when the meridional filament wrap angle equals and exceeds approximately 54°. (This "blow up" is characteristic of all other known analyses for filament-wound domes.) Methods existed for the cylinder-to-dome juncture discontinuity analysis, but no structural analysis method was available for detailed investigation of the vessel dome in the region of the polar boss.

This report covers a structural analysis of the dome region of metal-lined glass-filament-wound pressure vessels, which was conducted because of the critical nature of the boss-to-liner transition in filament-wound vessels, the mismatch of boss and filament-wound composite deflections and rotations, and the strain magnifications known to exist in this region due to the rigidity of the boss designs employed so far and the extensibility of the filament-wound composite on top of the boss. First, the pressure-vessel design criteria and membrane analysis are presented, followed by a discontinuity analysis of the vessel dome-to-cylinder juncture and a determination of the filament-winding pattern. Then the dome characterization in the vicinity of the polar boss is presented - elastic properties, deflections, rotations, and strains when subjected to internal pressure and boss reaction loads. Boss concepts are reviewed, and two configurations selected for detailed design and analysis. The detailed boss designs are then incorporated into the vessel design developed from the membrane and dome-to-cylinder analyses to result in two complete vessel designs for fabrication and structural evaluation under Contract NAS 3-10289.

III. DESIGN ANALYSES OF PRESSURE-VESSEL MEMBRANE, HEAD-TO-CYLINDER JUNCTURE, AND WINDING PATTERN

A. DESIGN CRITERIA

Two aluminum-lined glass-filament-wound pressure vessel designs are to be prepared with the following characteristics:

Liner: Aluminum, Type 1100-0, of 0.010-in.-thickness

Bosses: Two design configurations (each vessel to use one) of about 1.20-in.-OD at the filament-wound dome axis

Fiber Reinforcement: S-glass (HTS finish)

Resin Matrix: Epon 828/DSA/Empol 1040/BDMA (100/115.9/20/1)

Liner-to-Composite Adhesive: Adiprene L-100/Epi-Rez 5101/ MOCA (80/20/17)

Burst Pressure at +75°F: 3000 psig

Shape: Closed-end cylinder

Size: 12-in.-dia. by 18-in.-long

B. DESIGN-ALLOWABLE GLASS-FILAMENT STRENGTH

Aerojet has developed a systematic approach to the design of filament-wound vessels (Ref. 4,5, and 6) and is using it in a number of applications. The method involves the use of pressure-vessel design factors, corresponding to a range of dimensional parameters, to determine the allowable strength for each configuration. The factors are based on data collected over the past 7 years from Aerojet tests on several thousands of pressure vessels; these vessels ranged in diameter from 4 to 74 in. and had significant variations in their design parameters. Included as factors used for the selection of design-allowable values are the strength of the glass roving, resin content, envelope dimensions (length and diameter), internal pressure level, axial port diameters, temperature, sustained loading requirements, and cyclic loading requirements. The method was used in this analysis to establish realistic values for the allowable ultimate 75°F S-HTS glass-filament tensile strengths in the 12-in.-dia. by 18-in.-long aluminum-lined filament-wound test vessel.

1. Longitudinal Filaments

The allowable longitudinal-filament strength is given by

$$F_{f,1} = K_1 K_2 K_3 K_4 K_5 (\sec^2 \alpha) F_f$$

Symbols for this section are defined in Appendix A.

The following design factors (Ref. 6) are based on the specific vessel parameters:

Parameter	Design Factor
D_c = 12.00 in.	0.815 (K_1)
D_b/D_c = 0.11	1.015 (K_2)
L/D_c = 1.5	1.000 (K_3)
$t_{f,l}/D_c \approx 0.00235$	0.920 (K_4)
$T = 75^oF$	1.000 (K_5)
$\alpha = 4^o$ (from geometry of vessel)	

For S-HTS glass filaments, the minimum ultimate tensile strength, F_f, is 415,000 psi.

The single-pressure-cycle allowable ultimate longitudinal filament strength is therefore

$$F_{f,l} = (0.815)\ (1.015)\ (1.000)\ (0.920)\ (1.000)\ (1.004)\ (415{,}000)$$
$$= 316{,}000 \text{ psi}$$

2. Hoop Filaments

The allowable hoop-filament strength is given by

$$F_{f,h} = K_1\ K_4\ K_5\ (1 - \frac{\tan^2 \alpha}{2})\ F_f$$

The following design factors are based on the specific vessel parameters

Parameter	Design Factor
D_c = 12.00 in.	0.890 (K_1)
$t_{f,h}/D_c \approx$ 0.00424	0.960 (K_4)
$T = 75^oF$	1.000 (K_5)
$\alpha = 4^o$	

The single-pressure-cycle allowable ultimate hoop filament strength is therefore

$$F_{f,h} = (0.890)\ (0.960)\ (1.000)\ (1.000)\ \left[1-\frac{0.00489}{2}\right]\ 415{,}000$$
$$= 354{,}000 \text{ psi}$$

C. MEMBRANE ANALYSIS

1. Method

The vessel shape and component thicknesses were established with the previously developed computer program for analysis of metal-lined filament-wound pressure vessels (Ref. 3). The program was used to investigate the filament shell by means of a netting analysis, which assumes constant stresses along the filament path and that the resin matrix makes a negligible structural contribution. The filament and metal shells are combined by equating strains in the longitudinal and hoop directions and by adjusting the shell radii of curvature to match the combined material strengths at the design pressure.

The program established the optimum head contour and defined the component thicknesses and other dimensional coordinates, as well as the shell stresses and strains at zero pressure and the design pressure, the filament-path length, and the weight and volume of the components and complete vessel. It was also used to determine the stresses and strains in the two shells during vessel operation through the use of a series of pressures and temperatures.

2. Computer Input and Output

Input variables used for the computer pressure vessel design analysis are presented in Table 1. The computer output described the pressure vessel membrane shape, component thickness and weights, and stress and strain conditions. The portions of the liner configuration (Figure 1) and pressure vessel configuration (Figure 2) dealing with the pressure vessel membrane are taken from the computer output, except as noted below.

The longitudinal filament-wound composite thickness requirements computed for the test vessels, based on a minimum allowable ultimate longitudinal filament stress of 316,000 psi and a design burst pressure of 3000 psig at 75°F, are the following:

Longitudinal Filament-Wound Composite Thickness in Cylinder (t_L)	0.042 in.
Equivalent Filament Thickness in Longitudinal Direction of Cylinder ($t_{f,l}$)	0.028 in.

The computerized analysis used the same allowable for the hoop filaments as for the longitudinal filaments (i.e., 316,000 psi), and the hoop filament-wound composite thickness requirements were computed to be the following:

Hoop Filament-Wound Composite Thickness in Cylinder (t_H)	0.084 in.
Equivalent Filament Thickness in Hoop Direction of Cylinder ($t_{f,h}$)	0.057 in.

Because the actual hoop filament minimum allowable ultimate stress, $F_{f,h}$, is 354,000 psi, the hoop wound composite thickness from the computer analysis, t_H, was reduced to bring the hoop filament stress up to 354,000 psi in order to obtain a balanced design with equal probability of failure in the hoop and longitudinal filaments. The load carried by the hoop filaments of the computer analysis is

$$F_{f,h}\, t_H = (316{,}000 \text{ psi})\,(0.084 \text{ in.})$$

The new hoop-wound composite thickness, t_H', required to develop a stress in the hoop filaments of 354,000 psi is given by

$$t_H' = \frac{316{,}000}{354{,}000}\,(0.084 \text{ in.}) = 0.075 \text{ in.}$$

This hoop-wound composite thickness is reflected in Figure 2.

D. HEAD-TO-CYLINDER JUNCTURE DISCONTINUITY ANALYSIS

1. Objective

The purpose of this section of the report is to provide a discontinuity stress analysis of the head-to-cylinder juncture to establish the validity of the design shown in Figure 2.

2. Summary

A discontinuity analysis was conducted for the design shown in Figure 2. Only the section at the juncture of the head-to-cylinder, shown schematically in Figure 3, was considered in this analysis. Calculations indicate a maximum longitudinal composite stress of 213,300 psi (filament stress of 318,500 psi), which is 0.8% greater than the allowable design stress. This stress occurs in the cylindrical section approximately 0.1 inch from the tangent plane.

3. Analysis

Since the meridional radius of curvature of the head changes very slowly in the area adjacent to the juncture of the head and cylinder, the head may be considered cylindrical at the discontinuity. Equations for the deflection and rotation at the head-cylinder juncture are taken from Reference 7, cases 14 and 15, page 302. The deflection of the cylinder is

$$\delta_c = \delta_{c_p} - \frac{V_o}{2D_c \lambda_c^3} - \frac{M_o}{2D_c \lambda_c^2}$$

and, the rotation of the cylinder is

$$\theta_c = \frac{V_o}{2D_c \lambda_c^2} + \frac{M_o}{D_c \lambda_c}$$

Deflection of the head is

$$\delta_h = \delta_{hp} + \frac{V_o}{2D_h \lambda_h^3} - \frac{M_o}{2D_h \lambda_h^2}$$

and, the rotation of the head is

$$\theta_h = \frac{V_o}{2D_h \lambda_h^2} - \frac{M_o}{D_h \lambda_h}$$

The following relationships are used to adapt the deflection and rotation equations to filament-wound cylinders:

a. Composite Beam Properties

(1) Modulus

The composite modulus in the longitudinal direction is

$$E_L = \frac{E_{LL}\, t_L + E_{LM}\, t_M + E_{LH}\, t_H}{t_L + t_M + t_H}$$

where,

t_L = 0.042 in. (from Figure 2)

t_M = 0.010 in. (from Figure 1)

t_H = 0.075 in. (cylinder only, Figure 2)

E_{LH} = 0.0 (resin crazes)

The modulus of the longitudinal composite in the longitudinal direction (E_{LL}) is calculated from the following expression

$$E_{LL} = P_{vg} E_f \cos^2 \alpha_o$$

and with

E_f = 12.4×10^6 psi (S-HTS glass filaments)

P_{vg} = 0.673

$$\alpha_o = 3.82^\circ \text{ (from computer analysis)}$$

$$E_{LL} = 0.673\ (12.4 \times 10^6)\ (0.9956)$$

$$= 8.313 \times 10^6 \text{ psi}$$

Since the liner is strained beyond its yield stress, an effective modulus, based on total vessel strain, is used for the liner.

$$E_{LM} = \sigma_M\ (1 - \nu_M)\ \left(\frac{E_f}{\sigma_{f,\ell}}\right)$$

Where,

ν_M = 0.325 for aluminum

$\sigma_{f,\ell}$ = 316,000 psi for S-HTS glass filaments at 3000 psi internal pressure

σ_M = 13,400 psi (from computer analysis)

$$E_{LM} = 13{,}400\ (1-0.325)\ \left(\frac{12.4 \times 10^6}{316{,}000}\right)$$

$$= 0.355 \times 10^6 \text{ psi}$$

The composite modulus in the longitudinal direction for the cylinder is

$$E_{L_c} = \frac{8.313 \times 10^6\ (0.42) + 0.355 \times 10^6\ (0.010)}{0.042 + 0.010 + 0.075}$$

$$= 2.777 \times 10^6 \text{ psi}$$

and, for the head

$$E_{L_h} = \frac{8.313 \times 10^6\ (0.042) + 0.355 \times 10^6\ (0.010)}{0.042 + 0.010}$$

$$= 6.783 \times 10^6 \text{ psi}$$

The composite modulus in the hoop direction is

$$E_H = \frac{E_{HH} t_H + E_{HM} t_M + E_{HL} t_L}{t_L + t_M + t_H}$$

where,

$$E_{HH} = P_{vg}E_f$$

$$= 0.673\ (12.4 \times 10^6)$$

$$= 8.35 \times 10^6 \text{ psi}$$

and

$$E_{HL} = KE_f \sin^2 \alpha_o$$

$$= 0.673\ (12.4 \times 10^6)\ (0.00443)$$

$$= 0.037 \times 10^6 \text{ psi}$$

The effective modulus of the liner in the hoop direction is

$$E_{HM} = \sigma_M\ (1 - \nu_M) \left(\frac{E_f}{\sigma_{f,h}}\right)$$

with,

$\sigma_{f,h}$ = 354,000 psi for S-HTS hoop glass filaments at 3000 psi internal pressure

$$E_{HM} = 13,400\ (1 - 0.325)\ \left(\frac{12.4 \times 10^6}{354,000}\right)$$

$$= 0.317 \times 10^6 \text{ psi}$$

The composite modulus in the hoop direction for the cylinder is

$$E_{H_c} = \frac{8.35 \times 10^6\ (0.075) + 0.317 \times 10^6\ (0.010) + 0.037 \times 10^6\ (0.042)}{0.042 + 0.010 + 0.075}$$

$$= 4.968 \times 10^6 \text{ psi}$$

and, for the head

$$E_{H_h} = \frac{0.317 \times 10^6\ (0.010) \times 0.037 \times 10^6\ (0.042)}{0.042 + 0.010}$$

$$= 0.091 \times 10^6 \text{ psi}$$

(2) Neutral Axis

The neutral axis of the cylinder is

$$\bar{Y}_c = \frac{E_{LL} t_L (t_M + t_L/2) + E_{LM}(t_M)^2/2}{(t_L + t_M + t_H)\, E_{L_c}}$$

$$\bar{Y}_c = \frac{8.313 \times 10^6 (0.042)(0.031) + 0.355 \times 10^6 (0.01)^2/2}{0.127\ (2.777 \times 10^6)}$$

$$\bar{Y}_c = 0.031 \text{ in.}$$

and, for the head

$$\bar{Y}_h = \frac{E_{LL} t_L (t_M + t_L/2) + E_{LM}(t_M)^2/2}{(t_M + t_L)\, E_{L_h}}$$

$$\bar{Y}_h = \frac{8.313 \times 10^6 (0.042)(0.031) + 0.355 \times 10^6 (0.01)^2/2}{0.052\ (6.783 \times 10^6)}$$

$$\bar{Y}_h = 0.031 \text{ in.}$$

(3) Flexural Rigidity

The flexural rigidity is calculated from the equation

$$D = E_L I = \frac{1}{12}\left\{t_M^3 E_{LM} + t_L^3 E_{LL} + t_H^3 E_{LH}\right\}$$

$$+ t_M \left[\bar{Y} - t_M/2\right]^2 E_{LM} + t_L \left[\bar{Y} - (t_M + t_L/2)\right]^2 E_{LL}$$

$$+ t_H \left[\bar{Y} - (t_M + t_L + t_H/2)\right]^2 E_{LH}$$

Since $\bar{Y}_c = \bar{Y}_h$, the head and cylinder flexural rigidities are

$$D_c = D_h = \frac{(0.01)^3\ 0.355 \times 10^6 + (0.042)^3\ 8.313 \times 10^6}{12}$$

$$+ 0.01\ (0.031 - .005)^2\ 0.355 \times 10^6 = 53.753 \text{ lb-in.}$$

(4) Stiffness

The modulus of the beam foundation (stiffness) is

$$k = \frac{E_H (t_L + t_M + t_H)}{R_2^2}$$

where,

$$R_2 = R = 6.00 \text{ in. (from computer analysis)}$$

For the cylinder

$$k_c = \frac{4.968 \times 10^6 (0.127)}{(6)^2}$$

$$= 17{,}530 \text{ lb/in.}^3$$

and for the head

$$k_h = \frac{0.091 \times 10^6 (0.052)}{(6)^2}$$

$$= 131.4 \text{ lb/in.}^3$$

(5) Beam Characteristic

The beam characteristic (λ) is defined to be

$$\lambda^4 = \frac{k}{4D}$$

For the cylinder

$$\lambda_c^4 = \frac{17{,}530}{4\ (53.753)} = 81.53 \text{ in.}^{-1}$$

and for the head

$$\lambda_h^4 = \frac{131.4}{4(53.753)} = 0.6111 \text{ in.}^{-1}$$

b. Radial Membrane Deflections

(1) Cylinder

$$\delta_{c_p} = \frac{pR^2}{E_{H_c}(t_M + t_L + t_H)}$$

With p = 3000 psi

$$\delta_{c_p} = \frac{3000\ (6)^2}{4.968 \times 10^6\ (0.127)} = 0.1712 \text{ in.}$$

(2) Head

$$\delta_{H_p} = \frac{pR_2^{\,2}\ (2 - R_2/R_1)}{2E_{H_h}\ (t_M + t_L)}$$

With $1/R_1 = 0.331 \text{ in.}^{-1}$

$$\delta_{H_p} = \frac{3000\ (6)^2\ [2-6(0.331)]}{2(0.091 \times 10^6)(0.052)}$$

$$= 0.1598 \text{ in.}$$

c. Discontinuity Forces and Moments

(1) Head-to-Cylinder Juncture

The discontinuity force and moment at the juncture of the head to cylinder may be found by matching head and cylinder rotation and deflection. The deflection of the cylinder is

$$\delta_c = 0.1712 - \frac{V_o}{2(53.75)(27.13)} - \frac{M_o}{2(53.75)(9.029)}$$

$$\delta_c = 0.1712 - 0.00034\ V_o - 0.00103\ M_o$$

and the rotation of the cylinder is

$$\theta_c = \frac{V_o}{2(53.75)(9.029)} + \frac{M_o}{53.75(3.005)}$$

$$\theta_c = 0.00103\ V_o + 0.00619\ M_o$$

The deflection of the head is

$$\delta_h = 0.1598 + \frac{V_o}{2(53.75)(0.6912)} - \frac{M_o}{2(53.75)(0.7817)}$$

$$\delta_h = 0.1598 + 0.01345\ V_o - 0.1190\ M_o$$

and the rotation of the head is

$$\theta_h = \frac{V_o}{2(53.75)(0.7817)} - \frac{M_o}{53.75(0.8841)}$$

$$\theta_h = 0.01190\ V_o - 0.02104\ M_o$$

Equating rotations and deflections yields

$$M_o = \left(\frac{0.01190-0.00103}{0.00619 + 0.02104}\right) V_o$$

$$M_o = 0.39919\ V_o$$

and

$$V_o = \frac{(0.1712-0.1598) + (0.01190-0.00103)M_o}{0.01345 + 0.00034}$$

$$V_o = 0.82668 + 0.78825\ M_o$$

Simultaneous solution of the two equations yields

$$V_o = \frac{0.82668}{1-0.39919(0.78825)} = 1.206\ \text{lb/in.}$$

and

$$M_o = 0.39919\ (1.206) = 0.481\ \text{in.-lb/in.}$$

(2) Bending Moment Distribution

The bending moment distribution in the cylinder, including the moment due to shear, is calculated from the expression

$$M_c(Y) = e^{-\lambda_c Y}\left[M_o \cos \lambda_c Y + (M_o + \frac{V_o}{\lambda_c}) \sin \lambda_c Y\right]$$

and for the head

$$M_h(Y) = e^{-\lambda_h Y}\left[M_o \cos \lambda_h Y + (M_o - \frac{V_o}{\lambda_h}) \sin \lambda_h Y\right]$$

Results of calculations based on these equations are shown in Figure 4. It can be seen that the maximum bending moment occurs in the cylinder approximately 0.10 in. from the tangency plane.

d. Maximum Stress

The maximum stress occurs in the longitudinal composite and is a combination of membrane and bending stresses. The longitudinal composite stress resulting from pressure is

$$\sigma_{LL_p} = P_{vg}\, \sigma_{f,\ell} \cos^2 \alpha_o$$

where,

$$\sigma_{LL_p} = 0.673\ (316{,}000)(0.9955)$$

$$= 211{,}600 \text{ psi}$$

The maximum tensile bending stress in the outside fibers of the longitudinal composite is

$$\sigma_{LL_B} = \frac{My}{I_c}\left(\frac{E_{LL}}{E_L}\right)_c = \frac{ME_{LL}}{D_c}\,(\bar{Y} - t_M)$$

$$\sigma_{LL_B} = \frac{0.535(8.313 \times 10^6)(0.031-0.010)}{53.75}$$

$$\sigma_{LL_B} = 1740 \text{ psi}$$

and the maximum combined (tensile) stress is

$$\sigma_{LL} = \sigma_{LL_p} + \sigma_{LL_B}$$

$$\sigma_{LL} = 211{,}600 + 1740$$

$$\sigma_{LL} = 213{,}340 \text{ psi}$$

This longitudinal composite stress is equivalent to a longitudinal filament stress of 318,500 psi, which is 0.8% higher than the 316,000 psi allowable stress used for computer analysis of the membrane.

E. WINDING PATTERN ANALYSIS

The filament-wound vessel has two winding patterns: a longitudinal-in-plane pattern along the cylinder and over the end domes to provide the total filament-wound composite strength in the heads and the longitudinal strength in the cylindrical section; and a circumferential pattern applied along the cylinder for hoop strength in this section.

The winding pattern for the pressure vessel requires the application of a specific quantity of glass roving in predetermined orientations in order to obtain the desired burst pressure. The pressure vessel membrane analysis of Section III-C showed that the required filament-wound composite and equivalent glass-filament thicknesses are the following:

	Thickness, in.
Longitudinal filament-wound composite thickness in cylinder	0.042
Equivalent filament thickness in longitudinal direction of cylinder	0.028
Hoop filament-wound composite thickness in cylinder	0.075
Equivalent filament thickness in hoop direction of cylinder	0.051

1. Longitudinal Pattern

The pattern is analyzed here on the basis of actual winding data and laboratory tests of glass roving and composite specimens, which have shown that a cured single layer of 20-end roving created by side-by-side orientation has a thickness ($t_{s,1}$) of 0.007 in.

The required number of layers of longitudinal winding (L_L) to make up the longitudinal composite thickness (T_L) is given by

$$L_L = \frac{T_L}{t_{s,1}} = \frac{0.042}{0.007} = 6 \text{ layers}$$

Two layers are formed for each revolution of the winding mandrel. The number of revolutions required (N_1) is therefore

$$N_1 = \frac{L_L}{2} = \frac{6}{2} = 3 \text{ revolutions}$$

The winding-tape width (W_L) is given by

$$W_L = \frac{N_2 \; A}{t_{s,1} P_{vg}}$$

where

N_2 = number of 20-end roving strands per tape, selected as 3

A = cross section of 20-end roving = 420×10^{-6} in.^{2}

P_{vg} = glass-filament fraction in composite = 0.673

Thus,

$$W_L = \frac{(3)(420 \times 10^{-6})}{(0.007)(0.673)} = 0.268 \text{ in.}$$

The number of turns per revolution (N_3) must be an integer, and is given by

$$N_3 = \frac{\pi D_c \cos \alpha}{W_L + \epsilon_{t_p}} \quad \text{to the nearest integer}$$

where

D_c = vessel diameter = 12.00 in.

α = longitudinal in-plane winding angle = 3.82°

ϵ_{t_p} = space between tapes (which should equal zero)

Therefore,

$$N_3 = \frac{\pi (12.00)(0.998)}{0.268} = 140 \text{ turns per revolution}$$

2. Hoop Pattern

The required number of layers of hoop winding to make up the hoop composite thickness (t_H) is given by

$$L_H = \frac{t_H}{t_{s,h}}$$

where

$t_{s,h}$ = thickness of single cured layer of hoop winding

In this case $t_{s,h}$ may be set equal to 0.0075 in.

Then

$$L_H = \frac{0.075}{0.0075} = 10 \text{ layers}$$

The number of turns per inch of cylinder length (N_5) is given by

$$N_5 = \frac{L_c \, t_{s,h} \, P_{vg}}{N_4 \, A}$$

where

L_c = cylinder length, selected as 1 in.

N_4 = number of 20-end roving strands per tape, selected as 1

then

$$N_5 = \frac{(1.00)(0.0075)(0.673)}{(1)\ (420 \times 10^{-6})}$$

$$= 12.0 \text{ turns per inch layer.}$$

IV. DOME CHARACTERISTICS OF ALUMINUM-LINED GLASS FILAMENT-WOUND VESSEL

A. INTRODUCTION

The filament-wound pressure vessel dome (filament-wound composite, liner, and boss) analyzed here has been described in Section III and Figures 1 and 2. During analysis and characterization of the filament-wound composite component of this dome, modifications to the basic thickness, contour, and geometry were made only in the region of the polar boss by variations in winding tape width and composite stackup at the boss.

Two distinct methods exist for analyzing filament-wound composites: the netting analysis and the orthotropic analysis. In the netting analysis, which was used in Section III for design of the basic vessel, it is assumed that the resin has no load carrying ability, and that its only purpose is to hold the fibers in position. For vessel design, this analysis assumes that all the fibers are stressed uniformly and shapes the vessel dome contour to satisfy this condition. The netting analysis is used primarily for investigating the membrane stresses in fiber shells. It cannot be used for predicting the bending stresses and interlaminar shear stresses. In the orthotropic analysis, both the filaments and the resin are taken into consideration. The method consists of determining equivalent elastic constants for the filament-wound composite shell and using them in orthotropic shell theory.

In the absence of resin fracture or craze cracking, the orthotropic analysis should accurately describe dome properties and behavior under pressure loading. However, in practice, the glass-filament domes do craze as they strain, resulting in a partial breakdown of the resins influence on dome behavior. If resin fracture should ever be complete, the netting analysis would apply in describing dome properties and behavior. Real dome behavior lies between these two idealizations of the filament-wound structure. The present analysis investigated the filament-wound dome using both approaches to establish limits of dome behavior under pressure and boss loading.

B. STRAIN CHARACTERIZATION OF FILAMENT-WOUND SHELL

The meridional strain of the filament-wound composite shell at any point is

$$\epsilon_L = \frac{\sigma_L}{E_{LL}} - \nu_H \frac{\sigma_H}{E_{HL}}$$

where,

$$\sigma_L = \frac{N_L}{t_h} = \frac{pR_2}{2t_h}$$

and

$$\sigma_H = \frac{N_H}{t_h} = \frac{pR_2}{2t_h}\left(2 - \frac{R_2}{R_1}\right)$$

Analysis of the computer print-out in the region where the pressure vessel dome may be considered a shell ($\alpha_o \leq \alpha < 30^o$) reveals that the ratio of hoop to meridian radii of curvature is approximately equal to 2. Since ($2 - R_2/R_1$) is approximately zero, the hoop stress is approximately zero and the meridian strain is

$$\epsilon_L = \frac{\sigma_L}{E_{LL}} = \frac{N_L}{E_{LL} t_h}$$

For ease of calculation and a better presentation of parameters of interest, it was decided to normalize the strain at any point to the strain at the equator of the vessel

$$\epsilon_L / \epsilon_{L_o} = \frac{N_L / E_{LL} t_h}{(N_L / E_{LL} t_h)_o}$$

where, the subscript "o" refers to the value at the equator. The meridian force at any point is proportional to the hoop radius of curvature

$$N_L / N_{L_o} = \frac{pR_2/2}{pa/2} = R_2/a$$

so that the normalized strain may be defined by the relation

$$\epsilon_L / \epsilon_{L_o} = (R_2/a) \Big/ \left\{ E_{LL} t_h \Big/ E_{LL_o} t_{h_o} \right\}$$

The computer run for this particular shell was used to obtain values for α, R_2, R_1, $Z = x/a$, and t_h as shown in Table 2. A plot of Z vs. α was made from the data and is shown in Figure 5. It should be noted in the figure that the major portion of the pressure vessel (shell portion of vessel where liner thickness is constant) has wrap angles less than 20^o. In order to better show the deviation in parameters as the area of the boss is approached it was decided to use wrap angle (α) as the independent parameter for plots rather than the radial distance (x). Figures 6 and 7 show the normalized hoop radius of curvature and the normalized thickness of the composite, respectively, as a function of wrap angle. The only other parameter required to define the normalized strain is the modulus of elasticity in the meridian direction.

1. Modulus of Elasticity and Strain from Orthotropic Theory

The variation in modulus of elasticity with wrap angle for a glass/epoxy composite is shown in Figure 31 of Reference (8). Rather than recalculate values for this parameter, the curve described in Reference (8) was replotted and is shown in Figure 8. Using Figure 8 and the following relationship

$$E_{LL}/E_{LL_o} = (E_{LL}/E_F) / (E_{LL}/E_F)_o$$

in combination with the normalized thickness, the normalized extensional stiffness was determined and is plotted in Figure 9. The values of parameters depicted in Figures 6 and 9 were used to construct the curve of normalized strain for an unlined composite shell as shown in Figure 10.

a. Effect of Elastic Liner

In order to determine the effect of an elastic liner (liner stressed below its yield point) on the normalized strain, the liner and filament reinforced composite shells were treated as a single composite shell having an equivalent extensional stiffness. The strain of the equivalent composite shell is

$$\epsilon_{LC} = \frac{\sigma_{LC}}{E_{LC}} = \frac{N_L}{E_{LC} t_{hC}}$$

and, the normalized strain is

$$(\epsilon_{LC}/\epsilon_{LC_o}) = (R_2/a) / (E_{LC} t_{hC}/E_{LC_o} t_{hC_o})$$

The extensional stiffness of the equivalent composite shell at any point is

$$E_{LC} t_{hC} = E_{LL} t_L + E_{LM} t_M$$

$$E_{LC} t_{hC} = \left(\frac{E_{LL} t_L}{E_{LL_o} t_{L_o}}\right) E_{LL_o} t_{L_o} + \left(\frac{E_{LM} t_M}{E_{LM_o} t_{M_o}}\right) E_{LM_o} t_{M_o}$$

and, the normalized value is

$$\left(\frac{E_{LC} t_{HC}}{E_{LC_o} t_{hC_o}}\right) = \left(\frac{E_{LL} t_L}{E_{LL_o} t_{L_o}}\right)\left(\frac{E_{LL_o} t_{L_o}}{E_{LC_o} t_{hC_o}}\right) + \left(\frac{E_{LM} t_M}{E_{LM_o} t_{M_o}}\right)\left(\frac{E_{LM_o} t_{M_o}}{E_{LC_o} t_{hCo}}\right)$$

For a 0.010 in. thick aluminum liner with an elastic modulus of 10×10^6 psi

$$E_{LM_o} t_{M_o} = 10 \times 10^6 (0.01) = 1 \times 10^5 \text{ lb/in.}$$

and for the filament composite at the equator

$$E_{LL_o} t_{L_o} = \left(\frac{E_{LL_o}}{E_F} \right) E_F t_{L_o}$$

with

$$E_F = E_f P_{vg} + E_r (1-P_{vg})$$

$$E_F = \left[12.4 (0.67) + 0.5 (0.33) \right] \times 10^6$$

$$E_F = 8.47 \times 10^6 \text{ psi}$$

and, from Figure 8,

$$\left(E_{LL_o} / E_F \right) = 0.992$$

$$E_{LL_o} t_{L_o} = 0.992 (8.47 \times 10^6) (0.052) = 4.37 \times 10^5 \text{ lb/in.}$$

The extensional stiffness of the equivalent composite shell at the equator is

$$E_{LC_o} t_{h_o} = E_{LM_o} t_{M_o} + E_{LL_o} t_{L_o}$$

$$E_{LC_o} t_{h_o} = 1 \times 10^5 + 4.37 \times 10^5 = 5.37 \times 10^5 \text{ lb/in.}$$

and, the normalized extensional stiffness of the equivalent composite shell is

$$\frac{E_{LC} t_{hC}}{E_{LC_o} t_{hC_o}} = 0.186 \left(\frac{E_{LM} t_M}{E_{LM_o} t_{M_o}} \right) + 0.814 \left(\frac{E_{LL} t_L}{E_{LL_o} t_{L_o}} \right)$$

Definition of the metal-shell thickness variation is required in the region of the boss-flange in order to establish the extensional stiffness of the elastic liner in this area. Table 3 gives liner thickness data from the Figure 1 configuration.

Figure 6 was again used in combination with the normalized extensional stiffness (calculated from the values of liner thickness shown in Table 3) to establish the normalized strain for a filament composite shell with an elastic liner. All values of parameters are shown in Table 4 and normalized strain is plotted in Figure 10.

b. Effect of Plastic Liner

The effect of a liner in the plastic range (that is, a liner stressed above its yield point) on the strain of the shell is calculated using a similar method to that described in the preceding paragraphs. For a 0.010 in.-thick aluminum liner with a plastic modulus of 0.1 x 10^6 psi the extensional stiffness of the metal shell at the equator is

$$E_{LM_o} t_{M_o} = 0.1 \times 10^6 \, (0.01) = 0.01 \times 10^5 \text{ lb/in.}$$

and, the extensional stiffness of the equivalent composite shell at the equator is

$$E_{LC_o} t_{h_o} = 0.01 \times 10^5 + 4.37 \times 10^5 = 4.38 \times 10^5 \text{ lb/in.}$$

The normalized extensional stiffness of the equivalent composite shell at any point is

$$\frac{E_{LC} t_{hC}}{E_{LC_o} t_{hC_o}} = 0.002 \left(\frac{E_{LM} t_M}{E_{LM_o} t_{M_o}} \right) + 0.998 \left(\frac{E_{LL} t_L}{E_{LL_o} t_{L_o}} \right)$$

Data on the normalized extensional stiffness and normalized strain for the equivalent composite shell are shown in Table 5, and the normalized strain is plotted in Figure 10.

c. Discussion of Results

The meridional strain of a filament-wound composite shell with modulus of elasticity computed from orthotropic theory is shown in Figure 10. Although the accuracy of the curve is questionable for wrap angles greater than 30°, due to the neglected Poisson effect (hoop stress), it allows a basis for comparison of the effect of an elastic liner (stress below yield point) and a plastic liner (stress beyond yield point) up to the point where the boss-to-liner transition occurs. As shown in Figure 10, the unlined filament-wound dome had an increasing meridional strain up the dome: at the point where the liner-to-boss juncture would be located, the strain was 11% greater than at the equator; the maximum meridional strain occurred on top of where the boss would be located and was 50% greater than at the equator. At pressures above 140 psi, where the constant thickness portion of the liner is passed its yield stress everywhere on the dome, the liner had very little effect on strains at all points on the contour, and the strain pattern closely approximated that which occurred for an unlined dome.

2. Modulus of Elasticity and Strain from Netting Theory

In netting theory, the meridional modulus of elasticity is assumed to vary with wrap angle by the following expression:

$$E_{LL} = P_{vg} E_f \cos^2 \alpha$$

Data from computer output listed in Table 2 was used in combination with values obtained from the preceding equation to calculate the normalized extensional stiffness and strain of an unlined filament-wound shell. Calculated values are listed in Table 6 and a plot of normalized meridional strain is shown in Figure 11.

The effect of an elastic liner on the normalized meridional strain of the resulting equivalent composite shell is shown in Figure 11, while the data used to construct the plot is listed in Table 7. The method for establishing the extensional stiffness is the same as that described in the preceding section on orthotropic theory.

Referring to Figure 11, the unlined filament-wound dome with liner plastic had a meridional strain which was essentially constant along the contour. Inclusion of an elastic aluminum liner induced a similar strain spike (as in the orthotropic analysis) at the juncture of the liner-to-boss, but this spike is expected to dampen out as plastic flow is encountered at low vessel internal pressures.

C. RADIAL DEFLECTION OF FILAMENT-WOUND SHELL

The radial deflection (deflection normal to axis of rotation) of a shell of revolution subjected to membrane loading is expressed by the following relation

$$\delta = \frac{R}{t_h} \left[\frac{N_H}{E_{HL}} - \nu_L \frac{N_L}{E_{LL}} \right]$$

with

$$N_L = \frac{pR_2}{2}$$

$$N_H = \frac{pR_2}{2} \left(2 - \frac{R_2}{R_1} \right)$$

the radial displacement per unit pressure is

$$\delta/p = \frac{RR_2}{2t_h} \left[\frac{\left(2 - R_2/R_1\right)}{E_{HL}} - \frac{\nu_L}{E_{LL}} \right]$$

1. Composite Properties from Orthotropic Theory

Computer output was again used to define the geometric properties of the filament-wound shell at various points along the contour. Reference 8 was used to establish modulus of elasticity in the hoop and meridian direction, and Poisson's ratio at the required contour points. This data is summarized in Table 8 which also contains calculated values for radial deflection at each point.

Table 8 shows that the radial deflections of the shell were inward at the equator and up the dome until the boss region was approached, due to the high meridional load, very low hoop load, and Poisson's ratios for the materials.

2. Composite Properties from Netting Theory

In netting theory Poisson's ratio is zero, and the radial displacement of a point on the shell of revolution is described by the modified equation

$$\delta / p = \frac{RR_2 \left(2 - R_2/R_1 \right)}{2E_{HL} t_h}$$

Using the computer output of Table 8 and the following expression for the modulus of elasticity in the hoop direction

$$E_{HL} = P_{vg} E_f \sin^2 \alpha$$

the radial deflection at each point on the contour was calculated and results listed in Table 8. It should be noted that netting theory produced outward values for deflections over the entire dome.

3. Discussion of Results

Although radial deflections could be computed easily, the deflection in an orthogonal direction is needed to locate the deflected point in space, and the equations governing this orthogonal deflection require extensive numerical solution.

Because it was known that actual balanced-in-plane domes deflect outward, it was decided to review empirical data on dome deflections available at Aerojet from past programs. This review revealed the following:

- The existence of two zones of approximately linear load vs deflection behavior due to the departure from orthotropic properties with increasing strain; above the transition load (approximately 25% of ultimate) where crazing initiates, the deformation behaves as predicted by the netting analysis.

- Above the crazing threshold, deflections of points on the domes were essentially normal to the unpressurized surface.

Based on this, the netting analysis should be used to establish membrane strains, stresses, and deflection in glass filament-wound vessels.

The netting analysis computer program assumes that the vessel heads are wound with tape of negligible width. This assumption produces valid results for the entire dome except for an area immediately adjacent to the boss, where the composite thickness predicted by the analysis approaches infinity. This does not represent the actual situation (because finite tape widths are always used) and causes the analysis to "blowup." To determine the portion of the dome over which the analysis is valid, the computer output was analyzed to determine (1) the last good point where the inside surface of the windings did not curve in upon itself, and (2) the isotensoid feature of the filaments was maintained. For the 12-in.-dia vessel, this occurred at a normalized radial distance, $\bar{Z}$, of 0.254 (for reference, the boss diameter normalized radial distance, $\bar{Z}$, is 0.100). Coincidently, this is the point at which the metal liner design of Figure 1 starts thickening into the polar boss. The computer output thus describes the dome between $\bar{Z} = 1.000$ and $\bar{Z} = 0.254$, and other methods must be used to analyze the remainder of the dome. Discontinuity forces and moments exist here due to changes in section properties and curvature, and the presence of boss reaction loads. A discontinuity analysis will be used to tie the remainder of the dome to the membrane.

D. DISCONTINUITY ANALYSIS OF FILAMENT-WOUND COMPOSITE IN AREA OF BOSS/FLANGE

In the region of the boss/flange the filament-wound composite shell, which carries only membrane loads, blends into a rigid band of material 1.57 times the tape width which acts as a ring plate.* At the transition point, radii of curvature change from finite values in the shell region to infinite values for the ring plate. Figure 12 depicts a model of this region broken down into free bodies with the corresponding loads and their points of application. The flange of the boss is assumed to be disconnected from the metal liner at the discontinuity which implys a free floating metal boss. The horizontal discontinuity force (H_D) and bending moment (M_D) can be determined by setting up two equations of compatibility involving the rotation and displacements. Note in Figure 12 that provision was made to account for a uniformly distributed flange load or a concentrated load acting at any position along the flange which can be induced as a result of rotation of the bodies. Compatibility of deformations at the ring/shell juncture requires that

$$\left.\begin{aligned} \delta_R &= \delta_h \\ \theta_R &= \theta_h \end{aligned}\right\} \quad R = R_D$$

*The 1.6 factor was determined from measurement of a sectioned tank.

$$\delta_R^{H_T} - \delta_R^{M_R} = \delta_h^{p} - \delta_h^{H_D} - \delta_h^{M_D} \qquad \textbf{(1)}$$

$$\theta_R^{H_T} - \theta_R^{M_R} = \theta_h^{H_D} + \theta_h^{M_D} \qquad \textbf{(2)}$$

The ring loads are given by the following equations (see Figure 12).

$$V_D = \frac{pR_D}{2} \qquad N_L = \frac{pR_{2_D}}{2}$$

$$V_A = \frac{pR_D^2}{2(R_A + e)} \qquad H_T = H_D + N_D \cos \phi$$

$$M_R = \frac{1}{\bar{R}} \left[R_D M_D + R_D(R_D - \bar{R}) V_D + (R_A + e)(\bar{R} - R_A - e) V_A \right]$$

The ring deflections are given by the following:

$$\delta_R^{H_T} = \frac{R_D C_1 H_T}{B_{H_R}} \qquad C_1 = \left(\frac{R_D^2 + R_A^2}{R_D^2 - R_A^2} - \bar{\nu} \right)$$

$$\delta_R^{M_R} = 2 R_D \sin^2 \left(\theta_R^{M_R} / 2 \right) \sim 0$$

Ring rotations are given by:

$$\theta_R^{H_T} \sim 0$$

$$\theta_R^{M_R} = \frac{M_R \bar{R}^2}{D_R}$$

The extensional stiffness of the ring is

$$B_{H_R} = E_{H_R} t_R$$

and the ring flexural rigidity is

$$D_R = \frac{E_{H_R} t_R^3 \left(R_D - R_A\right)}{12 \left(1 - \nu_H \nu_L\right)}$$

Shell distortion equations for deflection and rotation of the shell as a result of the discontinuity loads were obtained from the work done by Greszczuk (Reference 9). These equations, describe a shallow homogeneous shell and must be modified to account for the orthotropic properties encountered in a composite material. The modified equations appear below, followed by definitions of the modifying factors.

$$\delta_h^{\,p} = \frac{pR_D R_{2_D}}{2}\left[\frac{2 - \left(R_2/R_1\right)_D}{B_H} - \frac{\nu_L}{B_L}\right]$$

$$\delta_h^{\,H_D} = \frac{R_D\, H_D}{W_d}\left[K_3\left(\frac{\nu_L K_2}{\xi_D B_L} - \frac{K_5}{B_H}\right) - K_1\left(\frac{K_6}{B_H} + \frac{\nu_L K_4}{\xi_D B_L}\right)\right]$$

$$\delta_h^{\,M_D} = \frac{R_D\, M_D}{R_{2_D} \phi_D^2\, W_d}\left[K_4\left(\frac{\nu_L K_2}{\xi_D\, B_L} - \frac{K_5}{B_H}\right) - K_2\left(\frac{K_6}{B_H} + \frac{\nu_L K_4}{\xi_D\, B_L}\right)\right]$$

$$\theta_h^{\,H_D} = \frac{\xi_D\, H_D}{B_H\, \phi_D\, W_d}\left[K_3\, K_4 + K_1\, K_2\right]$$

$$\theta_h^{\,M_D} = \frac{\xi_D\, M_D}{B_H \phi_D^3\, R_{2_D}\, W_d}\left[K_4^{\,2} + K_2^{\,2}\right]$$

where the extensional stiffnesses are

$$B_{H_h} = \sum_{1}^{i=n} E_{H_i}\, t_{h_i}\ , \quad B_L = \sum_{1}^{i=n} E_{L_i}\, t_{h_i}$$

and the flexural rigidity is

$$D_h = \sum_{1}^{i=n} E_{L_i} t_{h_i} \left[\frac{t_{h_i}^2}{12\,(1 - \nu_H \nu_L)_i} + (\bar{y} - y_i)^2 \right]$$

With these properties, the beam characteristic (λ_h) is established by the equation

$$\lambda_h^4 = \frac{B_{H_h} R_{2_D}^2}{4D_h}$$

The beam characteristic for the shell is used to establish Greszczuk's parameter (ξ_D) as

$$\xi_D = \lambda_h \phi_D \sqrt{2}$$

which is then used to evaluate the parameters, $k_1\ (\xi_D)$, ..., $K_n\ (\xi_D)$ the values of which are tabulated in Reference 9.

The compatibility equations in terms of influence coefficients can be written

$$U_R^{\,p}\, p + U_R^{\,H_D} H_D = U_h^{\,p}\, p - U_h^{\,H_D} H_D - U_h^{\,M_D} M_D \qquad \textbf{(3)}$$

and

$$-\beta_R^{\,p}\, p - \beta_R^{\,M_D} M_D = \beta_h^{\,H_D} H_D + \beta_h^{\,M_D} M_D \qquad \textbf{(4)}$$

The notation is such that $U_R^{\,p}$ is the deflection of the ring (R) resulting from unit pressure (p), and $\beta_h^{\,M_D}$ is the rotation of the shell (h) caused by the unit bending moment (M_D). Note that

$$\delta_R^{\,H_T} = \frac{R_D C_1}{B_{H_R}} \left[\frac{pR_{2_D}}{2} \cos \phi_D + H_D \right]$$

$$\delta_R^{\,H_T} = U_R^{\,p}\, p + U_R^{\,H_D} H_D$$

in transforming from Equation 1 to 3. Also, in transforming from Equation 2 to 4, the following is true

$$\theta_R^{M_R} = \frac{M_R \bar{R}^2}{D_R} = \frac{\bar{R}^2}{D_R}\left[\frac{pR_D^2}{2\bar{R}}(R_D - R_A - e) + \frac{R_D M_D}{\bar{R}}\right]$$

$$\theta_R^{M_R} = \beta_R^{\ p}\, p + \beta_R^{\ M_D} M_D$$

Equations 1A and 2A are solved simultaneously to arrive at the unknowns, H_D and M_D.

$$M_D = \frac{p\left[-\beta_R^{\ p}\left(U_R^{\ H_D} + U_h^{\ H_D}\right) - \beta_h^{\ H_D}\left(U_h^{\ p} - U_R^{\ p}\right)\right]}{\left(\beta_h^{\ M_D} + \beta_R^{\ M_D}\right)\left(U_R^{\ H_D} + U_h^{\ H_D}\right) - U_h^{\ M_D}\beta_h^{\ H_D}}$$

$$H_D = \frac{p\left[\beta_R^{\ p} U_h^{\ M_D} + \left(U_h^{\ p} - U_R^{\ p}\right)\left(\beta_h^{\ M_D} + \beta_R^{\ M_D}\right)\right]}{\left(\beta_h^{\ M_D} + \beta_R^{\ M_D}\right)\left(U_R^{\ H_D} + U_h^{\ H_D}\right) - U_h^{\ M_D}\beta_h^{\ H_D}}$$

The preceding equations were used to solve for rotations and deflections at the ring-plate/shell juncture for the design shown in Figure 12, using elastic properties of the composite derived from both netting and orthotropic theory. The results obtained are summarized in Table 9.

It can be seen from Table 9 that the results of the calculations are almost independent of the theory used to establish the elastic properties of the composite material. Further, the radial deflection at the composite ring-to-membrane juncture was independent of the type of flange-bearing load (distributed or concentrated) and its position, but rotation was strongly influenced by the magnitude and point of load application. At the vessel design burst pressure of 3000 psi, the radial deflection was 0.040 in. (i.e., the "slip" between the free-floating boss flange and composite ring-plate is 0.040 in.). The rotation of the composite section at the junction ranges between 1.5 and 3° at 3000 psi depending on the location of the bearing load.

Since the results of the discontinuity analysis are independent of the theory used to establish the elastic properties of the filament-wound composite in the area of the boss-flange, it can be concluded that netting theory properties are sufficient for establishing vessel designs.

The calculations were performed using single values for tape width (ring-plate width equal to 1.57 times the winding tape width of 0.268 in., or 0.424 in.) and boss diameter ($D_b/D_c = 0.1$). In order to establish the effect of these potentially variable parameters on the dome, further calculations were required for several combinations of tape width and boss diameter. The Aerojet-modified version of the computer program described in Reference 3 was used to obtain the geometric parameters at the ring-plate/shell juncture for several wrap diameters defined by the wrap radius parameter, X01. Note that X01 is not the boss radius ($D_b/2$) when finite tape widths (W_L) are considered, but it can be defined by the relation

$$X01 = (D_b + 1.57W_L)/2$$

This relation establishes a theoretical plane of wrap which is a better approximation of that which is actually achieved in practice.

Calculations were performed (using the geometric parameters from computer output and elastic properties based on netting theory) to obtain the effect of tape width and boss diameter on the deflection of the dome at the discontinuity. Results of these calculations are presented in Figure 13 which shows radial deflection, at the design pressure of 3000 psi, as a function of tape width and normalized boss diameter.

V. POLAR BOSS DESIGN CONCEPTS

The various polar boss configurations for glass-filament-wound metal-lined vessels considered during the study are shown schematically in Figure 14. The schematics indicate regions of the liner estimated to be in the elastic or plastic ranges. Areas of possible debonding caused by deflection and rotation of the composite on top of the boss are indicated. Each of the schematics is discussed below.

A. CONTRACT NAS 3-10289 BOSS DESIGN - (1)

This is the conventional design employed previously on this contract for a 6061 aluminum liner. In the two tanks tested, there was some unbonding noted when the tank was sectioned, as indicated in the sketch. This is consistent with the analytical results. It would be desirable to design the flange to rotate, thus uniformly distributing the load and reducing the peeling action. Metal liner plastic-to-elastic condition occurs in the transition area.

B. CONTRACTS NAS 3-6287 and NAS 3-6297 BOSS DESIGN - (2)

This is the conventional design employed on previous contracts for thin stainless steel liners. Although it is believed (from analysis) that some unbonding might have occurred, this is not known for a fact. This configuration has been acceptable for use with glass filament composites in single-cycle burst tests.

C. CONTRACT NAS 3-6292 BOSS DESIGN - (3)

This is the configuration used in a thick Inconel liner which was glass-filament overwrapped. The boss performed satisfactorily, although the ultimate filament stress level obtained was only 90% of that originally expected and most failures appeared to originate in filaments at the boss area.

D. MATCHED ROTATION FLANGE BOSS - (4)

A flange taper is provided to permit equal rotation of the filament-wound composite and boss flange, and to uniformly distribute boss reaction load. Mismatch of radial deflections may cause debonding as shown. Plastic-to-elastic condition occurs in the transition area.

E. SLIDING LINER BOSS - (5)

This scheme would provide some excess liner material to make up for radial deflection of the filament-wound composite. A slip surface would be required and need to be provided. Debonding could be expected in area shown. The plastic-to-elastic condition would occur inboard of the filament-wound composite and liner separation. The liner might have trouble recovering upon release of pressure. Pressure might deform the liner around the metal boss supporting the liner at the point of filament-wound composite and liner separation.

F. TUBE BOSS - TYPE A - (6)

This scheme involves a small fill tube (say a 2% boss) connected to the liner, a small winding angle, and a wide tape width. The small boss results in small deflections and rotations, a small boss reaction load, and a thin-wall tube. In the configuration shown, the uniform thickness tube will take the internal pressure load below its yield stress. To keep from shearing out, the thickness of the tube under the edge of the filament-wound composite needs to be about as thick as the basic tube; it tapers down to the basic liner thickness rapidly. Because the tube behaves elasticity, debonding between the tube and filament-wound composite can be expected as indicated. Plastic-to-elastic action in the liner would occur where the liner thickens into the tube.

G. TUBE BOSS - TYPE B - (7)

This configuration is the same as (6) above, except that a portion of the tube is thinned down so plastic deformation of the tube will occur in the hoop direction, matching the radial expansion of the opening in the filament-wound composite dome. The thin portion of the tube would be enough to take longitudinal loads and would be overwrapped as dictated by design details with glass or lower modulus material to permit proper hoop expansion. The thickness of the tube under the edge of the filament-wound composite and as the tube exits from the outside surface of the filament-wound composite would need to provide adequate shear strength and hoop tension strength. Because of the two thickened ring sections in the tube, some debonding is expected as indicated.

H. TUBE BOSS - TYPE C - (8)

This is the larger tube configuration ($\sim$10% of vessel diameter) based on same idea as (7) above. It is large enough to permit support of the mandrel easily in the winding machine.

I. FILAMENT REINFORCED PLASTIC BOSS WITH TUBE - TYPES A & B - (9) and (10)

This is similar to (6) except that a filament reinforced plastic boss is provided between the small tube and the filament-wound composite. This boss provides something to grip for positioning the mandrel in the winding machine. It would have a lower modulus than a metal member and would thus be more flexible. It would not be flexible enough to deflect radially with the filament-wound composite and debonding is expected as shown. Also, because three materials would be interfacing filament-wound composite, liner, filament reinforced plastic, debond could occur where the three materials intersect, as shown.

J. FILAMENT REINFORCED PLASTIC BOSS WITH TUBE - C - (11)

In this configuration (similar to the concept employed on Contract NAS 3—2562 Reference 10), a more flexible filament reinforced plastic boss is provided in conjunction with a larger tube size. The filament reinforced plastic boss would have sufficient strength to take boss shear and longitudinal loads.

In the hoop direction, it is envisioned that a low modulus hoop wrap (e.g. Dacron) would be used to permit radial expansion of the filament reinforced plastic boss and the thin tube with the opening in the filament-wound composite dome. Debonding is possible as indicated. A higher modulus, high-strength hoop wrap (e.g., glass) would be used on the filament reinforced plastic boss before it exits from the hole in the filament-wound composite.

K. PLASTIC SPRING BOSS - 12

In this scheme, pressure in the vessel is used to expand the liner past yield "plastic" against the opening in the filament-wound composite dome. The liner is flexible up to the opening and in the opening. Hoop wrap can be provided as needed to control radial deflection as the liner thickens as it exits from the opening in the filament-wound composite. A slip surface is provided on the other boss member which takes out the boss reaction load. Another schematic of this configuration is shown in Figure 15. Enough flexibility is provided to accommodate filament-wound composite deflection. Pressure acts to form the liner and reduced bond stresses.

L. BELLOWS SPRING BOSS - TYPES A AND B - 13 and 14

These both have bellows springs to provide more flexibility of the boss. However, because of the surface of revolution of the spring, the spring is restrained by the hoop stresses induced during expansion, and a high degree of flexibility is not provided. Debonding would probably result as indicated.

After review of the advantages and disadvantages of each of the concepts, Configurations 4 and 12 were selected for detailed design.

VI. DETAILED BOSS DESIGNS

A. PLASTIC SPRING BOSS

The basic features of this boss design concept are shown in Figure 16.

1. Design Assumptions

a. The vessel pressure acts over the entire Al-1100 liner surface forcing the liner to strain with the filament-wound composite. (Pressure vent holes are provided in the boss body and no seal exists between the liner and flange except at the end of the opening in the liner.)

b. A short cylinder of high-strength aluminum is provided to minimize distortion at the Al-1100 weld area and also to act as a hinge at its free end allowing the Al-1100 to strain with the composite.

c. The boss flange has a zero net pressure across its thickness; the reaction load is due to pressure acting over the port area only.

d. The Al-1100 liner slips over the boss flange surface.

2. Filament-Wound Composite

In order to establish the strain and rotational requirements of the boss for this design, a discontinuity analysis was performed at the ring-plate/shell juncture of the filament-wound composite. The tape width was assumed to be 0.268 in. and the boss diameter 1.2 in. (the opening in the filament-wound composite). These values correspond to a ring-plate width of 0.424 in. Computer outputs were used to establish geometry, and netting theory was used to establish properties of the filament-wound composite.

Results of this analysis are summarized below:

$$M_D = p\left[.2869\,e - .1017\right]$$

$$H_D = p\left[-.3811\,e - .9335\right]$$

$$\delta_D = \left[10.58\,p + .989\,H_D\right] \times 10^{-6}$$

$$\theta_D = \left[2.268\,H_D + 56.39\,M_D\right] \times 10^{-6}$$

At the design pressure of 3000 psi, the preceding variables have the following values:

Loading	N_L (lb/in.)	V_A (lb/in.)	V_D (lb/in.)	M_D (in.-lb/in.)	H_D (lb/in.)	δ_D (in.)	θ_D (deg)
Distributed (e = .212)	32,100	1937	1536	-122.7	-3042	.0287	0.79
Concentrated (e = .424)	32,100	1536	1536	+59.7	-3285	.0285	0.23

a. Ring Stress Analysis

Based on these values, the ring may be shown as a free body and the corresponding stresses calculated. For the case of a uniformly distributed load, the free body is shown below.

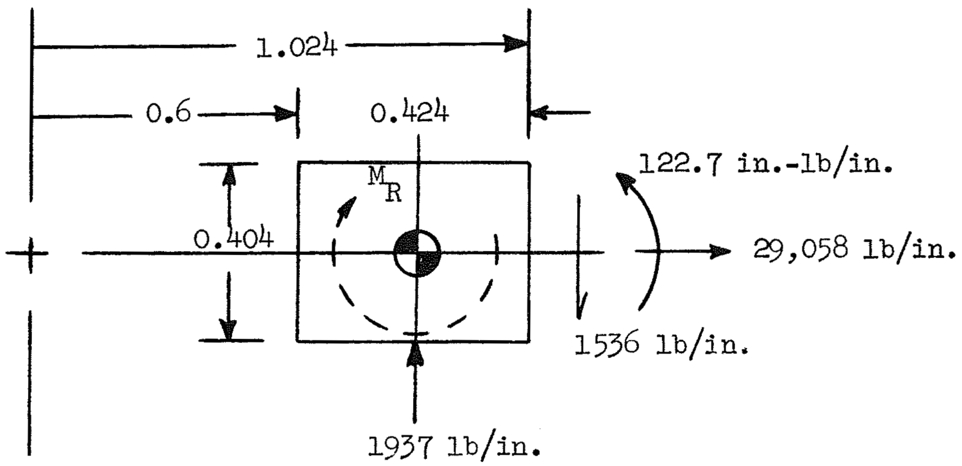

Resulting twisting moment

$$M_R = \frac{1}{0.812}\left[1.024(-122.7) + 1.024(.212)(1536) + .812(\cancel{6}\,0)\ 1937\right]$$

$$= 255.9 \text{ in.-lb/in.}$$

Maximum composite hoop stress (outside surface)

$$\sigma_{H_R} = \frac{H_T\ R_D}{t_R\ W_L} + \frac{M_R\ \bar{R}}{D_R}\left(\frac{B_{H_R}}{2}\right)$$

$$= \frac{29{,}058(1.024)}{.404(.424)} + \frac{255.9(.812)(2.118 \times 10^6)}{2(1.222 \times 10^4)}$$

$$\sigma_{H_R} = 173,700 + 18,000 = 191,700 \text{ psi}$$

Hoop filament stress

$$\sigma_f = \frac{\sigma_{H_R}}{P_{vg}} = \frac{191,700}{.67} = 286,000 \text{ psi}$$

Meridian composite stress (outside surface)

$$\sigma_{L_R} = \frac{H_T}{t_R} + \frac{6M_D}{t_R^{\ 2}}$$

$$= \frac{29,058}{.404} + \frac{6(122.7)}{(.404)^2}$$

$$\sigma_{L_R} = 71,900 + 4500 = 76,400 \text{ psi}$$

Filament stress (outside surface)

$$\sigma_f = \frac{\sigma_{L_R}}{P_{vg} \cos^2 \alpha_D} = \frac{76,400}{.67(.60738)^2}$$

$$\sigma_f = 309,100 \text{ psi}$$

All stresses are less than the allowable ultimate strength of the S-glass/epoxy composite for this particular design.

b. Ring Deflection at R_A

The deformation of the liner at the bend radius, R_A, (transition from plate to cylinder) is required for later calculations of composite/liner strain compatibility. Because the elastic properties of the ring vary across its width due to filaments oriented at various angles, assumptions must be made in order to define the expected deflection at R_A.*

---

*Refer to Figure 12 for definition of geometric and load parameters.

It is assumed that the radial deflection at R_A is caused by the total load, $H_T = N_L \cos \phi + H_D$, acting at radius, R_D, and may be expressed by the relation

$$\delta_A = \frac{H_T R_A}{B_{H_R}} \left(\frac{2 R_D^2}{R_D^2 - R_A^2} \right)$$

The deflection is now only a function of the effective extensional stiffness, B_{H_R}, of the ring.

(1) Assume $\alpha_R = \alpha_B = 52.6^\circ$

The extensional stiffness is

$$B_{H_R} = \left(B_{H_R} \right)_D = 5.243 \times 10^6 (.404) = 2.118 \times 10^6 \text{ lb/in.}$$

and, the deflection is

$$\delta_A = \frac{29{,}058(.6)(2)(1.024)^2}{2.118 \times 10^6 \left[(1.024)^2 - (.6)^2 \right]} = 0.025 \text{ in.}$$

The hoop strain is

$$\epsilon_{H_A} = \frac{\delta_A}{R_A} = \frac{0.025}{.6} = 0.042 \text{ in./in.}$$

(2) Assume $\alpha_R = 90^\circ$ (ring is all hoop wraps)

The extensional stiffness is

$$B_{H_R} = 8.308 \times 10^6 (.404) = 3.356 \times 10^6 \text{ lb/in.}$$

and, the deflection is

$$\delta_A = \frac{.025(2.118)}{3.356} = 0.016 \text{ in.}$$

The hoop strain is

$$\epsilon_{H_A} = \frac{0.016}{.6} = 0.027 \text{ in./in.}$$

(3) Assume $\epsilon_{H_D} = \epsilon_{H_A} = 0.028$ in./in.

The deflection at R_A is

$$\delta_A = \epsilon_{H_A} R_A = 0.028(.6) = 0.017 \text{ in.}$$

and, the resulting effective extensional stiffness is

$$B_{H_R} = \frac{.025(2.118 \times 10^6)}{.017} = 3.115 \times 10^6 \text{ lb/in.}$$

The effective modulus of the ring is

$$E_{H_R} = \frac{3.115 \times 10^6}{0.404} = 7.71 \times 10^6 \text{ psi}$$

Since assumption (3) provides an effective modulus midway between the actual values at R_A and R_D, the values of strain and deflection which correspond to this modulus will be used.

3. Boss Material Properties

a. 1100-0 Aluminum

Ultimate tensile strength, $F_{tu} = 13{,}000$ psi
Tensile yield strength, $F_{ty} = 5000$ psi
Ultimate tensile strain, $\epsilon_{tu} = 0.20$ in./in.
Elastic Poisson ratio, $\nu_E = 0.3$
Plastic Poisson ratio, $\nu_E = 0.5$
Elastic modulus, $E = 10 \times 10^6$ psi

Determination of the uniaxial plastic modulus was based on the following equation

$$E_p = \frac{F_{tu} - F_{ty}}{\epsilon_p}$$

where the parameters are defined in the stress/strain diagram below.

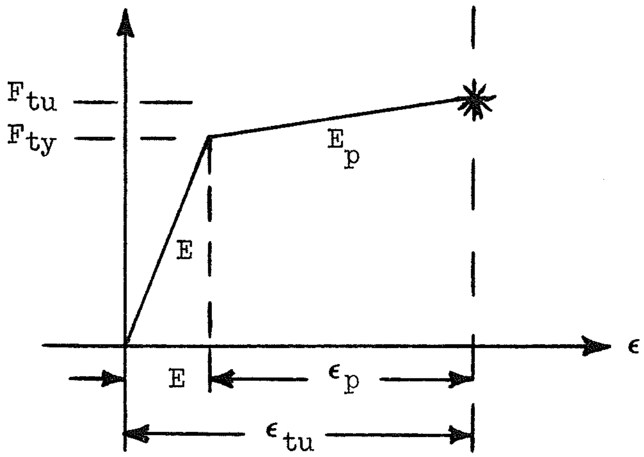

From the diagram

$$\epsilon_p = \epsilon_{tu} - \epsilon_E = \epsilon_{tu} - \frac{F_{ty}}{E}$$

and the plastic modulus is

$$E_p = \frac{F_{tu} - F_{ty}}{\epsilon_{tu} - \frac{F_{ty}}{E}}$$

For the 1100 material

$$E_p = \frac{(13,000 - 5000)}{0.20 - \frac{5000}{10 \times 10^6}} = 40,100 \text{ psi}$$

If the material is subjected to a 1:1 biaxial stress field, the strain equation in the plastic region can be written

$$\epsilon = \frac{F_{ty}\,(1 - \nu_E)}{E} + \frac{(\sigma - F_{ty})(1 - \nu_p)}{E_p}$$

$$\epsilon = \frac{5000\,(1 - .3)}{10 \times 10^6} + \frac{(\sigma - 5000)(1 - .5)}{4.01 \times 10^4}$$

$$\epsilon = 1.247 \times 10^{-5}\,\sigma - 0.062$$

It is interesting to note, that by this method at the ultimate strength of the material ($\sigma = F_{tu}$) the biaxial strain equals one half the ultimate uniaxial strain.

b. 2219-T87 Aluminum

Ultimate tensile strength, F_{tu} = 70,000 psi

Tensile yield strength, F_{ty} = 53,000 psi

Ultimate tensile strain, ϵ_{tu} = 0.10 in./in.

Elastic modulus, $E = 10 \times 10^6$ psi

Weld joint efficiency = 57%

The plastic modulus is determined, as above, from the equation

$$E_p = \frac{(70{,}000 - 53{,}000)}{0.10 - \dfrac{53{,}000}{10 \times 10^6}} = 179{,}500 \text{ psi}$$

The strain equation in the plastic region due to a uniaxial stress field ($\sigma_L = 0.0$) is

$$\epsilon_H = \frac{F_{ty}}{E} + \frac{(\sigma_H - F_{ty})}{E_p}$$

$$\epsilon_H = \frac{53{,}000}{10 \times 10^6} + \frac{(\sigma_H - 53{,}000)}{1.795 \times 10^5}$$

$$\epsilon_H = 0.557 \times 10^{-5}\sigma_H - 0.290$$

4. Flange Design

Require that the flange of the boss must have the same rotation as the composite ring portion of the head. Thus, the reaction load may be assumed to be distributed uniformly over the flange bearing area and Case 21 of ref. 7 applies.

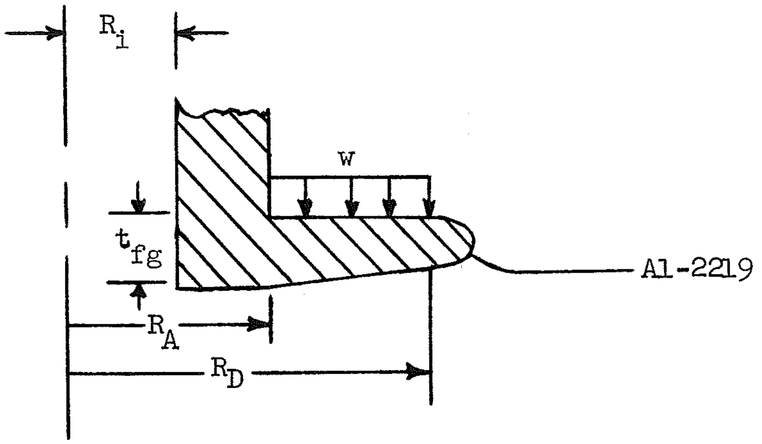

$$t_{fg}^{\ 3} = \frac{\lambda_{21}\ w\ R_D^{\ 3}}{E\theta_R}, \qquad \lambda_{21} = f\left(\frac{R_D}{R_A}\right)$$

$$\theta_R = 4.60 \times 10^{-6}\ p = 4.60 \times 10^{-6}\ (3000)$$

$$\theta_R = 0.0138 \text{ rad}$$

$$w = \frac{p\ R_A^{\ 2}}{R_D^{\ 2} - R_A^{\ 2}} = \frac{3000\ (.6)^2}{(1.024)^2 - (.6)^2}$$

$$w = 1568 \text{ psi}$$

$$\lambda_{21} = .0694 + .1579\left(\frac{.207}{.5}\right) = 0.1348 \text{ (ref. 7, p. 241)}$$

$$t_{fg}^{3} = \frac{0.1348\ (1568)(1.024)^3}{10 \times 10^6\ (.0138)} = 0.00164 \text{ in.}^3$$

$$t_{fg} = 0.118 \text{ in.}$$

Check bending stress

$$\sigma_B = \frac{\beta_{21}\ w\ R_D^{\ 2}}{t_{fg}^{\ 2}}$$

$$\beta_{21} = 0.410 + 0.64 \left(\frac{.207}{.5}\right) = 0.675$$

$$\sigma_B = \frac{0.675\ (1568)(1.024)^2}{(0.118)^2} = 79{,}700 \text{ psi}$$

$$\text{M.S.} = \frac{F_{ty}}{\sigma_B} - 1 = \frac{53{,}000}{79{,}700} - 1 = \underline{\underline{\text{NEG}}}$$

Therefore, a concentrated load must be used. Use Case 22 of ref. 7, with the requirement of matched rotations for design only.

$$t_{fg}^{\ 3} = \frac{\lambda_{22}\ W\ R_D}{E\theta_R}$$

$$W = p\ \pi\ R_A^{\ 2}$$

$$W = 3000\ \pi\ (.6)^2 = 3400 \text{ lb}$$

$$\lambda_{22} = .1052 + .1338 \left(\frac{.207}{.5}\right) = 0.2074$$

$$\theta_R = 1.35 \times 10^{-6}\ p = 1.35 \times 10^{-6}\ (3000)$$

$$= 0.00405 \text{ rad}$$

$$t_{fg}^{\ 3} = \frac{.2074\ (3400)(1.024)}{10 \times 10^6\ (.00405)} = 0.01783$$

$$t_{fg} = \underline{\underline{0.261}} \text{ in.}$$

Check bending stress

$$\sigma_B = \frac{\beta_{22}\ W}{t_{fg}^{\ 2}}$$

$$\beta_{22} = .428 + .325 \left(\frac{.207}{.5}\right) = 0.563$$

$$\sigma_B = \frac{0.563\ (3400)}{(.261)^2} = 28{,}100 \text{ psi}$$

The margin of safety is

$$\text{M.S.} = \frac{53{,}000}{28{,}100} - 1 = \underline{\underline{+0.89}}$$

5. Hinge Design

A model of the proposed hinge is shown in the following schematic

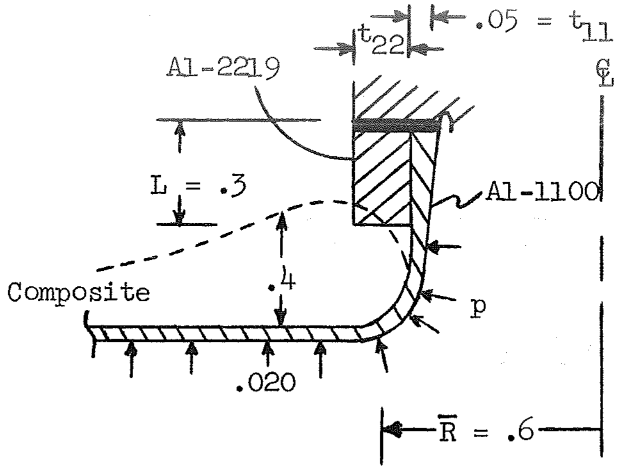

The effect of varying the thickness of the hinge, t_{22}, on the resulting stresses was determined by a detailed analysis and results are contained in the appendix. Assuming a weld occurs at the fixed point of the hinge, the allowable tensile yield strength of the 2219 aluminum alloy is

$$(F_{ty})_{weld} = 0.57(53{,}000) = 30{,}000 \text{ psi}$$

Inspection of the table of results in the appendix indicates that a hinge thickness of 0.15 in. should be adequate for this application.

a. Stress Analysis

Since the hinge (Al-2219) and the liner (Al-1100) bend together with the application of pressure, the total thickness of the combined materials must be used in stress calculations.

$$t = t_{11} + t_{22} = 0.15 + 0.05 = 0.20 \text{ in.}$$

Assuming the Al-1100 is in the plastic range and the Al-2219 is elastic at the design pressure of 3000 psi, the flexural rigidity of the equivalent hinge is

$$D = \Sigma EI \sim \left(\frac{Et^3}{12\,(1 - \nu^2)} \right)_{2219}$$

$$D = \frac{10 \times 10^6\ (.15)^3}{12\ (.91)} = 3091 \text{ lb-in.}^2\text{/in.}$$

The stiffness is

$$k = \frac{\Sigma Et}{R^2} \sim \frac{(Et)_{2219}}{R^2}$$

and the beam characteristic is

$$\lambda^4 = \frac{k}{4D} = \left[\frac{3\,(1 - \nu^2)}{R^2\, t^2}\right]_{2219}$$

$$\lambda^4 = \frac{3(.91)}{\left[.6(.15)\right]^2} = 337 \text{ in.}^{-1}$$

The neutral axis of the hinge referenced to the inside surface of the 1100 liner is

$$\bar{y} \sim \bar{y}_{22} = 0.125 \text{ in.}$$

The basis for all of the above approximations is that the ratio of the modulii of elasticity of 2219 (elastic) and 1100 (plastic) is

$$\frac{E_{22}}{E_{11}} = \frac{4 \times 10^4}{10 \times 10^6} \doteq 0.004$$

(1) Al-2219, Meridional Bending Stress

$$\sigma_{L_B} = \frac{M\,(\bar{y} - t_{11})\,E_{22}}{D}$$

$$\sigma_{L_B} = \frac{77.3\,(.125 - .05)(10 \times 10^6)}{3091}$$

$$\sigma_{L_B} = 18{,}800 \text{ psi}$$

The margin of safety is

$$M.S. = \frac{30,000}{18,800} - 1 = \underline{\underline{+0.60}}$$

(2) Al-1100, Maximum Meridional Stress

Using the results of Section V-A-2-b, which defines the strain at $R_A = 0.6$ to be the same as the strain at $R_D = 1.024$

$$\epsilon_{H_A} = \epsilon_{H_D}$$

and the results in Section V-A-3-a, which defines 1100 liner strain, under a 1:1 biaxial stress field, to be

$$\epsilon = 1.247 \times 10^{-5} \sigma - 0.062$$

the stress in the 1100 at R_A becomes

$$\sigma_{L_A} = \sigma_{H_A} = \frac{\left(\epsilon_{H_D} + 0.062\right) \times 10^5}{1.247}$$

For, $\epsilon_{H_D} = 0.028$ in./in.

$$\sigma_{L_A} = \frac{(.028 + .062) \times 10^5}{1.247} = 7220 \text{ psi}$$

Assuming that the load in the liner is transferred around the corner at R_A, then load equilibrium requires that the direct (membrane) stress in the 1100 at the weld be proportional to the stress at r_A.

$$N_{L_{11}} = N_{L_A} = \sigma_{L_A} t_A$$

and

$$\sigma_{L_{11}} = \frac{\sigma_{L_A} t_A}{t_{11}} = \frac{7220(.02)}{.05} = 2890 \text{ psi}$$

The maximum bending strain in the Al-1100 at the weld is

$$\epsilon_L = \frac{M_y}{D}$$

$$\epsilon_L = \frac{77.3(.125)}{3091} = 313 \times 10^{-5} \text{ in./in.}$$

and the corresponding stress at this strain level is

$$\sigma_L = \frac{(313 + 6200)}{1.247} = 5220 \text{ psi}$$

The maximum combined meridional stress is

$$\sigma_{L_{max}} = 5220 + 2890 = 8110 \text{ psi}$$

The margin of safety is

$$\text{M.S.} = \frac{13{,}000}{8110} - 1 = \underline{\underline{+0.60}}$$

b. Deflections and Rotations

The equations developed in the appendix are used to check the deflections and rotations of the hinge.

(1) Fixed End (Weld)

$$\delta = \frac{3000(.6)^2}{10 \times 10^6(.15)} - \frac{1.606(635)}{2(3091)(78.62)} + \frac{2.020(77.3)}{2(3091)(18.35)} = 0$$

$$\theta = \frac{2.020(635)}{2(3091)(18.35)} - \frac{1.935(77.3)}{4.284(3091)} = 0$$

(2) Free End

$$\delta = \frac{3000(.6)^2}{10 \times 10^6(.15)} + \frac{\overbrace{0.752}^{C_3'}(635)}{2(3091)(78.62)} - \frac{\overbrace{1.749}^{C_5'}(77.3)}{2(3091)(18.35)}$$

$$\delta = \left[0.720 + 0.982 - 1.192\right] \times 10^{-3} = 0.510 \times 10^{-3} \text{ in.}$$

$$\theta = \frac{\overbrace{1.749}^{C_4'}(635)}{2(3091)(18.35)} - \frac{\overbrace{1.303}^{C_6'}(77.3)}{4.284(3091)}$$

$$\theta = \left[9.790 - 7.606\right] \times 10^{-3} = 2.184 \times 10^{-3} \text{ rad}$$

$$\theta = 0.12 \text{ degrees}$$

6. Friction at Liner to Boss Flange Surface

During vessel pressurization, the Al-1100 liner must slide on the order of 0.017 to 0.025 in. at the burst point of 3000 psig. The sliding should be a linear function of pressure, as should the friction force between the two surfaces. The normal force, N_{fr}, between the liner and flange is due to the pressure acting over the port area only. The friction force, F_{fr}, may be expressed as

$$F_{fr} = \mu N_{fr}$$

$$N_{fr} = p \pi R_A^2$$

The maximum value of the normal force is

$$N_{MAX} = (3000 \text{ psi})(\pi)(0.066 \text{ in.})^2 = 3380 \text{ lb}$$

The load carrying capability of the 0.010-in.-thick liner, L, at the R_D diameter is

$$L = (\sigma)(t)(\pi)(2R_D) = (5000\ \text{psi})(0.010)(\pi)(2)(1.024\ \text{in.})$$

$$= 3220\ \text{lb}$$

The coefficient of friction, μ, aluminum-to-aluminum is greater than 1.00, while μ between Teflon and aluminum is about 0.04.

If a Teflon coating is applied to one of the aluminum surfaces, the friction force will be reduced from a value of over 3380 lb at 3000 psi to

$$F_{fr} = \mu N_f = (0.04)(3380) = 130\ \text{lb}$$

B. MATCHED ROTATION FLANGE BOSS

Basic features of this boss design concept are shown in Figure 17.

1. Design Assumptions (see Figure 18)

a. The Al-1100 metal shell gradually increases in thickness from 0.010 in. to 0.050 in. at the weld radius (R_w).

b. An Al-2219-T87 boss flange of thickness, t_{fg}, is joined to the metal shell by means of a weld at R_w.

c. The Al-1100 metal shell plastically deforms with the filament-reinforced composite, but the more rigid Al-2219 resists deformation, causing a mismatch of rotations between the composite ring and the metal flange for all radii less than R_w.

d. The total boss load is concentrated on the reaction circle defined by the weld radius, R_w.

2. Composite Ring Rotation

In order to calculate the rotation of the composite ring, the load model (see Figure 18) must conform to the model established in Section IV.

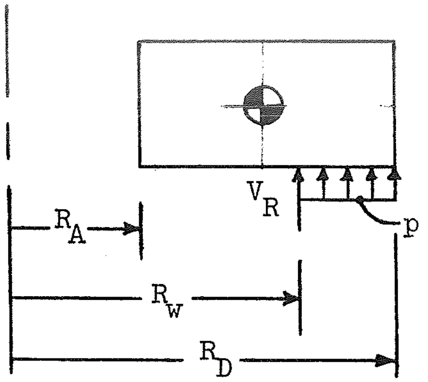

No. 1, Actual Applied Loads

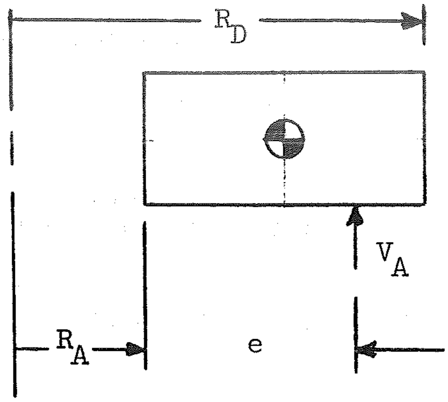

No. 2, Equivalent Load Model

The equivalent load model is found by replacing the concentrated load (V_R) and pressure load (p) with a single concentrated load (V_A) at a distance (e) from the inside of the ring; the distance (e) establishes an equivalent moment system

$$\Sigma M_1 = \Sigma M_2$$

$$V_R R_W (R_W - R_A) + V_p \left(\frac{R_W + R_D}{2} - R_A\right)\left(\frac{R_W + R_D}{2}\right) = V_A\, e\, (R_A + e)$$

where

$$V_A = \frac{p\, R_D^2}{2(R_A + e)}$$

$$V_R = \frac{p\, \pi\, R_W^2}{2\, \pi\, R_W} = \frac{p\, R_W}{2}$$

$$V_p = \frac{p\, \pi\, (R_D^2 - R_W^2)}{2\, \pi \left(\frac{R_D + R_W}{2}\right)} = p\, (R_D - R_W)$$

and, by substitution, the distance, e, is found to be

$$e = \frac{1}{R_D^2}\left[R_W^2 (R_W - R_A) + (R_D^2 - R_W^2)\left(\frac{R_W + R_D}{2} - R_A\right)\right]$$

With

$$R_D = 1.024 \text{ in.}, \quad R_A = 0.6 \text{ in.} \quad \text{and} \quad R_W = 0.995 \text{ in.}$$

$$e = \frac{1}{(1.024)^2} \left\{ (.995)^2(.395) + \left[(1.024)^2 - (.995)^2\right] \left[\frac{2.019}{2} - .6\right] \right\}$$

$$e = 0.396 \text{ in.}$$

From Section V-A-2, the ring moment and shear at the burst pressure are

$$H_D = -3000 \left[.3811(.396) + .9355\right] = -3259 \text{ lb/in.}$$

$$M_D = 3000 \left[.2869(.396) - .1017\right] = +35.73 \ \frac{\text{in.-lb}}{\text{in.}}$$

and the ring rotation is

$$\theta_R = \left[2.268(-3259) + 56.39(35.73)\right] \times 10^{-6} = 0.00538 \text{ radians}$$

3. Bending Stress at Root of Flange

The thickness of the flange required to match the rotation of the composite ring at R_W is calculated in accordance with formulas described on page 242 of ref. 7 (Case 22).

$$t_{fg} = \left[\frac{\lambda_{22} \, W \, R_W}{E\theta_R}\right]^{1/3}$$

where

$$W = p \, \pi \, R_W^{\,2} = 3000 \, \pi \, (.995)^2 = 9331 \text{ lb}$$

and by interpolation

$$\frac{R_W}{R_A} = 1.658$$

$$\lambda_{22} = 0.1052 + (.239 - .1052)\,\frac{.158}{.5} = 0.1475$$

The flange thickness is

$$t_{fg} = \left[\frac{0.1475(9331)(.995)}{10 \times 10^6(.00538)}\right]^{1/3} = 0.294 \text{ in.}$$

and the maximum bending stress is calculated from the formula

$$\sigma_B = \frac{\beta_{22}\,W}{t_{fg}^{\,2}}$$

With

$$\beta_{22} = 0.428 + (.753 - .428)\,\frac{.158}{.5} = 0.531$$

the bending stress is

$$\sigma_B = \frac{0.531(9331)}{(.294)^2} = 57{,}300 \text{ psi}$$

and the margin of safety is

$$\text{M.S.} = \frac{70{,}000}{57{,}300} - 1 = \underline{\underline{+0.22}}$$

4. Strain Analysis

It is assumed that a bond does not exist between the composite ring plate and the Al-2219 portion of the boss flange at the burst pressure; the Al-2219 flange does not restrict the strain of the composite ring plate. It is further assumed that a bond does exist between the Al-1100 metal shell and the composite shell up to some point located near the weld. These assumptions imply strain compatibility and load equilibrium between the Al-1100 and the composite shell, and load transfer only from the Al-1100 through the weld into the Al-2219. The resulting calculated values for strain in the Al-1100 will be the maximum expected values.

The equation for the tangential strain of the ring-plate is

$$\epsilon_t = \frac{\sigma_t}{E_t} - \nu_{rt} \frac{\sigma_r}{E_r}$$

and, the radial strain is

$$\epsilon_r = \frac{\sigma_r}{E_r} - \nu_{tr} \frac{\sigma_t}{E_t}$$

Neglecting the low bending moment, the applied tangential and radial stresses are, respectively,

$$\sigma_t = \frac{H_T R_D^2 (R^2 + R_A^2)}{R^2 t (R_D^2 - R_A^2)}$$

$$\sigma_r = \frac{H_T R_D^2 (R^2 - R_A^2)}{R^2 t (R_D^2 - R_A^2)}$$

a. Ring-Plate/Shell Junction $R = R_D$

$H_T = 2.9 \times 10^4$ lb/in.

$t = 0.404 + 0.050 = 0.454$ in.

The applied tangential stress is

$$\sigma_{t_D} = \frac{2.9 \times 10^4 \left[(1.024)^2 + (.6)^2\right]}{0.454 \left[(1.024)^2 - (.6)^2\right]}$$

$\sigma_{t_D} = 130{,}700$ psi

and the radial stress is

$$\sigma_{r_D} = \frac{2.9 \times 10^4}{0.454} = 63{,}900 \text{ psi}$$

Based on a wrap angle of 52.6°, the orthotropic properties of the filament composite are

$$E_t = 0.45\ (8.47 \times 10^6) = 3.81 \times 10^6 \text{ psi}$$

$$E_r = 0.32\ (8.47 \times 10^6) = 2.71 \times 10^6 \text{ psi}$$

$$\nu_{rt} = 0.4$$

$$\nu_{tr} = 0.6$$

Assuming the Al-1100 is in the plastic range, the properties are

$$E = 0.04 \times 10^6 \text{ psi}$$

$$\nu = 0.5$$

The corresponding properties of the total composite are

$$E_t = \frac{[3.81(.404) + .04(.05)] \times 10^6}{0.454}$$

$$= 3.39 \times 10^6 \text{ psi}$$

$$E_r = \frac{[2.71(.404) + .04(.05)] \times 10^6}{0.454}$$

$$= 2.42 \times 10^6 \text{ psi}$$

$$\nu_{rt} = \frac{3.81(.404)(.4) + .04(.05)(.5)}{3.81(.404) + .04(.05)}$$

$$= 0.4$$

$$\nu_{tr} = \frac{2.71(.404)(.6) + .04(.05)(.5)}{2.71(.404) + .04(.05)}$$

$$= 0.6$$

The tangential strain is

$$\epsilon_{t_D} = \frac{13.07 \times 10^{-2}}{3.39} - \frac{.4(6.39 \times 10^{-2})}{2.42}$$

$$\epsilon_{t_D} = 0.0280 \text{ in./in.}$$

and the radial strain is

$$\epsilon_{r_D} = \frac{6.39 \times 10^{-2}}{2.42} - \frac{.6(13.07 \times 10^{-2})}{3.39}$$

$$\epsilon_{r_D} = 0.00327 \text{ in./in.}$$

It should be noted that both these values fall within the plastic portion of the stress/strain curve for Al-1100, but neither value is greater than the ultimate strain capability (ϵ_{tu} = 0.2 in./in.) of the material.

b. Al-2219/Al-1100 Junction $R = R_W$

The applied tangential stress is

$$\sigma_{t_W} = \frac{2.9 \times 10^4 (1.024)^2 \left[(.995)^2 + (.6)^2\right]}{.454(.995)^2 \left[(1.024)^2 - (.6)^2\right]}$$

$$\sigma_{t_W} = 132{,}700 \text{ psi}$$

and the radial stress is

$$\sigma_{r_W} = \frac{2.9 \times 10^4 (1.024)^2 \left[(.995)^2 - (.6)^2\right]}{.454(.995)^2 \left[(1.024)^2 - (.6)^2\right]}$$

$$\sigma_{r_w} = 61{,}900 \text{ psi}$$

With a wrap angle of 54.8°, the filament composite properties are

$$E_t = 0.48(8.47 \times 10^6) = 4.07 \times 10^6 \text{ psi}$$

$$E_r = 0.31(8.47 \times 10^6) = 2.63 \times 10^6 \text{ psi}$$

$$\nu_{rt} = 0.38$$

$$\nu_{tr} = 0.6$$

The properties of the total composite are

$$E_t = \frac{[4.07(.404) + .04(0.5)] \times 10^6}{0.454} = 3.63 \times 10^6 \text{ psi}$$

$$E_r = \frac{[2.63(.404) + .04(.05)] \times 10^6}{0.454} = 2.34 \times 10^6 \text{ psi}$$

$$\nu_{rt} = \frac{4.07(.404)(.38) + .04(.05)(.5)}{4.07(.404) + .04(.05)} = 0.38$$

$$\nu_{tr} = \frac{2.63(.404)(.6) + .04(.05)(.5)}{2.63(.404) + .04(.05)} = 0.6$$

The tangential strain is

$$\epsilon_{t_w} = \frac{13.27 \times 10^{-2}}{3.63} - \frac{.38(6.19 \times 10^{-2})}{2.34}$$

$$\epsilon_{t_w} = 0.0265 \text{ in./in.}$$

and the radial strain is

$$\epsilon_{r_w} = \frac{6.19 \times 10^{-2}}{2.34} - \frac{0.6(13.27 \times 10^{-2})}{3.63}$$

$$\epsilon_{r_w} = 0.00452 \text{ in./in.}$$

In order to determine the strain of the Al-2219 flange, the load transmitted through the weld must be determined. This load is dependent on the resultant stresses in the Al-1100; the stresses can be determined from the strain equation in Section VI-A-3 modified to account for an unequal biaxial stress field. The resulting equations are

$$\epsilon_t = -\ 0.062 + 2.49 \times 10^{-5}\ (\sigma_t - .5\,\sigma_r)$$

$$\epsilon_r = -\ 0.062 + 2.49 \times 10^{-5}\ (\sigma_r - .5\,\sigma_t)$$

Substituting the calculated values for strain into the equations and solving the equations simultaneously results in the following stresses

$$\sigma_t = 6512 \text{ psi}$$

$$\sigma_r = 5921 \text{ psi}$$

Since the Al-2219 is the same thickness as the Al-1100 at the weld, these are also the values for applied stress in the Al-2219. The resulting strains are

$$\epsilon_{t_w} = \frac{6512 - .3(5921)}{10 \times 10^6}$$

$$\epsilon_{t_w} = 0.00047 \text{ in./in.}$$

and

$$\epsilon_{r_w} = \frac{5921 - .3(6512)}{10 \times 10^6}$$

$$\epsilon_{r_w} = 0.00040 \text{ in./in.}$$

Comparison of these strain levels with those calculated for the Al-1100 leads to the conclusion that, in the area of the weld, the Al-2219 flange is rigidly restrained as the Al-1100 deforms plastically.

c. Ring-Plate Inside Diameter $(R = R_A)$

Although the composite ring-plate does not influence the strain of the Al-2219 flange, based on the initial assumptions, it is of interest to know the expected value of strain at the inner surface of the ring-plate.

For a wrap angle of 90°, the orthotropic properties of the filament composite are

$$E_t = 8.47 \times 10^6 \text{ psi}$$

$$E_r = .34(8.47 \times 10^6) = 2.88 \times 10^6 \text{ psi}$$

$$\nu_{rt} = 0.08$$

$$\nu_{tr} = 0.25$$

The radial stress (σ_r) is zero and the tangential stress is

$$\sigma_{t_A} = \frac{2.9 \times 10^4 (1.024)^2 (2)}{0.404 \left[(1.024)^2 - (.6)^2\right]}$$

$$\sigma_{t_A} = 218{,}600 \text{ psi}$$

The tangential strain is

$$\epsilon_{t_A} = \frac{21.86 \times 10^{-2}}{8.47} = 0.0258 \text{ in./in.}$$

and the radial strain is

$$\epsilon_{r_A} = -\frac{0.25\ (21.86 \times 10^{-2})}{8.47}$$

$$\epsilon_{r_A} = -\ 0.00645 \text{ in./in.}$$

The relatively large tangential strain of the composite ring-plate compared to the low strains associated with Al-2219 flange indicates the shear distortion required of the bond material. This shear distortion coupled with the peal action induced by the mismatch in rotation of the flange and the ring-plate at $R = R_A$, tends to justify the assumed non-existence of the bond at the burst pressure.

VII. COMPLETE VESSEL DESIGNS

A. ALUMINUM LINER WITH PLASTIC SPRING BOSS

The boss design developed in Section VI was incorporated into the vessel membrane design of Section III, to result in the vessel liner design shown in Figure 19.

B. ALUMINUM LINER WITH MATCHED ROTATION FLANGE BOSS

Figure 20 shows the liner design resulting from incorporation of the boss design of Section V into the vessel membrane design of Section III.

C. COMPLETE VESSEL

Figure 21 presents the complete design configuration for the aluminum-lined glass-filament-wound vessel, incorporating either the plastic spring boss or the matched rotation flange boss.

VIII. SUMMARY OF RESULTS

A method was developed for analysis and detailed investigation of the dome ends of metal-lined glass-filament-wound vessels in the vicinity of an axially located polar boss. It represents an extension and supplement to the methods generally used for membrane analysis of filament-wound composite pressure-vessel shells (domes and cylinder), and for discontinuity analysis of the dome-to-cylinder juncture.

The analytical method was developed for and applied to a specific pressure-vessel design configuration: a 12-in.-dia by 18-in.-long closed-end, cylindrical, glass-filament-wound vessel lined with 0.010-in.-thick aluminum, with aluminum polar bosses with diameters equal to 10% of the vessel diameter located axially on each dome end, designed for a burst pressure of 3000 psi at 75°F. First, criteria for the pressure-vessel design were reviewed and available glass-filament strengths established for the longitudinal and circumferential windings. A membrane analysis was then conducted for the cylindrical section and the vessel domes from the dome-to-cylinder juncture up the head to the vicinity of the axial polar boss using a previously developed computer program. A head-to-cylinder discontinuity analysis was then performed to determine forces and moments at the juncture and maximum stresses. The maximum stress due to the discontinuity was only 0.8% higher than the membrane stress. Following this, the vessel filament winding pattern was determined.

Then the metal-lined glass-filament-wound vessel domes were characterized when subjected to internal pressure and boss reaction loads with emphasis on the axial polar boss regions. The meridional wrap angle as a function of normalized radial distances is shown graphically; most of the vessel head had wrap angles less than 20°. Normalized hoop radius of curvature and normalized filament-wound composite thickness are presented graphically as a function of wrap angle. Elastic properties, deflections, rotations, and strains were determined by orthotropic analysis and netting analysis.

It was from orthotropic analysis that the glass-filament-wound dome had an increasing strain up the dome; at the point where the metal liner-to-boss transition would be located, the strain was 11% greater than at the equator. The maximum meridional strain occurred on top of where the boss would be located and was 50% greater than at the equator.

Netting analysis resulted in essentially constant meridional strain up the dome.

Although radial deflection could be computed easily, the deflection in an orthogonal direction was needed to locate the deflected point in space; the equations governing this orthogonal deflection required extensive numerical solution. Instead, empirical data on dome deflections were reviewed. It was determined that, for glass filament-wound vessels, two zones of approximately linear load vs deflection exist due to the departure from orthotropic properties with increasing strain; above the transition load (approximately 25% of ultimate) where crazing initiates, the deformation behaves as predicted by netting analysis. Above the crazing threshold, deflections of points on the domes were essentially normal to the unpressurized surface. Based on this, it was determined that the netting analysis should be used for glass-filament-wound vessels for establishing strains, stresses, and deflections.

In the area of the dome immediately adjacent to the boss, the composite thickness increases rapidly, and discontinuity forces and moments exist here due to changes in section properties and curvature, necessitating a discontinuity analysis of the section. The discontinuity analysis analyzed the filament-wound composite buildup at the boss as a ring-plate and accounted for the flange bearing loads (distributed or concentrated) of a free-floating boss. Ring loads, deflections, and rotations were determined. The results were almost independent of the theory used to establish elastic properties. Radial deflection at the composite ring-plate-to-membrane juncture was independent of the type of flange bearing load (distributed or concentrated) and its position, but rotation was strongly influenced by the magnitude and point of load application. For example, at the vessel design burst pressure, the radial deflection was 0.040 in. (i.e., the "slip" between the free-floating boss flange and composite ring-plate is 0.040 in.); the rotation of the composite section at the junction ranged from 1.5 and 3^{o} depending on location of the bearing load. Since results of the discontinuity analysis were independent of theory used to establish elastic properties, it was concluded that netting theory properties are sufficient for establishing vessel designs.

Axial polar-boss design concepts for metal-lined glass-filament-wound vessels are reviewed. Detailed structural analysis and designs for two selected metal polar bosses are then presented: (1) a boss with matched rotation flange butt welded to the aluminum liner membrane, and (2) a plastic spring boss in which the thin liner extends into the opening in the filament-wound composite at the axial port and another boss member is provided to take out the boss reaction load. These designs were incorporated into the membrane analysis pressure-vessel designs were established during initial portions of the work. These configurations have been selected for evaluation by means of fabricating and testing pressure vessels.

TABLE 1. DESIGN CRITERIA

12-in.-dia by 18-in.-long Aluminum-Lined Glass-Filament-Wound Pressure Vessels

Geometry and Pressure

Diameter, in.	12.000
Length, in.	18.000
Polar Boss Diameter, in.	1.200
Metal Liner Thickness, in.	0.010
Design Burst Pressure at 75°F, psig	3000
at -320°F, psig	3750
at -423°F, psig	3750

Material Properties

	Aluminum 1100-0	Glass-Filament-Wound Composite
Density, lb/in.^{3}	0.102	0.072
Coefficient of thermal expansion, in./in. - °F at +75 to -423°F	8.910×10^{-6}	2.010×10^{-6}
Tensile-yield strength, psi	8,000	-
Derivative of yield strength with respect to temperature, psi/°F	-7.9	-
Proportional limit, psi	5,000	-
Derivative of proportional limit with respect to temperature, psi/°F	-7.9	-
Elastic modulus, psi	10.25×10^6	12.4×10^6
Derivative of elastic modulus with respect to temperature, psi/°F	-1382	-2410
Plastic modulus, psi	116,500	-
Derivative of plastic modulus with respect to temperature, psi/°F	-516	-
Poisson's ratio	0.325	-
Derivative of Poisson's ratio with respect to temperature, 1/°F	0.201×10^{-4}	-
Volume fraction of filament in composite	-	0.673
Longitudinal filament, design-allowable stress, psi at +75°F	-	316,000
at -320°F	-	395,000
at -423°F	-	395,000

TABLE 2. FILAMENT-WOUND SHELL PARAMETERS

From Computer Run, t_{h_o} = .04183 in.					Modulus Based on Orthotropic Theory			
z (Fig. 5)	α, degree	R_2	R_2/a (Fig. 6)	t_h/t_{h_o} (Fig. 7)	E_{LL}/E_F (Fig. 8)	$\frac{E_{LL}}{E_{LL_o}}$	$\frac{E_{LL}t_h}{(E_{LL}t_h)_o}$ (Fig. 9)	$\epsilon_{LL}/\epsilon_{LL_o}$ (Fig. 10)
1.000	3.82	6.000	1.000	1.000	0.992	1.000	1.000	1.000
0.903	6.03	6.626	1.104	1.110	0.990	0.998	1.108	0.996
0.803	7.21	7.434	1.239	1.253	0.975	0.983	1.232	1.006
0.703	8.39	8.456	1.409	1.435	0.967	0.975	1.399	1.007
0.598	9.89	9.883	1.647	1.694	0.960	0.968	1.640	1.004
0.506	11.64	11.582	1.930	2.012	0.930	0.938	1.887	1.023
0.389	15.10	14.843	2.474	2.660	0.877	0.884	2.351	1.052
0.312	18.84	18.100	3.017	3.381	0.800	0.806	2.725	1.107
0.213	28.00	24.608	4.101	5.293	0.623	0.628	3.324	1.234
0.187	32.42	26.873	4.479	6.328	0.533	0.537	3.398	1.318
0.171	35.89	28.203	4.701	7.213	0.476	0.480	3.462	1.358
0.152	41.12	29.419	4.903	8.705	0.398	0.401	3.491	1.404
0.130	50.13	29.205	4.868	10.21	0.323	0.326	3.33	1.460
0.122	54.76	27.977	4.663	10.06	0.310	0.313	3.15	1.478
0.100	90.00	27.087	4.515	8.65	0.340	0.343	2.97	1.520

Spherical from computer

Measured

TABLE 3. LINER THICKNESS

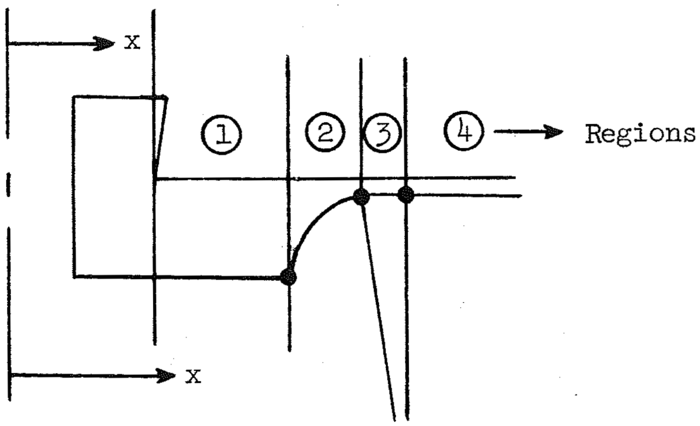

SCHEMATIC OF METAL BOSS

α, Degree	z	x = za, in.	t_M, in.	t_M/t_{M_o}	Region
3.8 to 21.5	1.0 to 0.276	6.0 to 1.655	0.010	1.000	4 to 3
23.25	0.254	1.524	0.013	1.300	3
25.21	0.235	1.410	0.020	2.000	3
26.5	0.225	1.347	0.025	2.500	3 to 2
28.00	0.213	1.278	0.038	3.800	2
32.42	0.187	1.122	0.132	13.200	2
35.89	0.171	1.026	0.302	30.200	2
37.0 to 90.0	0.169	1.015	0.392	39.200	2 to 1

TABLE 4. FILAMENT-WOUND SHELL WITH ELASTIC ALUMINUM LINER

(Modulus Based on Orthotropic Theory)

α, degree	$\left(E_{LL} t_h / E_{LL_o} t_{h_o}\right)$	$\left(E_{LM} t_M / E_{LM} t_{M_o}\right)$	$\left(E_{LC} t_{hC} / E_{LC_o} t_{hC_o}\right)$	R_2/a	$\left(\epsilon_L / \epsilon_{L_o}\right)_C$
3.82	1.000	1.00	1.000	1.000	1.000
6.03	1.108		1.088	1.104	1.015
7.21	1.232		1.189	1.239	1.042
8.39	1.399		1.325	1.409	1.063
9.89	1.640		1.521	1.647	1.083
11.64	1.887		1.722	1.930	1.121
15.10	2.351		2.100	2.474	1.178
18.84	2.725		2.404	3.017	1.255
21.5	2.96	1.00	2.595	3.38	1.303
23.25	3.09	1.3	2.757	3.587	1.301
25.21	3.20	2.0	2.977	3.812	1.280
26.5	3.26	2.5	3.119	3.98	1.276
28.0	3.324	3.8	3.413	4.101	1.202
32.42	3.398	13.2	5.221	4.479	0.858
35.89	3.462	30.2	8.435	4.701	0.557
37.0	3.47	39.2	10.116	4.74	0.469
41.12	3.491	39.2	10.133	4.903	0.484
50.13	3.33	39.2	10.002	4.868	0.487

TABLE 5. FILAMENT-WOUND SHELL

WITH PLASTIC ALUMINUM LINER

(Modulus Based on Orthotropic Theory)

α, degree	$\left(E_{LC} t_{hC} / E_{LC_o} t_{h_o}\right)$	$\left(\epsilon_L / \epsilon_{L_o}\right)_C$
3.82	1.000	1.000
6.03	1.108	0.996
7.21	1.232	1.006
8.39	1.398	1.008
9.89	1.639	1.005
11.64	1.885	1.024
15.10	2.348	1.054
18.84	2.722	1.108
21.5	2.956	1.143
23.25	3.086	1.162
25.21	3.198	1.192
26.5	3.258	1.222
28.0	3.325	1.233
32.42	3.418	1.310
35.89	3.515	1.337
37.0	3.541	1.339
41.12	3.562	1.376
50.13	3.402	1.431
90.00	3.042	1.484

TABLE 6. FILAMENT-WOUND SHELL

(Modulus Based on Netting Theory)

α, degree	cos α	$E_{LL}/P_{vg}E_f = \cos^2 \alpha$	$\frac{E_{LL}}{E_{LL_o}}$	$\frac{E_{LL}t_h}{E_{LL_o}t_{h_o}}$	$\epsilon_L/\epsilon_{L_o}$
3.82	0.99778	0.996	1.000	1.000	1.000
6.03	0.99447	0.989	0.993	1.102	1.002
7.21	0.99209	0.984	0.988	1.238	1.001
8.39	0.98930	0.979	0.983	1.411	0.999
9.89	0.98514	0.971	0.974	1.650	0.998
11.64	0.97944	0.959	0.963	1.938	0.996
15.10	0.96547	0.932	0.936	2.490	0.994
18.84	0.94642	0.896	0.899	3.040	0.992
21.5	0.93042	0.866	0.869	3.406	0.992
23.25	0.91879	0.844	0.848	3.621	0.991
25.21	0.90475	0.819	0.822	3.863	0.987
26.5	0.89493	0.801	0.804	3.996	0.996
28.0	0.88295	0.780	0.783	4.144	0.990
32.42	0.84414	0.713	0.715	4.525	0.990
35.89	0.81014	0.656	0.659	4.753	0.989
37.00	0.79864	0.638	0.640	4.800	0.988
41.12	0.75333	0.568	0.570	4.962	0.988

TABLE 7. FILAMENT-WOUND SHELL
WITH ELASTIC ALUMINUM LINER

(Modulus Based on Netting Theory)

α, degree	$E_{LC}t_{hC} / E_{LC_o}t_{hC_o}$	$\left(\epsilon_L / \epsilon_{L_o}\right)_C$
3.82	1.000	1.000
6.03	1.083	1.019
7.21	1.194	1.038
8.39	1.335	1.055
9.89	1.529	1.077
11.64	1.764	1.094
15.10	2.213	1.118
18.84	2.661	1.134
21.5	2.958	1.143
23.25	3.189	1.125
25.21	3.516	1.084
26.5	3.718	1.070
28.0	4.080	1.005
32.42	6.139	0.730
35.89	9.486	0.496
37.0	11.198	0.423
41.12	11.330	0.433
50.13	10.724	0.454

TABLE 8. RADIAL DEFLECTION DATA FOR FILAMENT-WOUND SHELL

Pt. No.	Computer Output					Orthotropic Analysis				Netting	
	R, in.	α, degree	R_2, in.	R_1, in.	t_h, in.	ν_L *	E_{LL}/E_F *	E_{HL}/E_F *	δ/p*** x 10^{-6}	E_{HL}/E_F	δ/p*** x 10^{-6}
1	6.000	3.82	6.000	3.031	0.052	0.260	0.992	0.339	-8.46	0.004	+208.
31	5.420	6.03	6.626	3.356	0.058	0.275	0.990	0.338	-7.48	0.011	+88.1
42	4.815	7.21	7.434	3.771	0.065	0.282	0.975	0.336	-6.73	0.016	+60.0
49	4.216	8.39	8.456	4.299	0.075	0.300	0.967	0.334	-6.05	0.021	+44.9
54	3.586	9.89	9.883	5.042	0.088	0.310	0.960	0.332	-4.91	0.030	+32.3
59	3.038	11.64	11.582	5.941	0.105	0.332	0.930	0.330	-4.14	0.041	+24.6
64	2.331	15.10	14.843	7.726	0.138	0.385	0.877	0.327	-2.98	0.068	+17.5
68	1.871	18.84	18.100	9.633	0.176	0.450	0.800	0.320	-2.14	0.104	+13.5
73	1.281	28.00	24.608	14.352	0.275	0.570	0.623	0.310	+0.03	0.220	+8.94
74	1.121	32.42	26.873	16.854	0.329	0.598	0.533	0.310	+1.03	0.287	+7.80
75	1.024	35.89	28.203	19.123	0.375	0.598	0.476	0.312	+1.98	0.344	+7.07
76	0.913	41.12	29.419	23.781	0.453	0.575	0.398	0.335	+2.97	0.432	+6.30
**77	0.782	50.13	29.205	51.399	0.531	0.457	0.323	0.412	+5.33	0.589	+6.29
**78	0.735	54.76	27.977	27.977	0.523	0.390	0.310	0.485	+1.90	0.667	+3.55
**79	0.600	90.00	27.087	27.087	0.450	0.085	0.340	1.000	+1.63	1.000	+2.17

* Ref. 8.

** Invalid due to computer "blow up".

*** in./psi

TABLE 9. CALCULATED PARAMETERS AT RING-PLATE/SHELL JUNCTURE OF VESSEL SHOWN IN FIGURE 2

(RING PLATE WIDTH = .424 in.)

Orthotropic Theory

Location e, in.	of Load, V_A	M_D/p*	H_D/p*	N_L/p $\frac{lb}{in.}/psi$	$\delta/px10^{-6}$ in./psi	$\theta/px10^{-6}$ rad./psi
0	Load acts at root of flange	-.0955	-6.593	+14.1	+12.2	-16.0
.212	Distributed Load, Resultant acts at C.G of Ring	-.0130	-6.638		+12.1	-12.5
.246	$M_D = 0$	0	-6.645		+12.1	-11.9
.424	Load acts at discontinuity	+.0694	-6.682	+14.1	+12.1	- 9.1

Netting Theory

Location e	of Load, V_A	M_D/p*	H_D/p*	N_L/p $\frac{lb}{in.}/psi$	$\delta/px10^{-6}$ in./psi	$\theta/px10^{-6}$ rad./psi
0	Load acts at root of flange	-.1150	-6.720	+14.1	+14.4	-16.0
.212	Distributed load	-.0281	-6.781		+14.3	-12.6
.246	For comparison only (see ortho)	-.0141	-6.790		+14.3	-12.0
.424	Load acts at discontinuity	+.0588	-6.841		+14.2	- 9.2
.280	$M_D = 0$	0	-6.800	+14.1	+14.3	-11.5

* M_D/p and H_D/p are each in units of $\frac{in.-lb}{in.}/psi$ and $\frac{lb}{in.}/psi$ respectively.

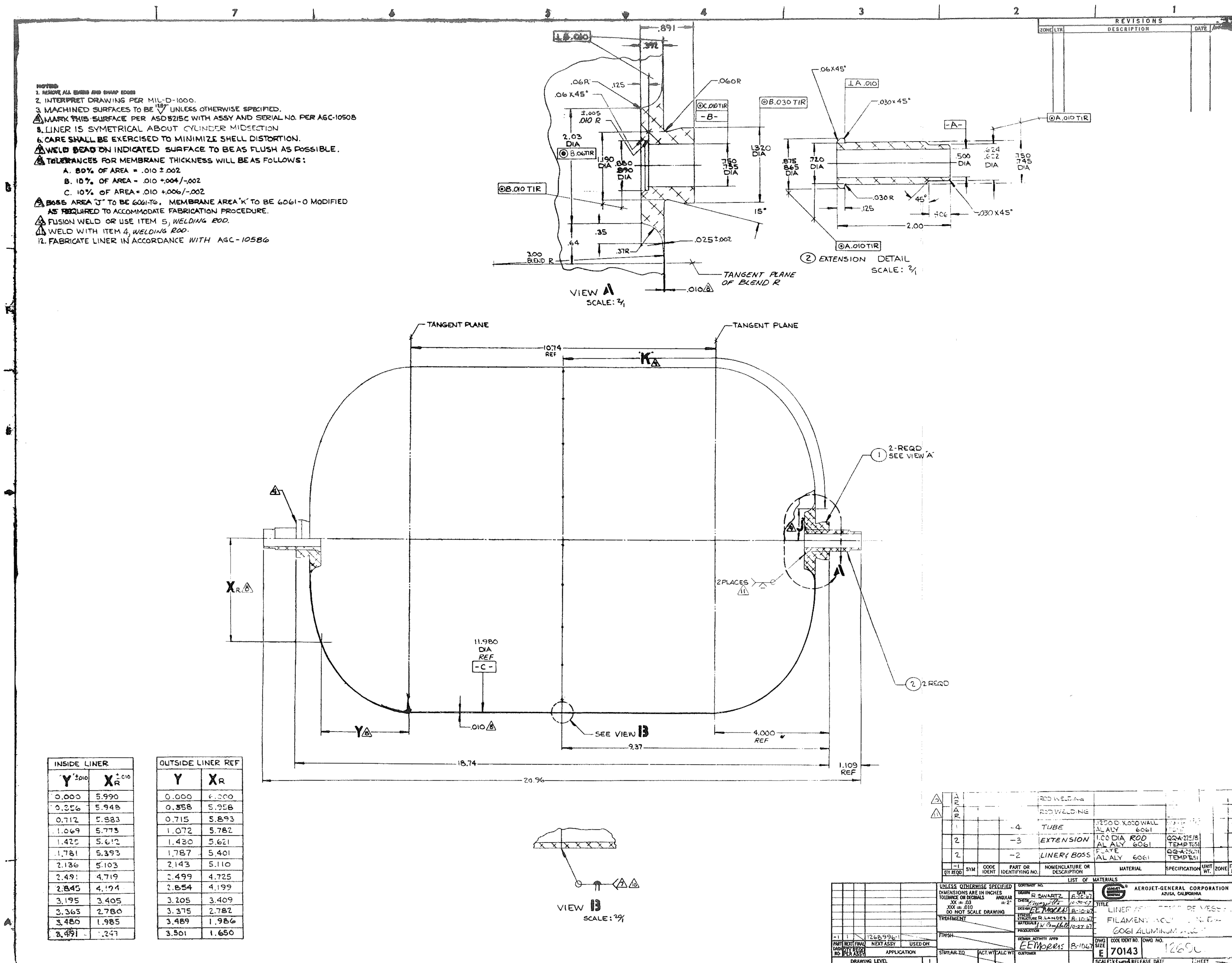

INSIDE LINER	
$Y^{\pm.010}$	$X_R^{\pm.010}$
0.000	5.990
0.356	5.948
0.712	5.883
1.069	5.773
1.425	5.612
1.781	5.393
2.136	5.103
2.491	4.719
2.845	4.194
3.195	3.405
3.363	2.780
3.480	1.985
3.491	1.247

OUTSIDE LINER REF	
Y	X_R
0.000	6.000
0.358	5.958
0.715	5.893
1.072	5.782
1.430	5.621
1.787	5.401
2.143	5.110
2.499	4.725
2.854	4.199
3.205	3.409
3.375	2.782
3.489	1.986
3.501	1.650

Figure 1. 12-in.-dia by 18-in.-long Aluminum Liner

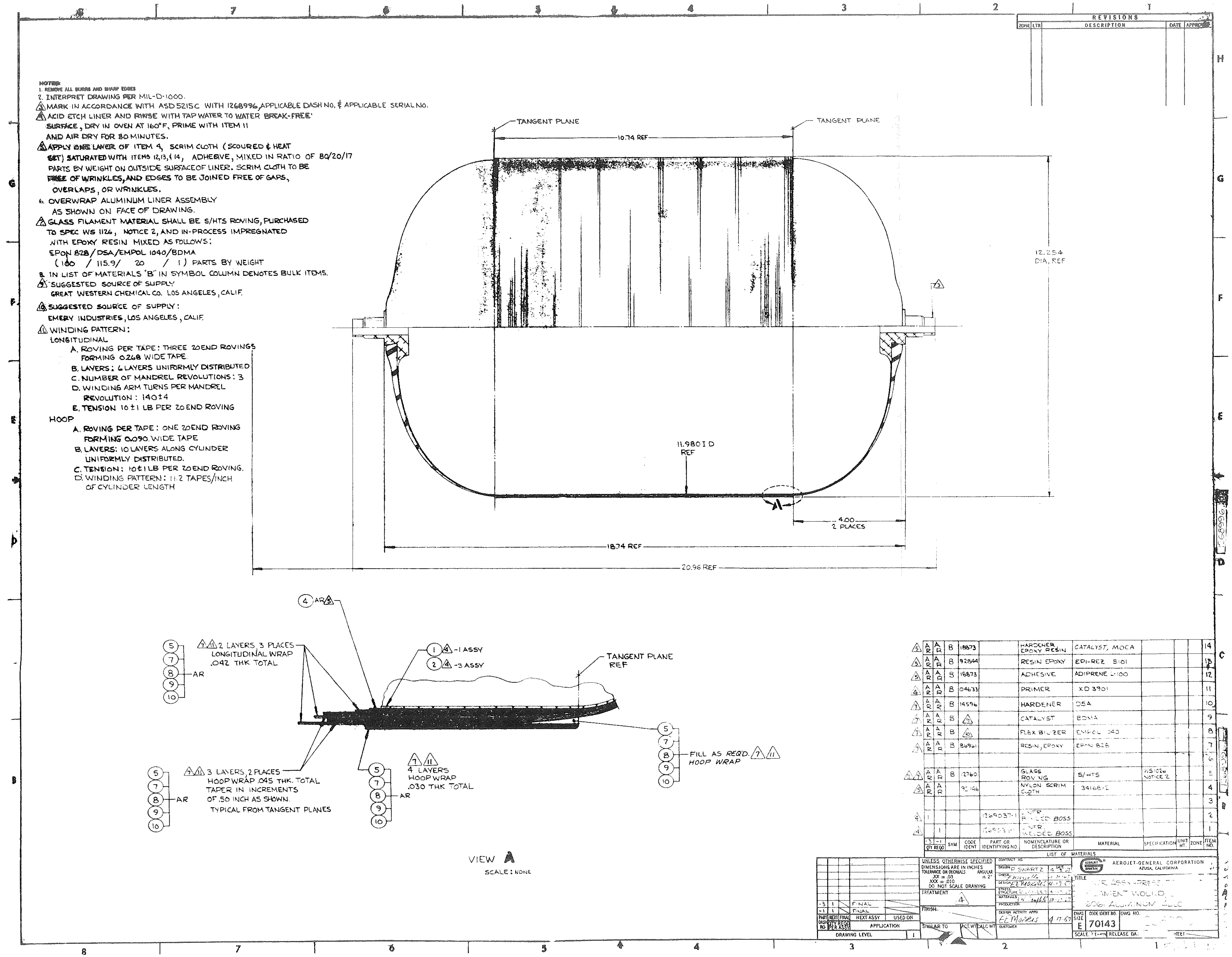

Figure 2. 12-in.-dia by 18-in.-long Aluminum-Lined Glass-Filament-Wound Vessel

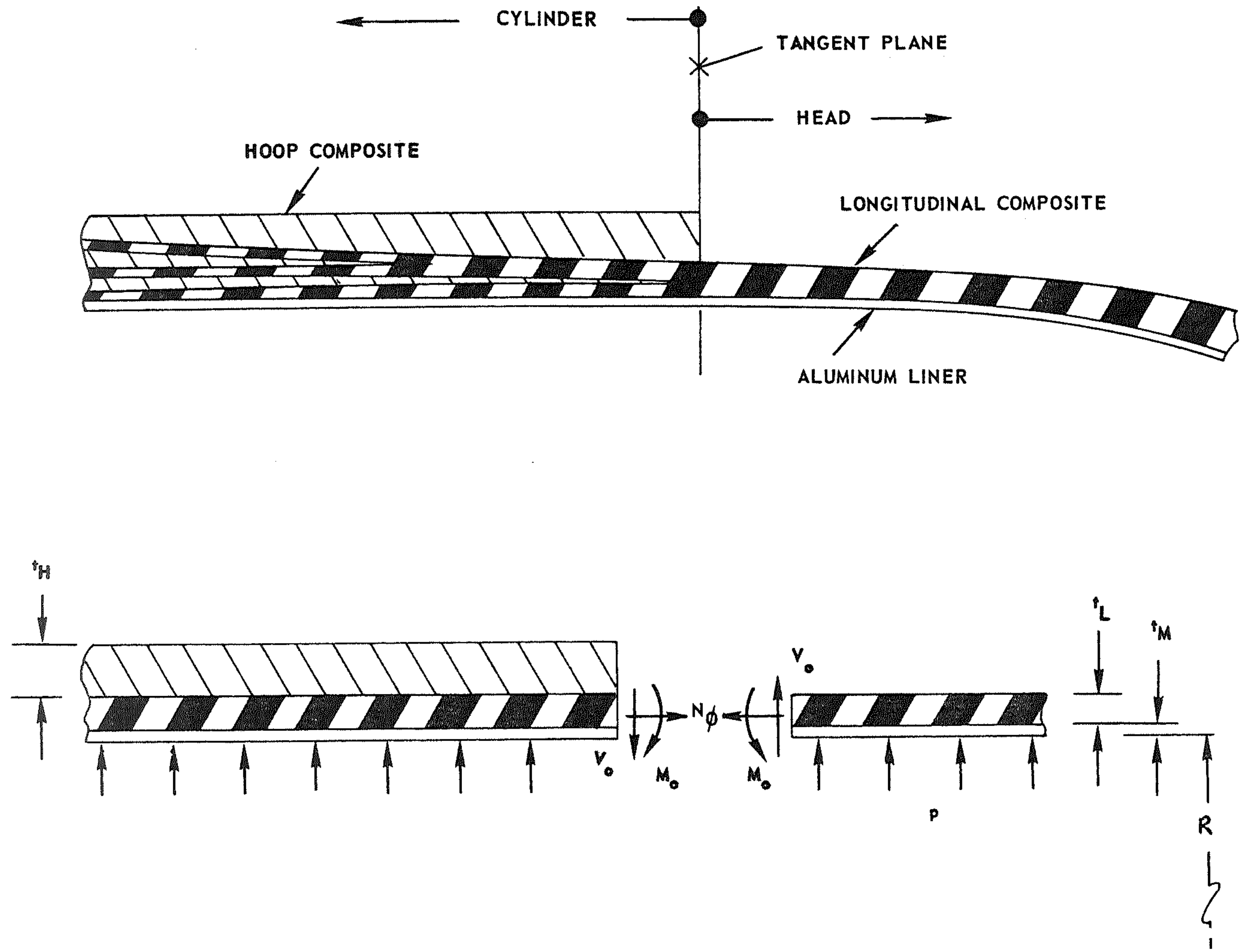

Figure 3. Beam System for Analysis

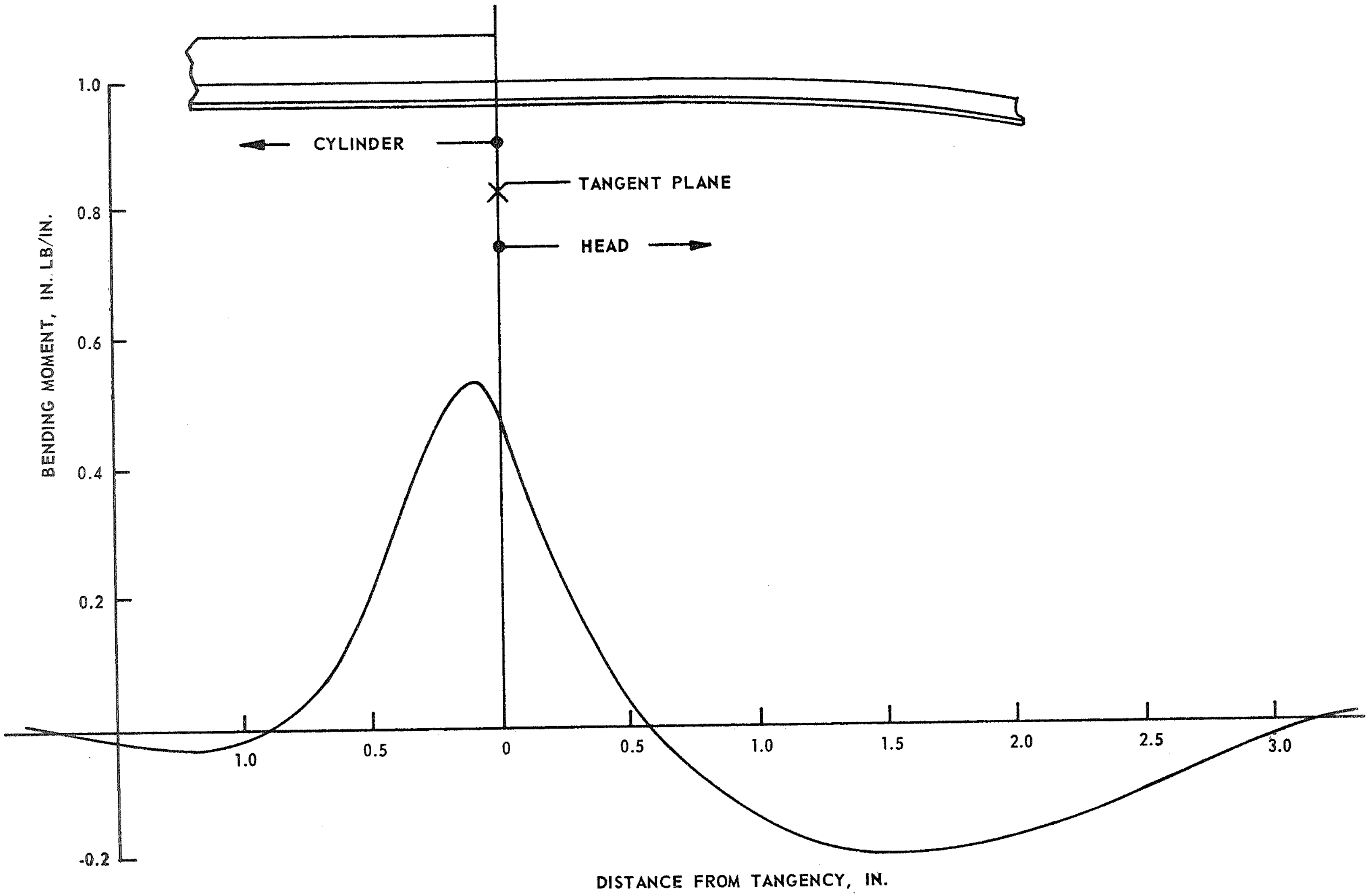

Figure 4. Bending Moment Distribution at Head-to-Cylinder Juncture

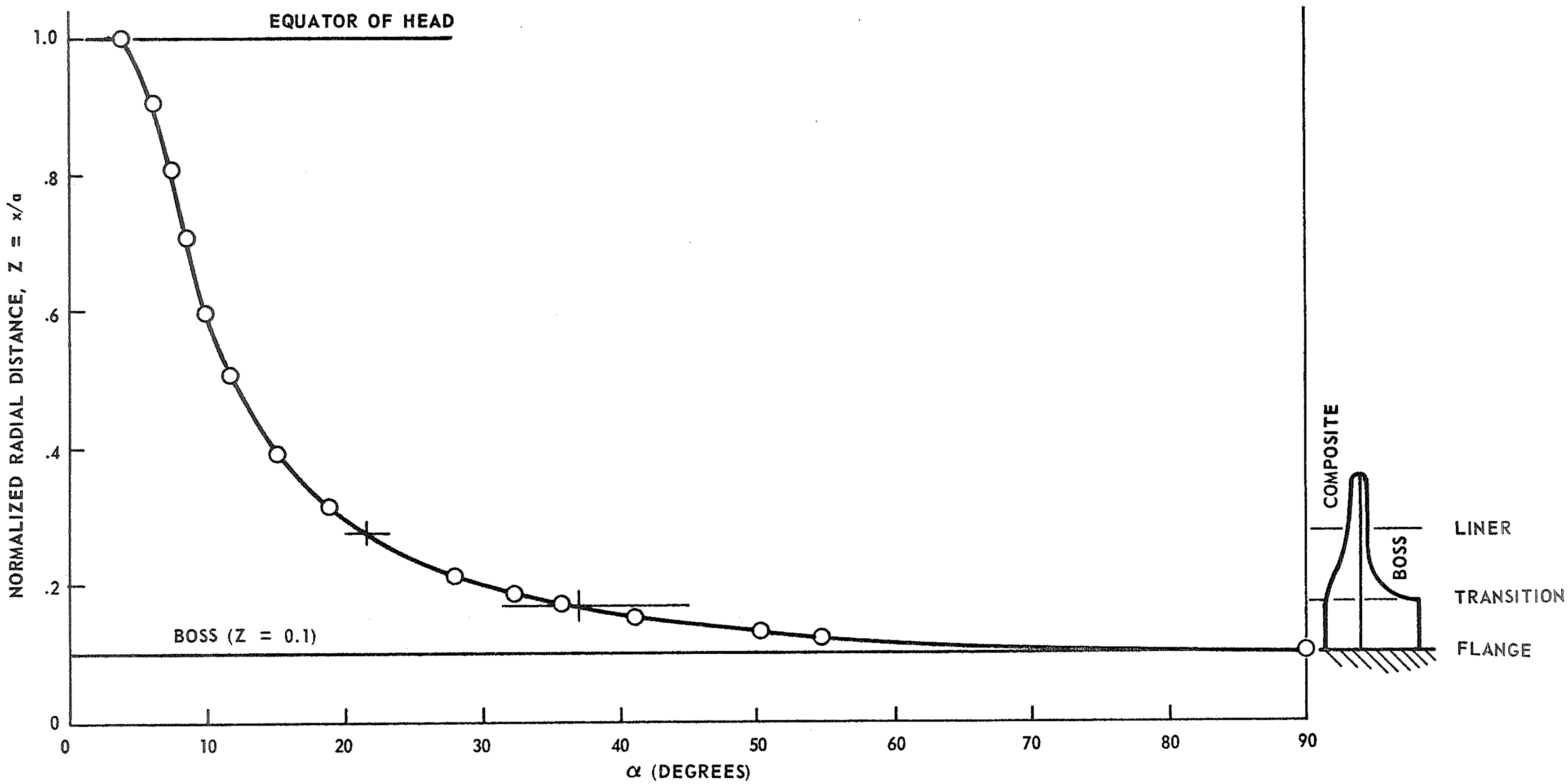

Figure 5. Longitudinal Filament Wrap Angle vs Radial Position

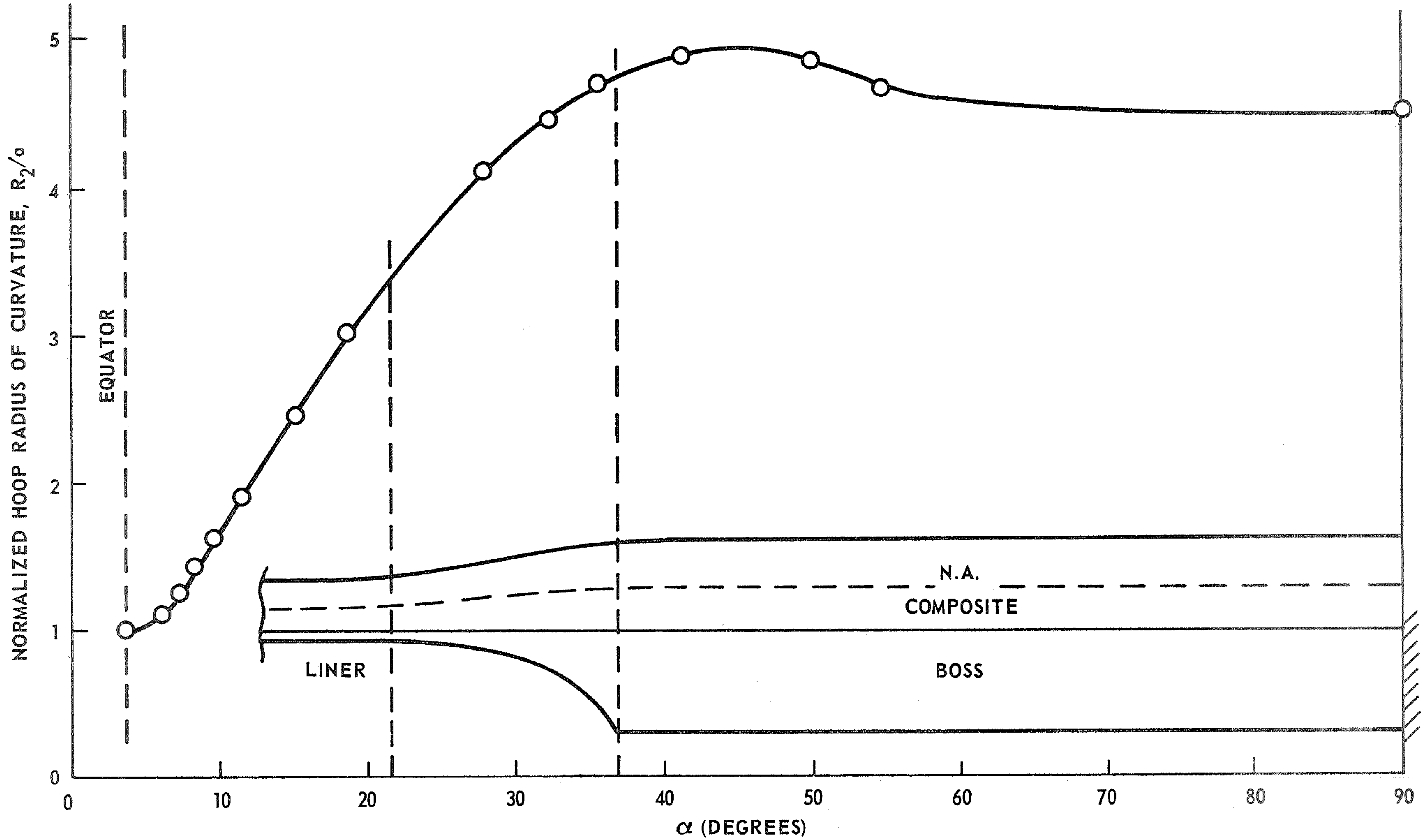

Figure 6. Normalized Hoop Radius of Curvature vs Wrap Angle

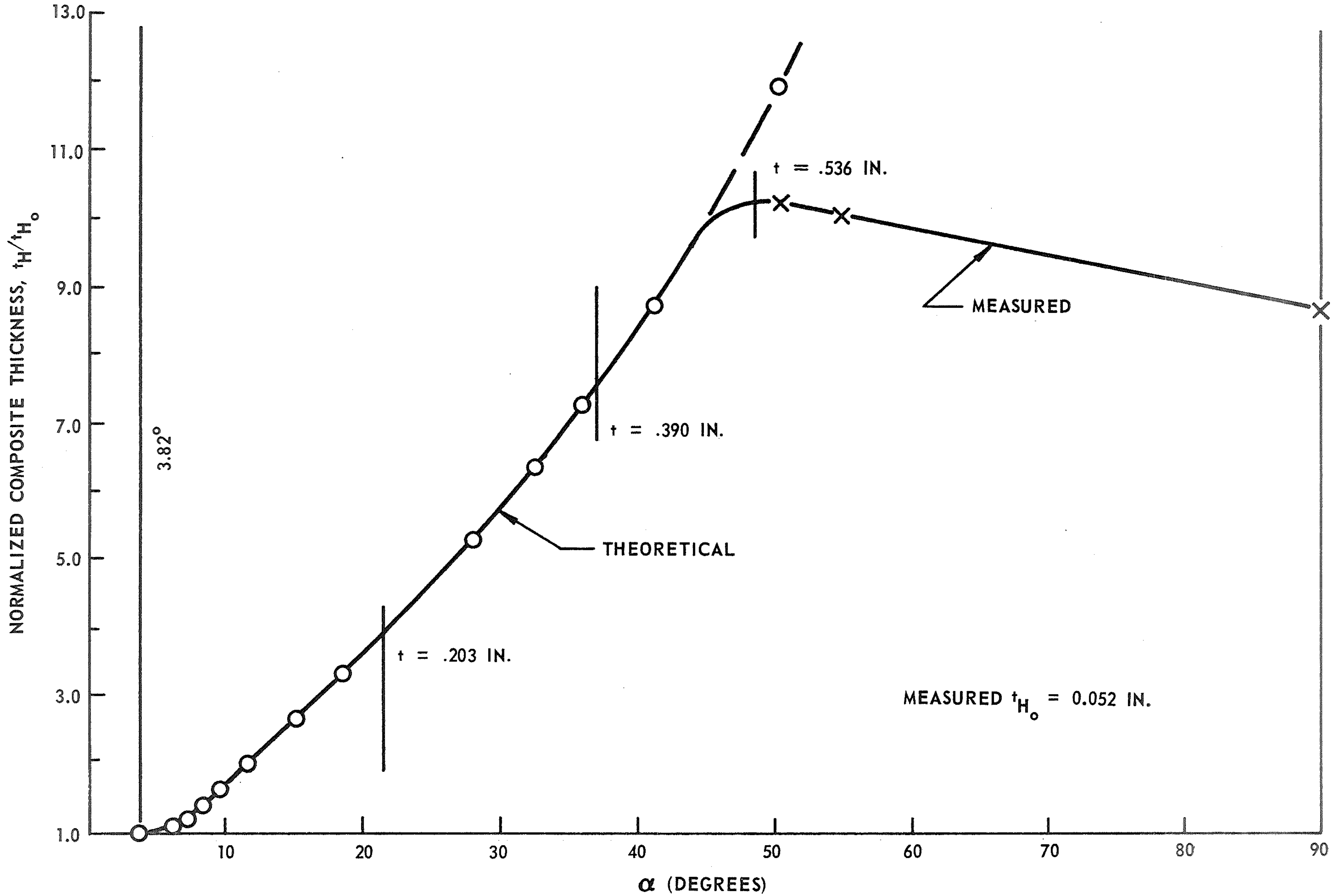

Figure 7. Normalized Composite Thickness vs Wrap Angle

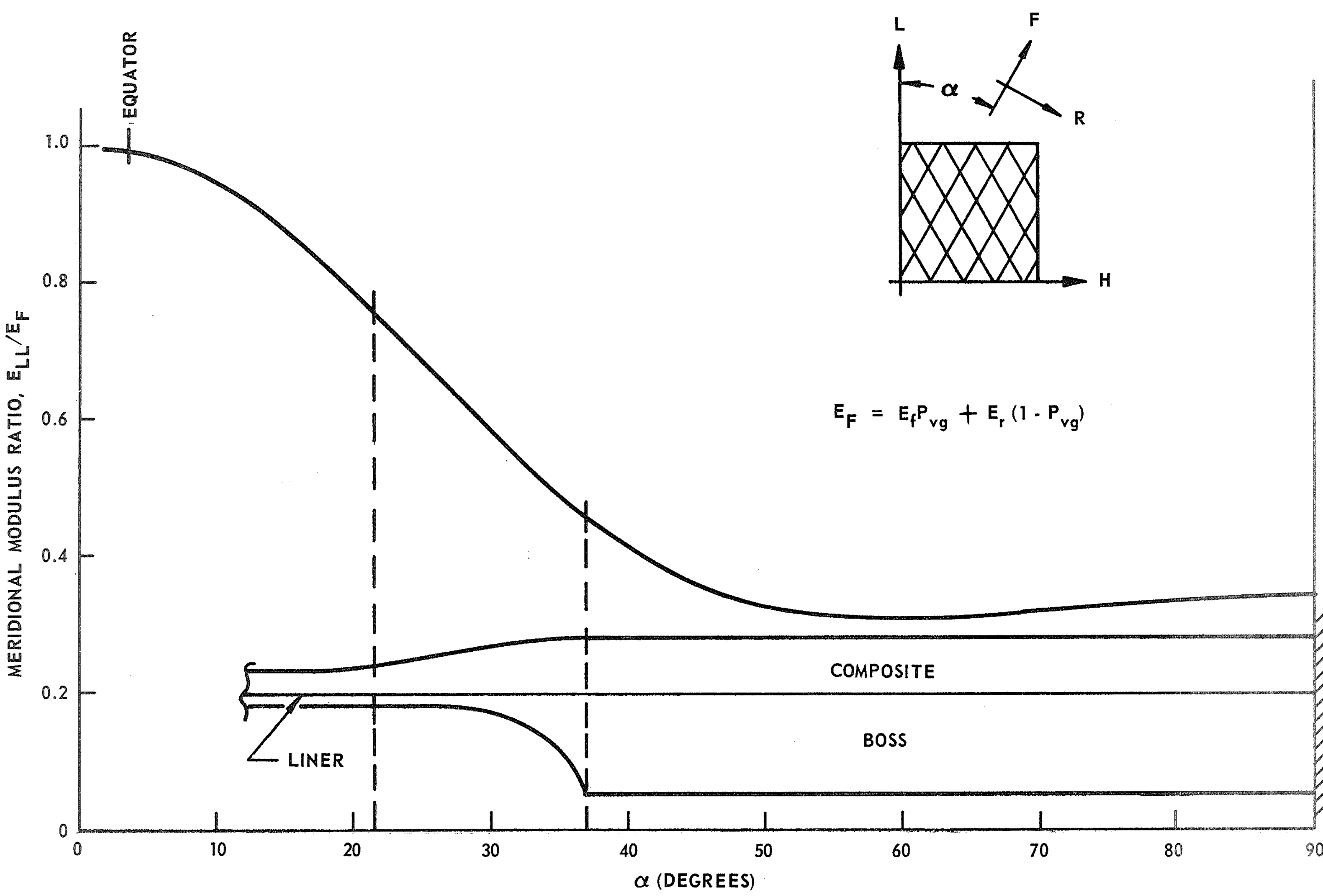

Figure 8. Meridional Modulus Ratio vs Wrap Angle

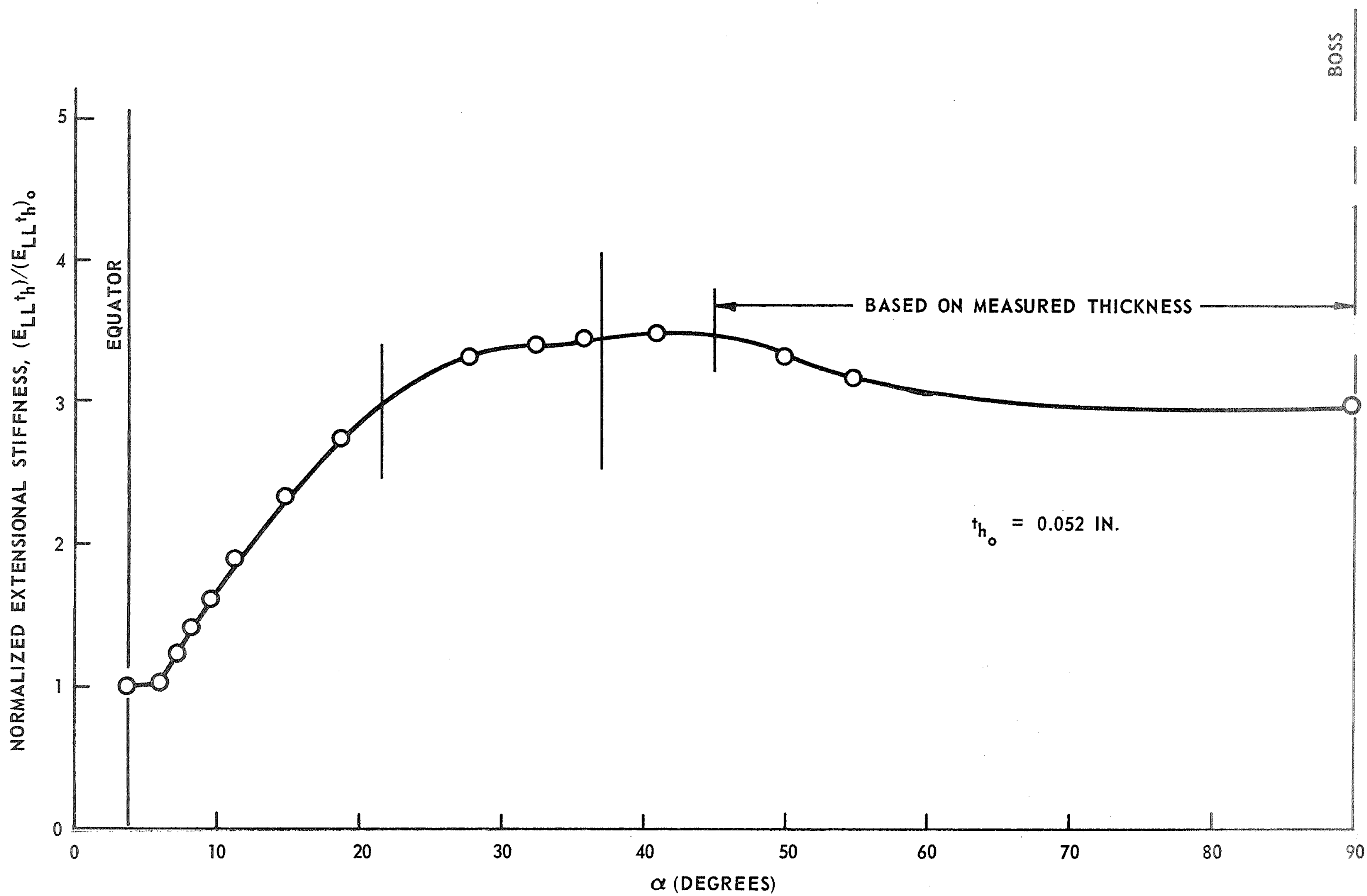

Figure 9. Normalized Extensional Stiffness vs Wrap Angle

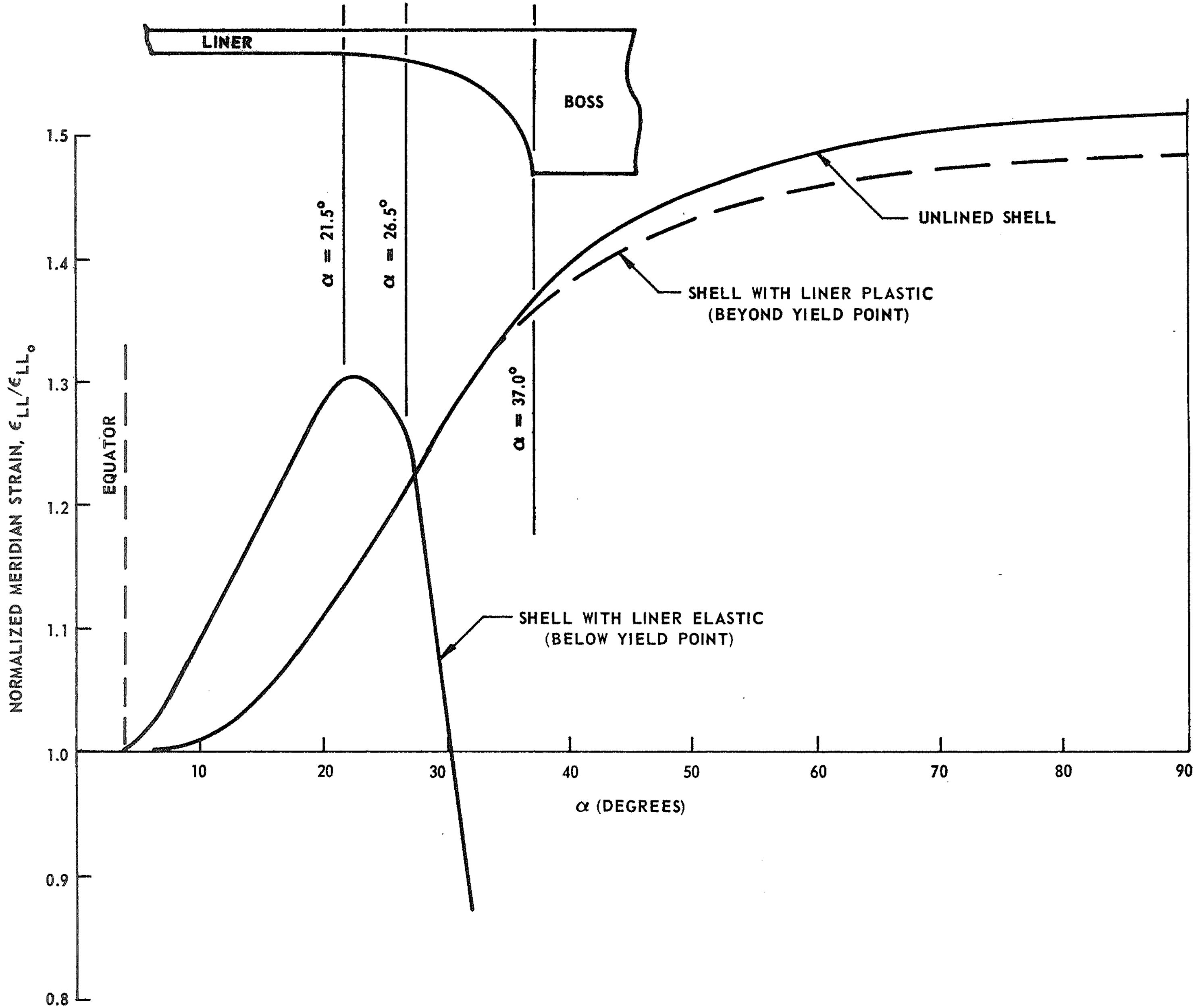

Figure 10. Effect of Liner Condition on Meridional Strain Distribution - Orthotropic Analysis

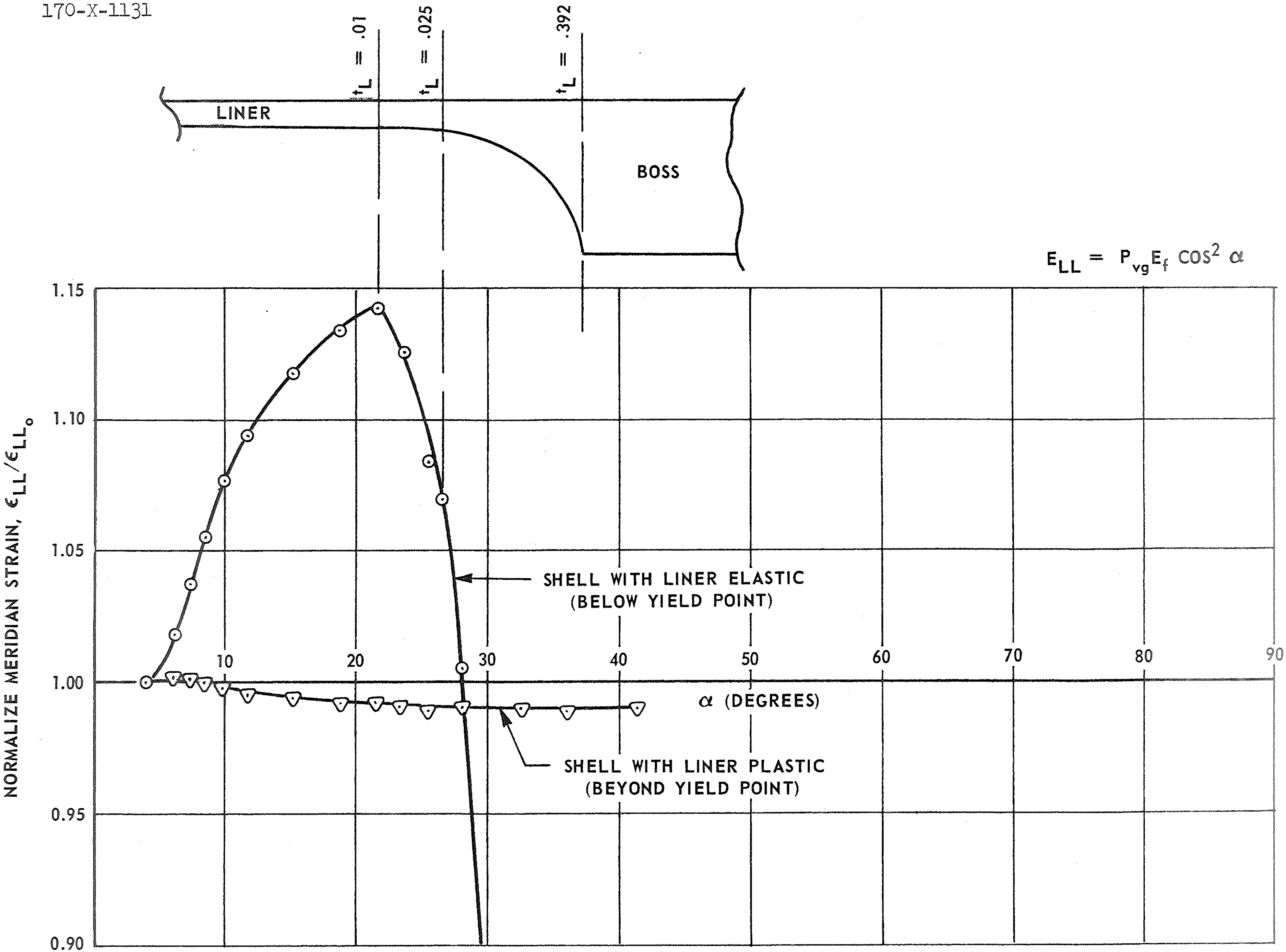

Figure 11. Effect of Liner Condition on Meridional Strain Distribution of Filament-Wound Shell-Netting Analysis

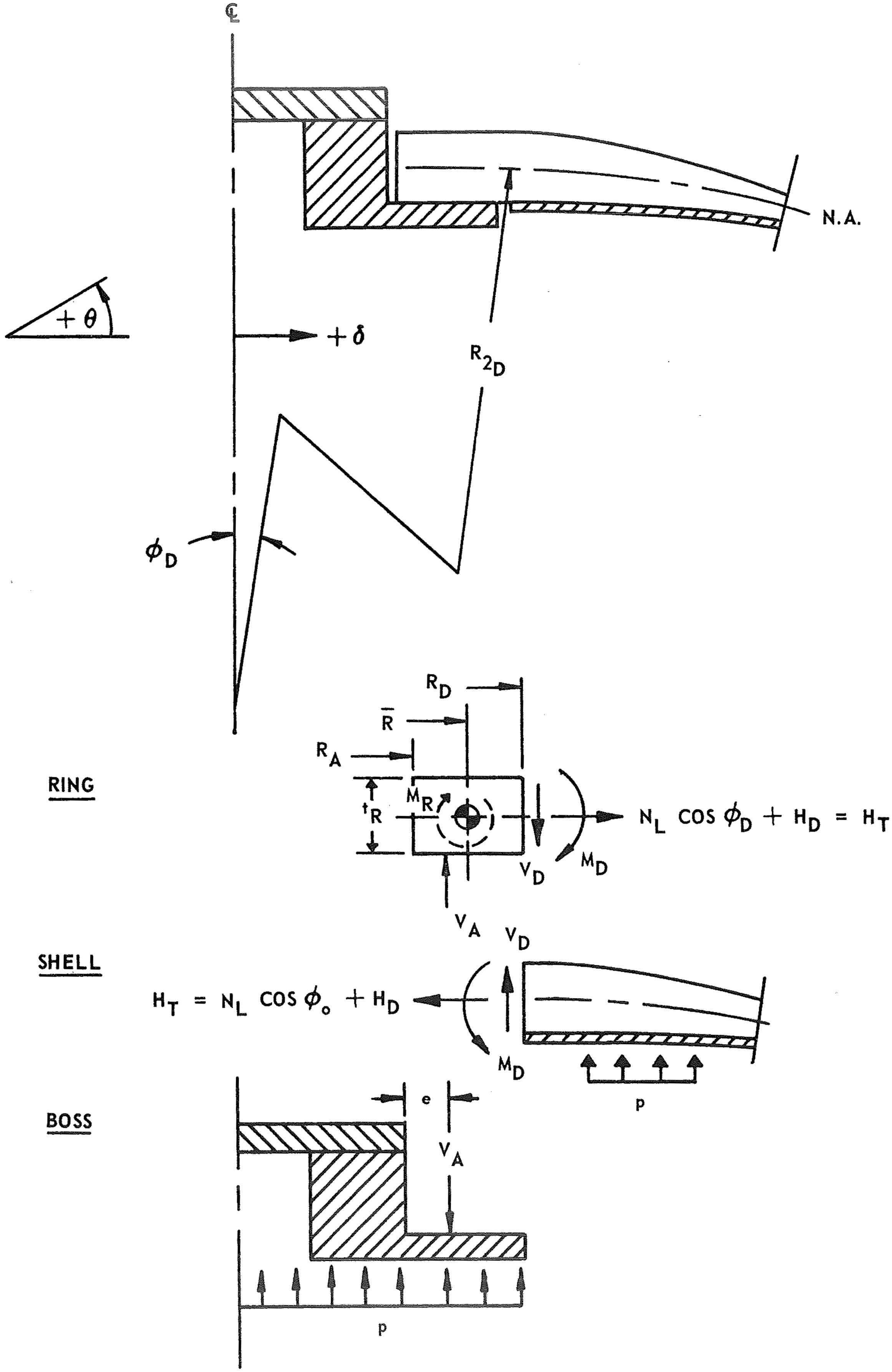

Figure 12. Model of Axial Port Region of Metal-Lined Filament-Wound Vessel Dome

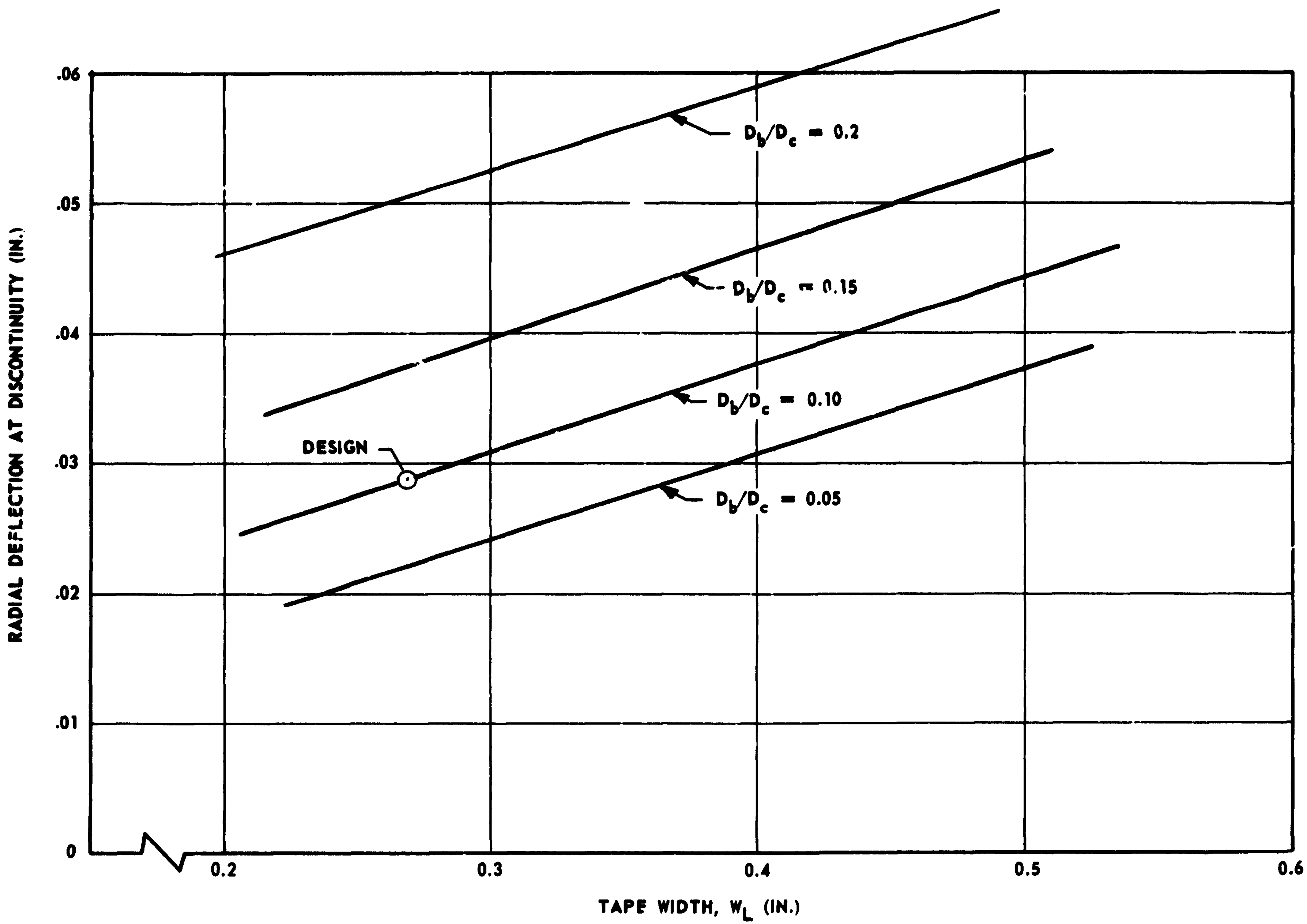

Figure 13. Deflection at Ring-Plate/Shell Juncture

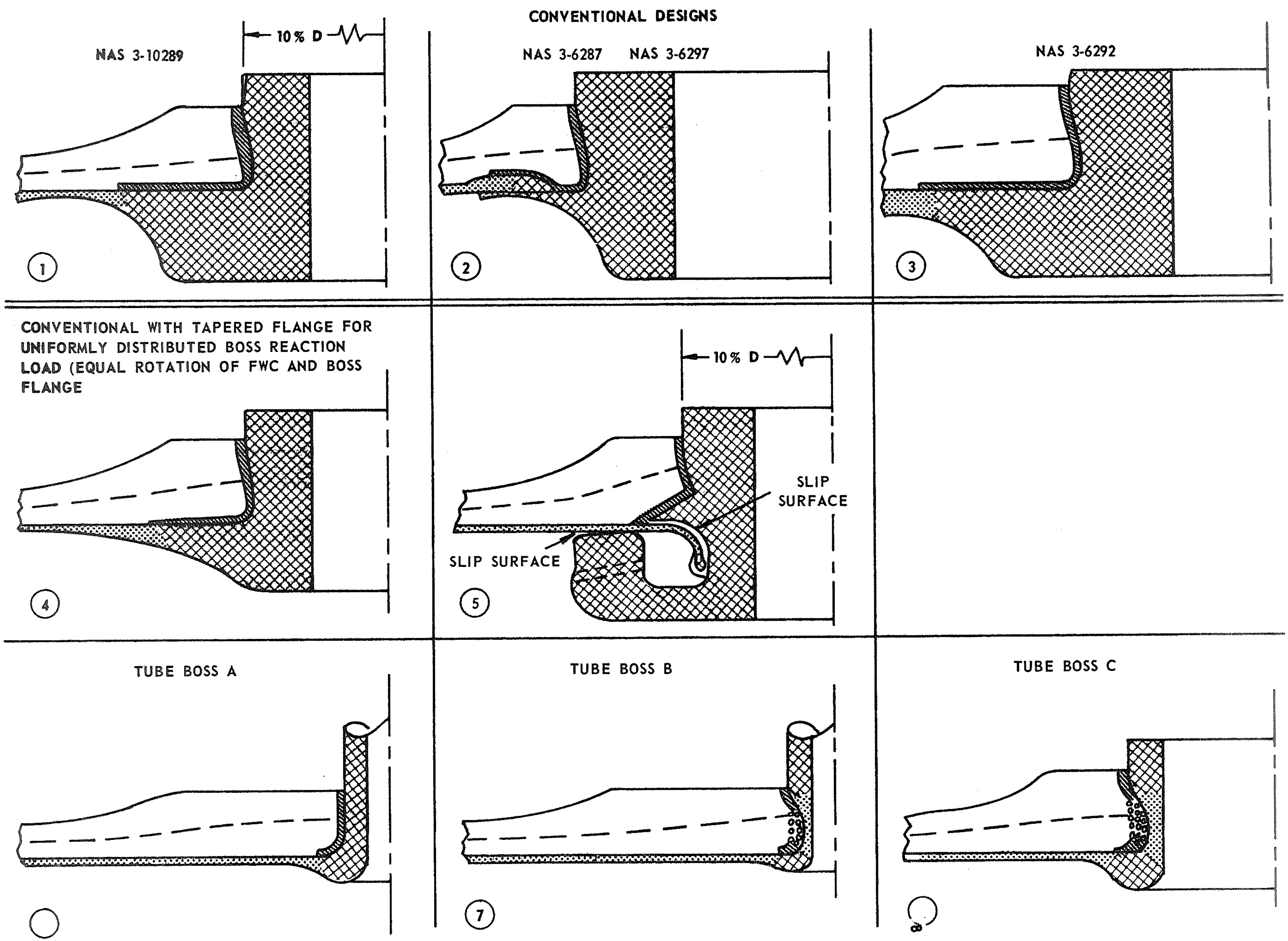

Figure 14. Polar Boss Design Configuration
Sheet 1 of 2

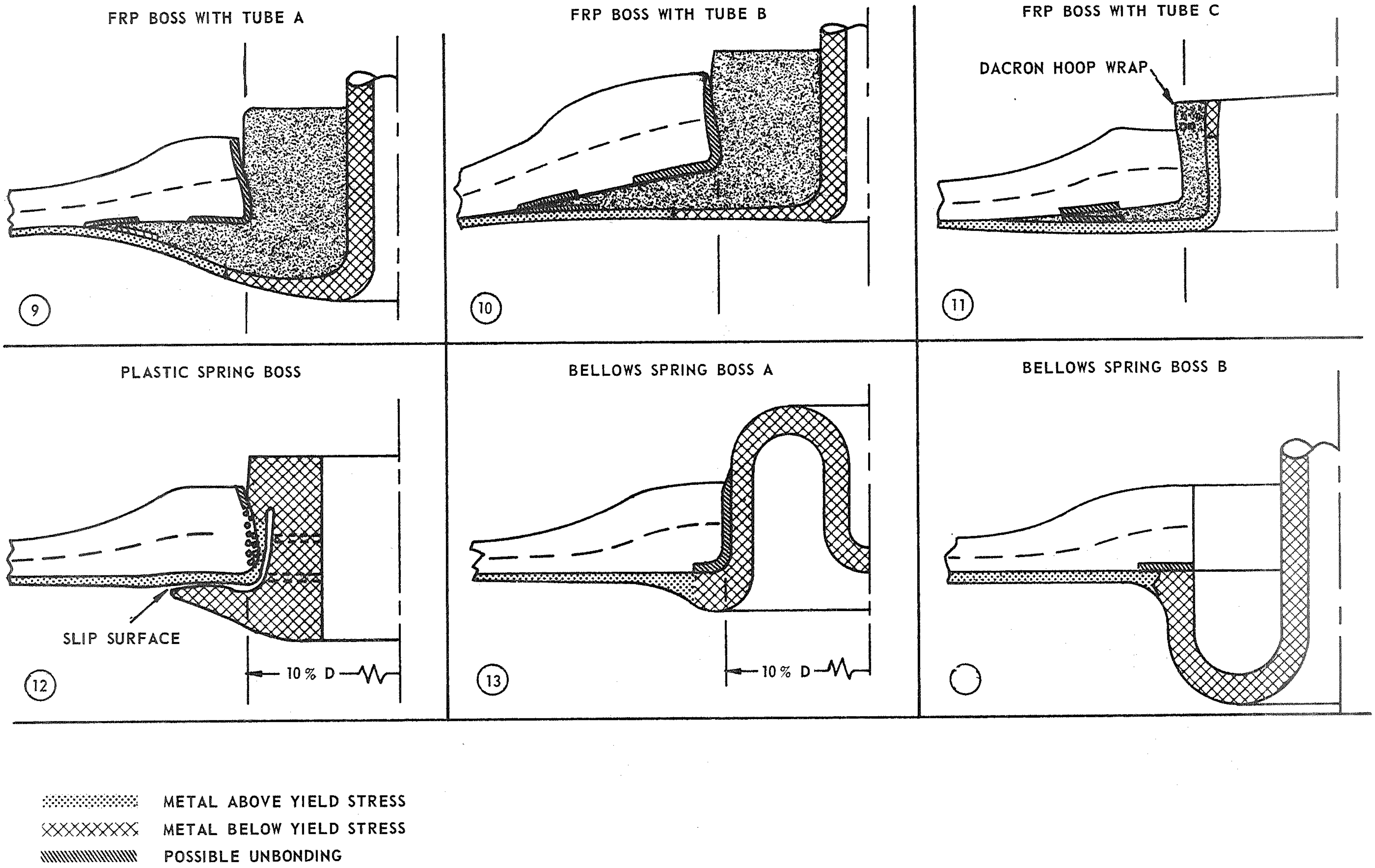

Figure 14. Polar Boss Design Configuration
Sheet 2 of 2

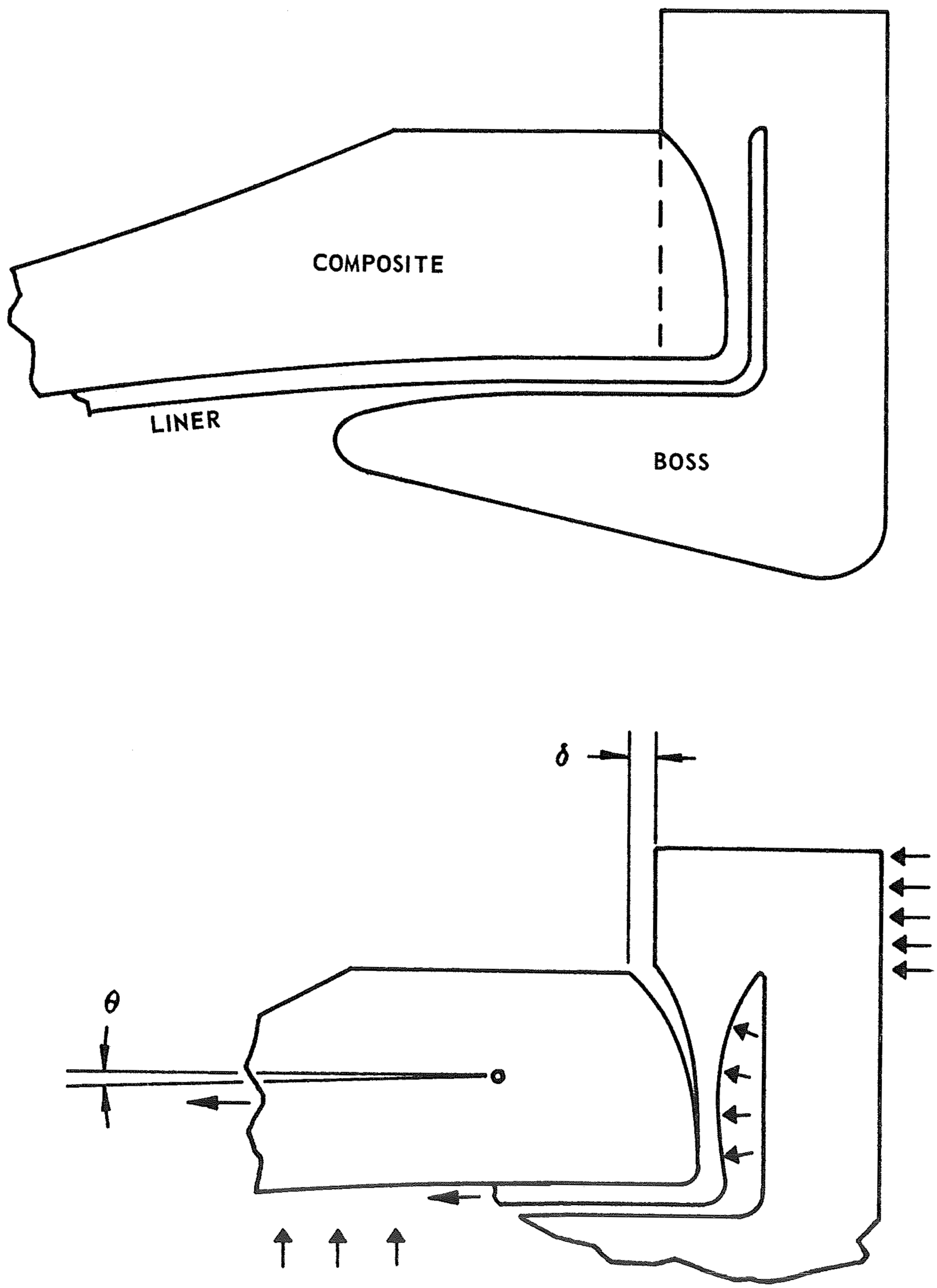

Figure 15. Schematic of Plastic Spring Boss

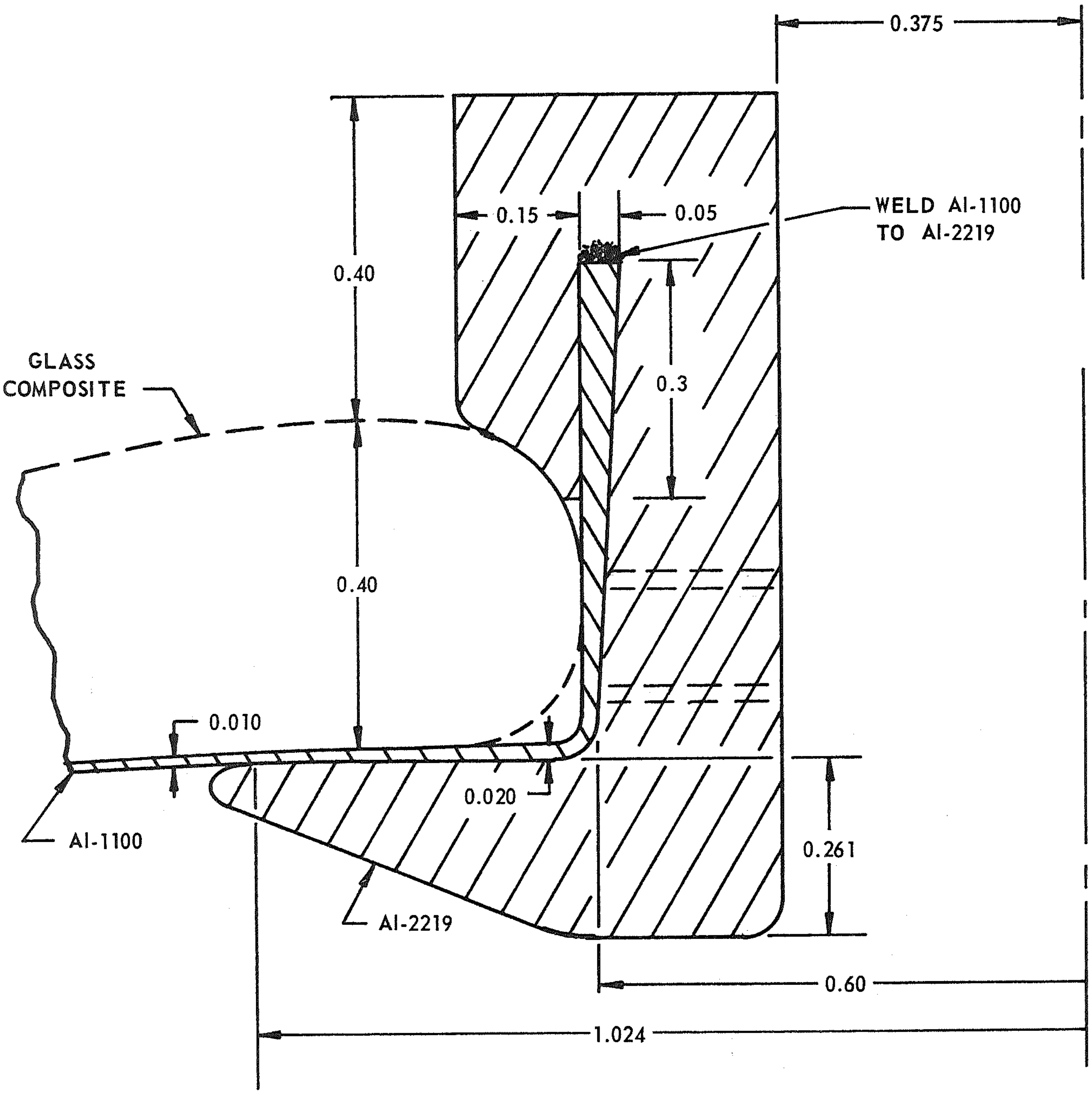

Figure 16. Plastic Spring Boss

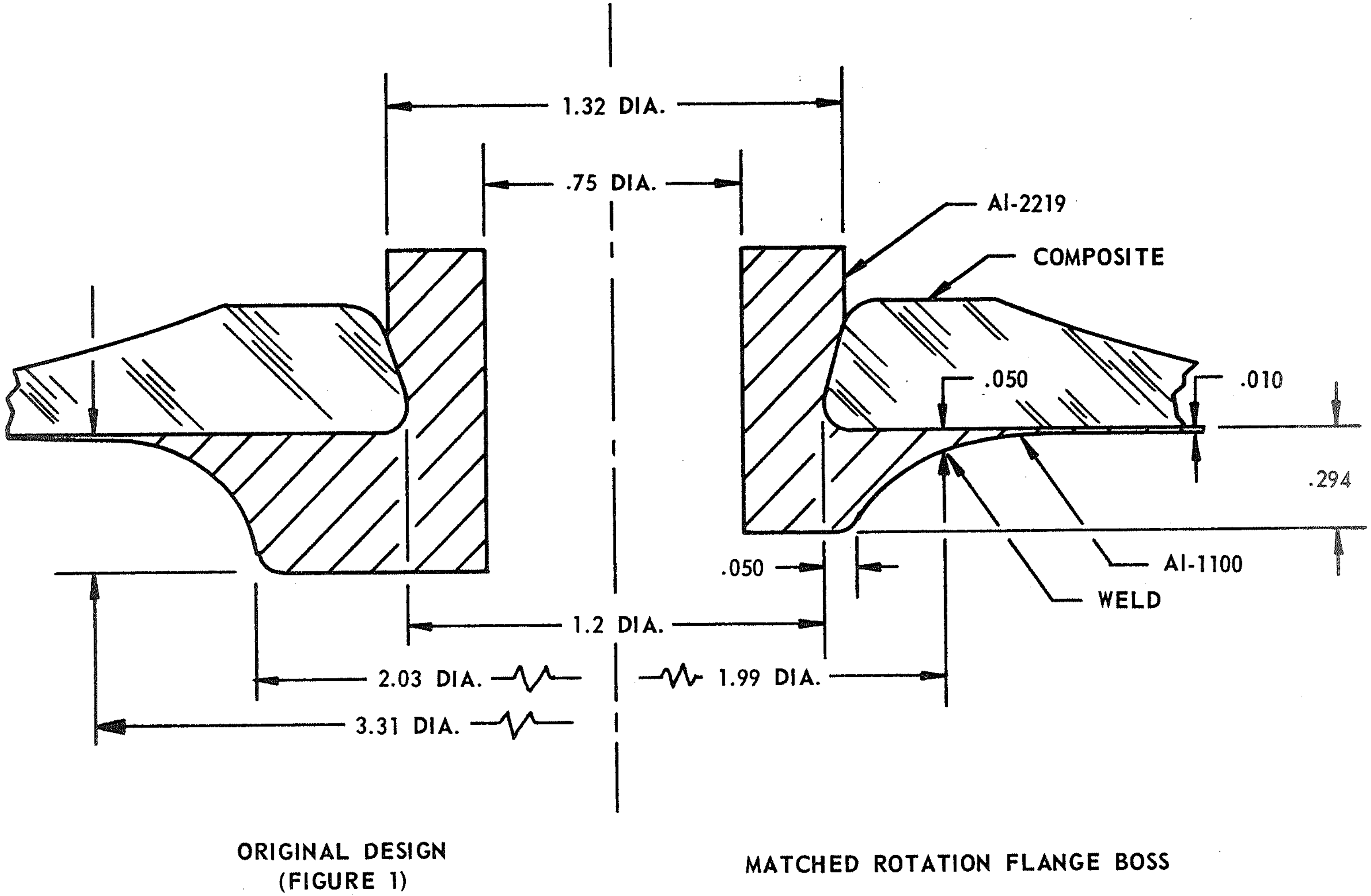

Figure 17. Matched-Rotation Flange Boss

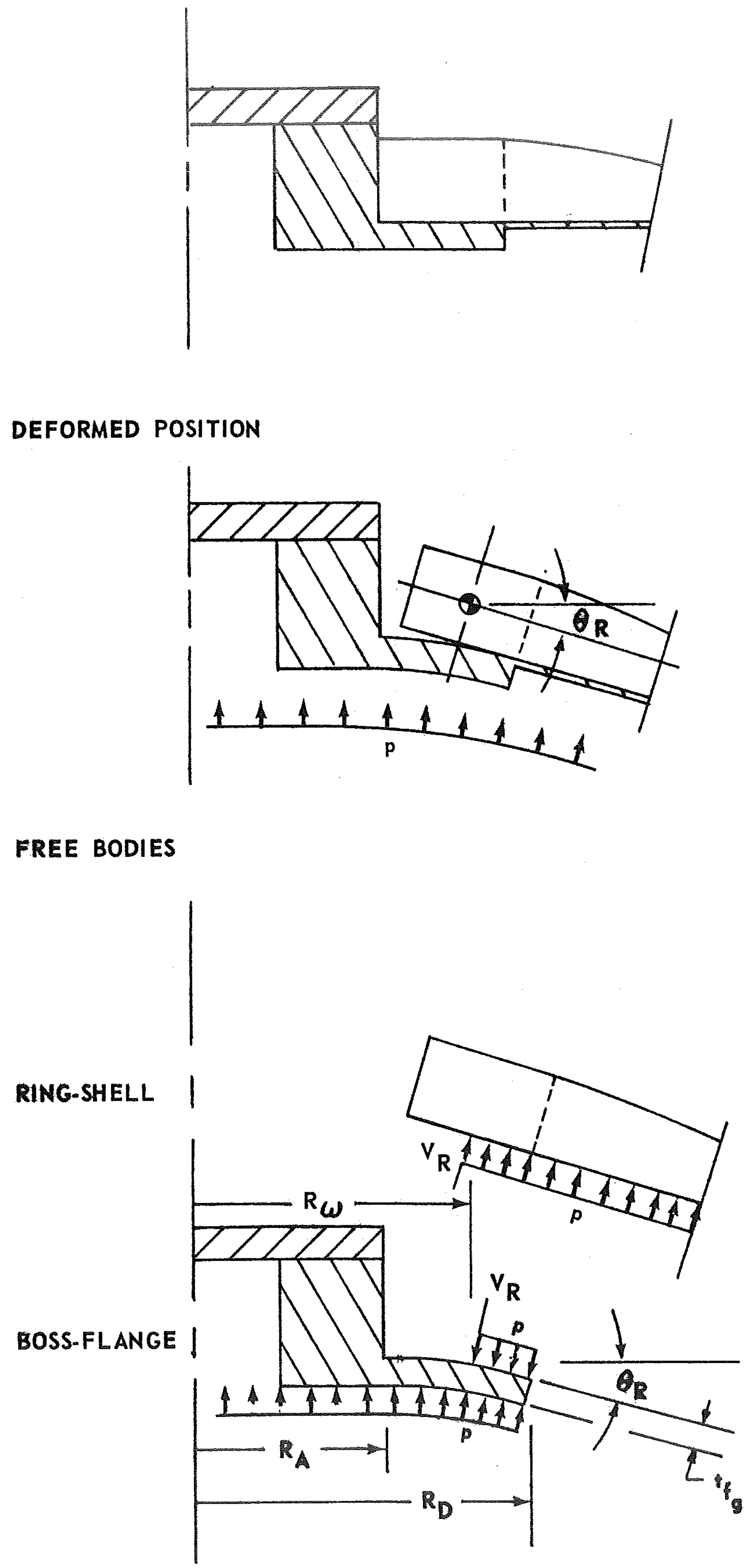

Figure 18. Model of Matched-Rotation Flange Boss

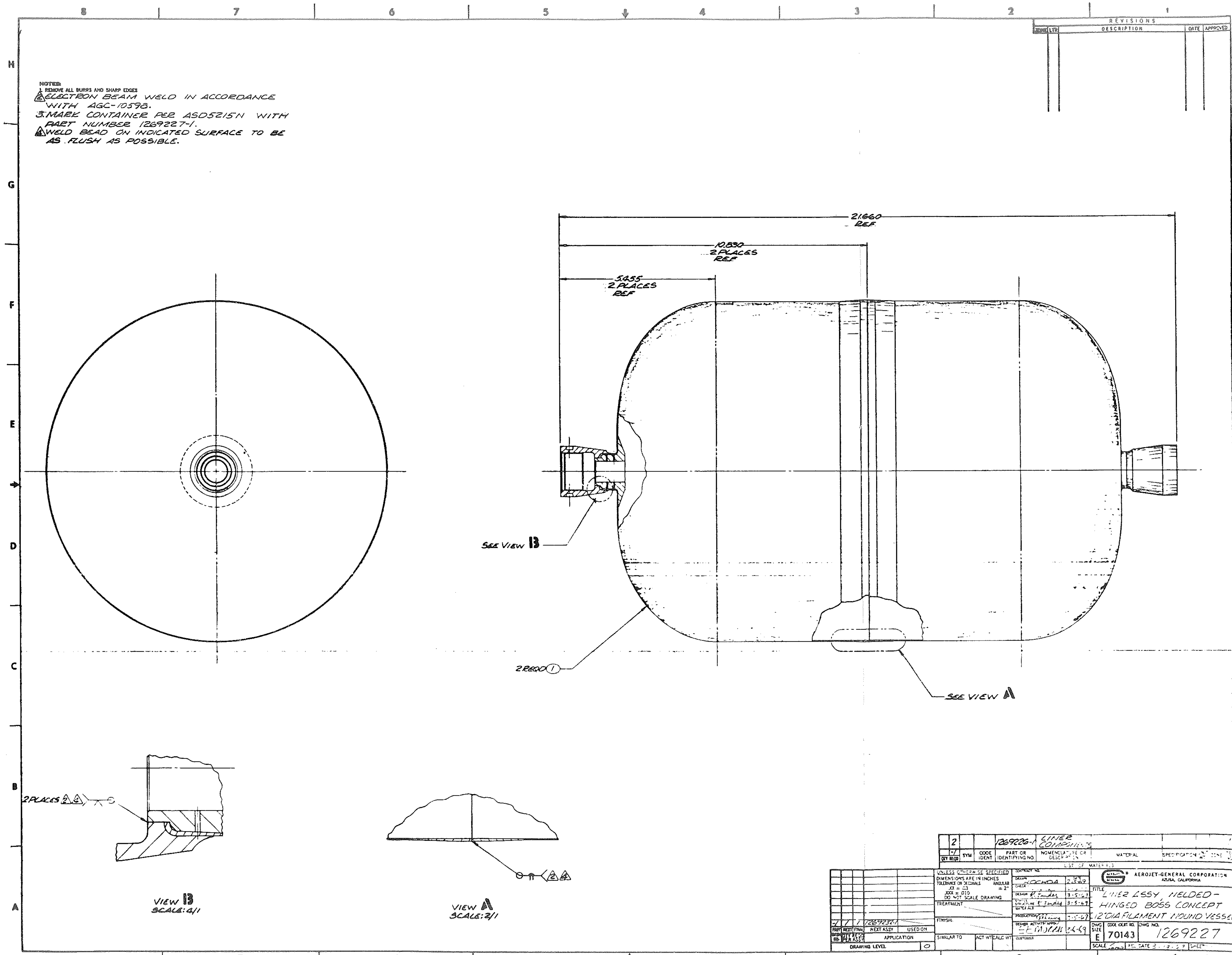

Figure 19. Aluminum Liner with Plastic Spring Boss

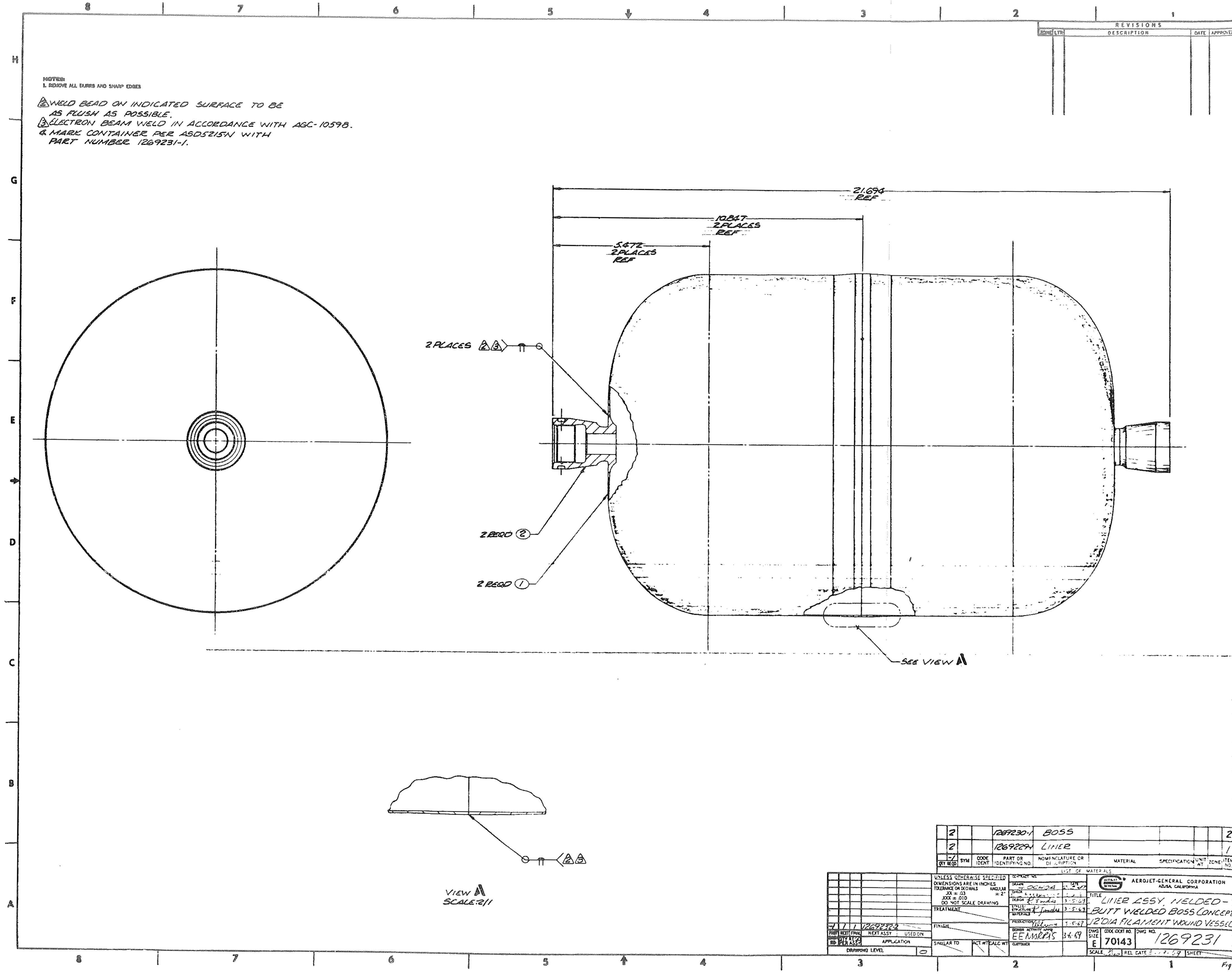

Figure 20. Aluminum Liner with Matched-Rotation Flange Boss

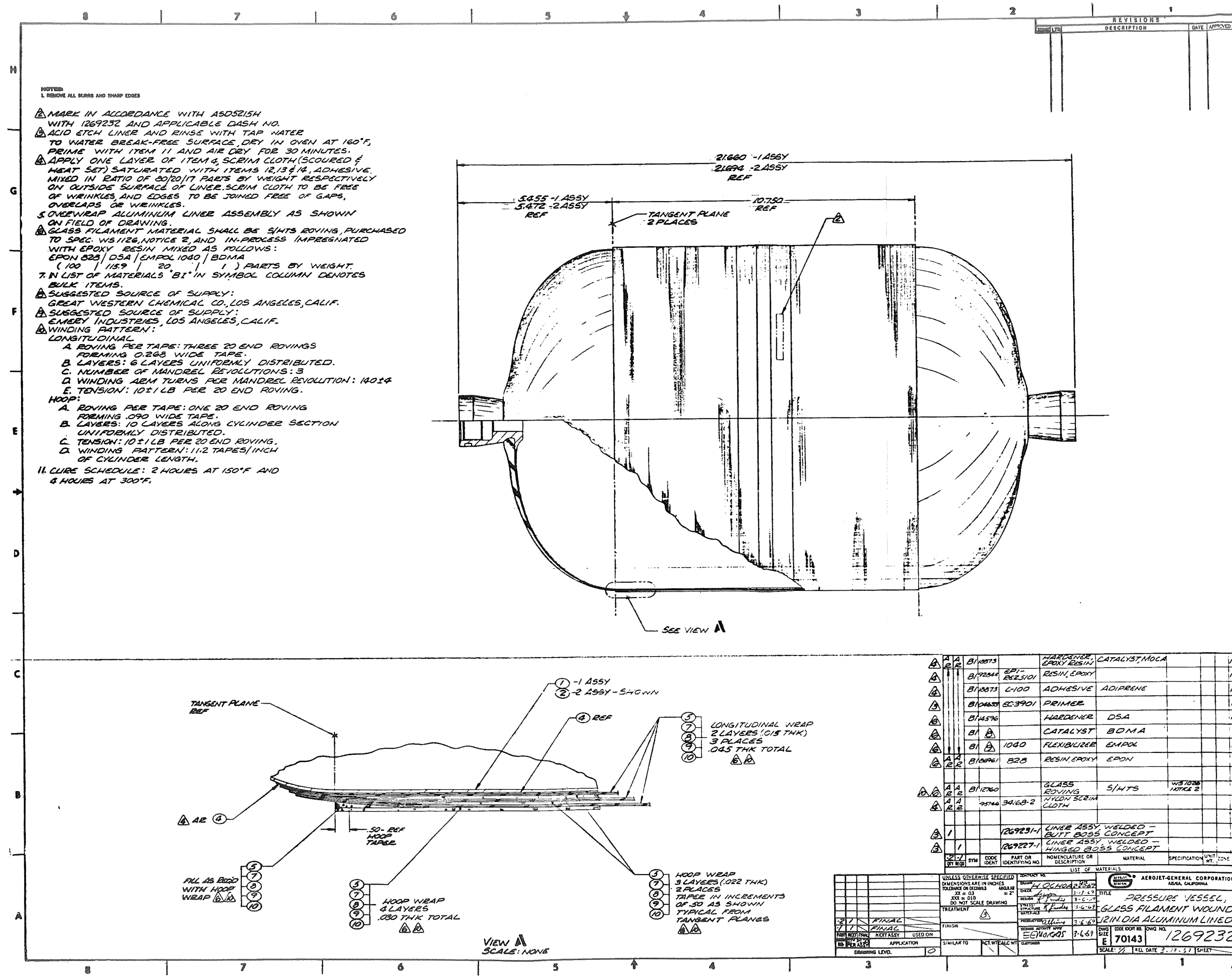

Figure 21. Aluminum-Lined Glass-Filament-Wound Vessel

APPENDIX A

SYMBOLS

APPENDIX A

SYMBOLS

	Definition	Units
A	cross section of 20-end roving	in.^{2}
a	chamber radius	in.
B	extensional stiffness	lb/in.
C_1 =	$(R_D^2 + R_A^2)/(R_D^2 - R_A^2) - \nu$	
D	flexural rigidity or diameter	lb-in. or in.
E	modulus of elasticity	psi
e	distance defined in Figure 12	in.
F	allowable ultimate strength of filament	psi
F_{fr}	friction force	lb
H	horizontal force	lb/in.
H_T	total load per inch	lb/in.
I	moment of inertia	in.^{3}
$K_1, \ldots, K_6$	design factors defined in text	
$k_1(\xi), \ldots, k_6(\xi)$, $W_d(\xi)$	functions defined in ref. 8	
k	foundation modulus	lb/in.^{3}
L	total vessel length	in.
L_c	total cylinder length	in.
L_H	number of hoop layers	
L_L	number of longitudinal layers	
M	bending moment	in.-lb/in.
N	membrane force	lb/in.
N_1	number of revolutions	
N_2	number of strands per tape, longitudinal	

SYMBOLS (cont.)

	Definition	Units
N_3	number of turns per revolution	
N_4	number of strands per tape, hoop	
N_5	turns per inch of cylinder	$in.^{-1}$
P_{vg}	glass filament fraction in composite	
p	internal pressure	psi
R	radius	in.
R_1	radius of curvature in meridian direction	in.
R_2	radius of curvature in hoop direction	in.
T	temperature	deg. F
t	thickness	in.
t_H	hoop composite thickness	in.
t_L	longitudinal composite thickness	in.
$t_{s,\ell}$	thickness of single layer of longitudinal composite	in.
$t_{s,h}$	thickness of single layer of hoop composite	in.
U	influence coefficient for deflection	
V	shear force	lb/in.
W	total applied load	lb
W_L	winding tape width	in.
w	distributed load	lb/in.
x	radial coordinate	in.
XO1 =	$(D_b + 1.57\ W_L)/2$	
y	axial coordinate	in.
$\overline{Y}$	distance to neutral axis	in.
z =	x/a	

SYMBOLS (cont.)

Greek	Definition	Units
α	angle between filament path and meridian direction	degrees
β	influence coefficient for rotation	
β_{21}	influence coefficient (ref. 7, p. 215)	
β_{22}	influence coefficient (ref. 7, p. 215)	
δ	radial deflection	in.
ϵ	strain	in./in.
ϵ_{tp}	space between tapes	in.
θ	rotation	radians
λ	beam characteristic	in.$^{-1}$
λ_{21}	influence coefficient from ref. 7, p. 215	
λ_{22}	influence coefficient from ref. 7, p. 215	
μ	coefficient of friction	
ν	Poisson's ratio	
ξ =	$\lambda\phi\sqrt{2}$	
σ	stress	
ϕ	central angle subtended by circular opening at vertex	radians

Subscripts

A	location defined in figure 12	
B	due to bending	
b	boss	
C	composite	
c	cylinder	
D	location defined in figure 12	

SYMBOLS (cont.)

Subscripts	Definition	Units
E	elastic condition	
F	filament composite	
f	filament	
fg	flange	
f,h	hoop filaments	
f,ℓ	longitudinal filaments	
H	hoop direction	
HH	hoop direction, hoop composite	
HL	hoop direction, longitudinal composite	
HM	hoop direction, metal liner	
h	filament composite head	
i	inside	
L	longitudinal direction	
LH	longitudinal direction, hoop composite	
LL	longitudinal direction, longitudinal composite	
LM	longitudinal direction, metal liner	
M	metal liner	
O	at tangent plane	
p	due to pressure or plastic condition	
R	ring	
r	resin or radial direction	
t	tangential direction	
tu	ultimate tensile	

SYMBOLS (cont.)

Subscripts	Definition	Units
ty	tensile yield	
w	location defined in figure 18	
11	refers to Al-1100 alloy	
22	refers to Al-2219 alloy	

APPENDIX B

SHORT CYLINDER ANALYSIS FOR HINGE DESIGN

The purpose of this analysis is to provide equations for determining the effect of thickness on stresses, strains, rotations, and deflections of short cylinders rigidly fixed at one end.

At the fixed end of the cylinder*

$$\text{(K)} \begin{cases} \delta_p = \dfrac{pR^2}{Et}, \quad \delta_v = \dfrac{C_3 V}{2 D \lambda^3}, \quad \delta_m = \dfrac{C_5 M}{2 D \lambda^2} \\[2ex] \theta_v = \dfrac{C_4 V}{2 D \lambda^2}, \quad \theta_m = \dfrac{C_6 M}{\lambda D} \end{cases}$$

Note: See Reference 7, p. 297 for $C_i = f(\lambda L)$

(1) $\theta_v - \theta_m = 0$ no rotation

(2) $\delta_p + \delta_m - \delta_v = 0$ no deflection

Shear load in terms of bending moment is

$$\text{(3)} \quad V = 2 \left(\frac{C_6}{C_4} \right) \lambda M$$

The bending moment is

$$\text{(4)} \quad M = \frac{2 \lambda^2 D \delta_p}{\dfrac{2 C_3 C_6 - C_4 C_5}{C_4}}$$

let

$$C_7 = \frac{2 C_3 C_6 - C_4 C_5}{C_4}$$

<u>Where</u>

$$\lambda^4 = \frac{3 (1 - v^2)}{R^2 t^2}$$

---

*Reference 7.

$$D = \frac{Et^3}{12\,(1 - v^2)}$$

Meridional Bending Stress

$$\sigma_{\phi_m} = \frac{6M}{t^2} = \frac{12\,D\,\lambda^2\,\delta_p}{C_7\,t^2} = \frac{12\,Et^3\,[3(1 - v^2)]^{1/2}\,pR^2}{C_7\,t^2\,12(1 - v^2)\,Rt\,Et}$$

$$\sigma_{\phi_m} = \left(\frac{3}{1 - v^2}\right)^{1/2} \frac{pR}{C_7\,t}$$

Direct Hoop Stress due to M

$$\sigma_{\theta_m} = \frac{2\,\lambda^2\,RM}{t} = \frac{4\,\lambda^4\,RD\,\delta_p}{C_7\,t} = \frac{12\,(1 - v^2)\,R\,Et^3\,pR^2}{C_7\,t\,R^2\,t^2\,12\,(1 - v^2)\,Et}$$

$$\sigma_{\theta_m} = \frac{pR}{C_7\,t}$$

Hoop Membrane Stress

$$\sigma_{\theta_p} = \frac{pR}{t}$$

Hoop Bending Stress

$$\nu\sigma_{\phi_m} = \left(\frac{3}{1 - \nu^2}\right)^{1/2} \frac{\nu\,pR}{C_7\,t}$$

Direct Hoop Stress due to V

$$\sigma_{\theta_v} = \frac{2\lambda RV}{t} = \frac{8\,\lambda^4\,R\,D\,C_6\,\delta_p}{C_4\,C_7\,t}$$

$$\sigma_{\theta_v} = \frac{2\,C_6}{C_4}\,\sigma_{\theta_m}$$

$$\sigma_{\theta_v} = \left(\frac{2\,C_6}{C_4\,C_7}\right) \frac{pR}{t}$$

Maximum Combined Hoop Stress

$$\sigma_{\Theta_{max}} = \sigma_{\Theta_p} + \sigma_{\Theta_m} - \sigma_{\Theta_V} \pm \nu\sigma_{\phi_m}$$

$$\sigma_{\Theta_{max}} = \frac{pR}{C_7\ t}\left[C_7 + 1 - \frac{2\ C_6}{C_4} \pm \nu\left(\frac{3}{1-\nu^2}\right)^{1/2}\right]$$

Deflection

$$\delta = \frac{pR^2}{Et} - \frac{C_3\ V}{2\ D\ \lambda^3} + \frac{C_5\ M}{2\ D\ \lambda^2}$$

Rotation

$$\Theta = \frac{C_4\ V}{2\ D\ \lambda^2} - \frac{C_6\ M}{\lambda D}$$

The deflection and rotation at the free end are

$$\delta = \frac{pR^2}{Et} + \frac{|C_3'|\ V}{2\ D\ \lambda^3} - \frac{|C_5'|\ M}{2\ D\ \lambda^2}$$

$$\Theta = \frac{|C_4'|\ V}{2\ D\ \lambda^2} - \frac{|C_6'|\ M}{\lambda D}$$

The preceding equations are now used, in the section that follows, to determine the effect of cylinder thickness, t, on stress and distortions of the short cylinder.

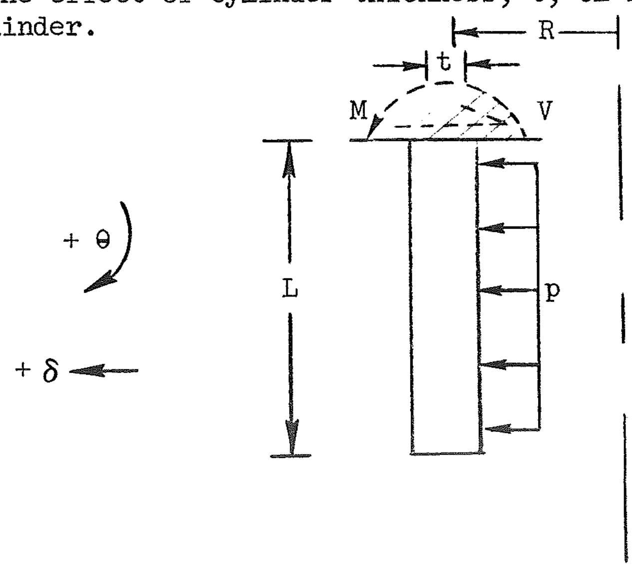

Find effect of "t" on stresses for the following fixed parameters

$L = 0.3$ in., $R = 0.6$ in., $p = 3000$ psi

$\nu = 0.3$, $E = 10 \times 10^6$

$$\sigma_{\phi_{max}} = \frac{3000\ (.6)\left(\frac{3}{.91}\right)^{1/2}}{C_7 t} = \frac{3269}{C_7 t}$$

$$\sigma_{\theta_{max}} = \frac{3000(.6)}{C_7 t}\left[C_7 + \left(\frac{C_4 - 2\ C_6}{C_4}\right) \pm .3\ \left(\frac{3}{.91}\right)^{1/2}\right]$$

$$\sigma_{\theta_{max}} = \frac{1800}{C_7 t}\left[C_7 - \left(\frac{2\ C_6 - C_4}{C_4}\right) \pm 0.545\right]$$

$$M = \frac{3000(.6)}{6C_7}\left(\frac{3}{.91}\right)^{1/2} t = \frac{545\ t}{C_7}$$

$$V = \frac{C_6}{C_4 C_7}\left(\frac{1}{3(.91)}\right)^{1/4}\ 3000(.6)^{1/2}\ t^{1/2}$$

$$V = \frac{1809\ C_6}{C_4 C_7}\ t^{1/2}$$

$$\lambda = \frac{1}{t}\ \frac{[.3(.91)]^{1/4}}{(.6)^{1/2}} = \frac{1.659}{t^{1/2}}$$

$$C_7 = \frac{2\ C_3 C_6 - C_4 C_5}{C_4}$$

TABLE B-1

SUMMARY OF SHORT CYLINDER PARAMETERS

t	λ	λL	C_3	C_4, C_5	C_6	C_7	V	M	$\sigma_{\theta_{max}}$	$\sigma_{\phi_{max}}$	σ_s
.10	5.247	1.574	1.355	1.497	1.383	1.007	525	54.1	+12,600 - 6,900	32,500	5300
.15	4.284	1.285	1.606	2.020	1.935	1.057	635	77.3	+ 7,800 - 4,600	20,600	4200
.20	3.710	1.113	1.838	2.612	2.698	1.185	705	92.0	+ 5,000 - 3,200	13,800	3500

APPENDIX B SYMBOLS

$C_1, \ldots, C_6$	coefficients defined in Reference 7	
$C_1', \ldots, C_6'$	coefficients defined in Reference 7	
C_7	$(2\ C_3C_6 - C_4C_5)/2$	
E	modulus of elasticity	psi
L	cylinder length	in.
M	bending moment	in.-lb/in.
p	pressure	psi
R	cylinder average radius	in.
t	cylinder thickness	in.
V	shear load	lb/in.
δ	radial deflection	in.
θ	rotation	radians
λ	beam characteristic	$in.^{-1}$
ν	Poisson's ratio	
σ	stress	

Subscripts

m	due to moment
p	due to pressure
v	due to shear
θ	hoop direction
ϕ	longitudinal direction
s	shear

REFERENCES

1. E. E. Morris, F. J. Darms, R. E. Landes, and J. W. Campbell, Parametric Study of Glass-Filament-Reinforced Metal Pressure Vessels, NASA CR 54-855 (Aerojet-General report prepared under Contract NAS 3-6292), April 1966.

2. E. E. Morris, Glass-Fiber-Reinforced Metallic Tanks for Cryogenic Service, NASA CR-72224 (Aerojet-General report prepared under Contract NAS 3-6292), June 1967.

3. F. J. Darms and R. E. Landes, Computer Program for the Analysis of Filament-Reinforced Metal-Shell Pressure Vessels, NASA CR-72124 (Aerojet-General Report prepared under Contract NAS 3-6292), May 1966.

4. F. J. Darms, R. Molho, and B. E. Chester, Improved Filament-Wound Construction for Cylindrical Pressure Vessels, ML-TDR-64-63, Volumes I and II, March 1964.

5. F. J. Darms and E. E. Morris, "Design Concepts and Procedures for Filament-Wound Composite Pressure Vessels," Paper presented at American Society for Mechanical Engineers Aviation and Space Conference, 16-18 March 1965, at Los Angeles, California.

6. Structural Materials Handbook, Aerojet-General Corporation, Structural Materials Division, February 1964.

7. R. J. Roark, Formulas for Stress and Strain, 4th Edition, McGraw-Hill Book Company, 1965.

8. UCLA Course X414 PQ Notes Entitled "Analysis and Design of Modern Pressure Vessels," Lecture 10, Analysis of Filament-Wound Pressure Vessels, by L. B. Greszczuk, 12 July 1963.

9. L. B. Greszczuk, Effect of Reinforcement Geometry on the Stresses in Spherical Shells, Paper 578C, SAE, October 1962.

10. J. M. Toth, et al., Investigation of Structural Properties of Fiber-Glass Filament-Wound Pressure Vessels at Cryogenic Temperature, NASA CR 54393, September 1965.

DISTRIBUTION

REPORT COPIES R D	RECIPIENT	DESIGNEE
	National Aeronautics & Space Administration Lewis Research Center 21000 Brookpark Road Cleveland, Ohio 44135	
1	Attn: Contracting Officer, MS 500-313	
5	Liquid Rocket Technology Branch, MS 500-209	
1	Technical Report Control Office, MS 5-5	
1	Technology Utilization Office, MS 3-16	
2	AFSC Liaison Office, MS 4-1	
2	Library	
1	Office of Reliability & Quality Assurance, MS 500-111	
1	D. L. Nored, Chief, LRTB, MS 500-209	
3	J. R. Barber Project Manager, MS 500-209	
1	E. W. Conrad, MS 500-204	
1	R. H. Kemp, MS 49-1	
2	Chief, Liquid Experimental Engineering, RPX Office of Advanced Research &Technology NASA Headquarters Washington, D.C. 20546	
2	Chief, Liquid Propulsion Technology, RPL Office of Advanced Research & Technology NASA Headquarters Washington, D.C. 20546	
1	Director, Launch Vehicles & Propulsion, SV Office of Space Science & Applications NASA Headquarters Washington, D.C. 20546	
1	Chief, Environmental Factors & Aerodynamics Code RV-1 Office of Advanced Research & Technology Washington, D.C. 20546	
1	Chief, Space Vehicles Structures Office of Advanced Research & Technology NASA Headquarters Washington, D.C. 20546	

REPORT COPIES R	D	RECIPIENT	DESIGNEE
1		Director, Advanced Manned Missions, MT Office of Manned Space Flight NASA Headquarters Washington, D.C. 20546	
6		NASA Scientific & Technical Information Facility P.O. Box 33 College Park, Maryland 20740	
1		Director, Technology Utilization Division Office of Technology Utilization NASA Headquarters Washington, D.C. 20546	
1	1	National Aeronautics & Space Administration Ames Research Center Moffett Field, California 94035 Attn: Library	C. A. Syvertson
1		National Aeronautics & Space Administration Flight Research Center P.O. Box 273 Edwards, California 93523 Attn: Library	
1		National Aeronautics & Space Administration Goddard Space Flight Center Greenbelt, Maryland 20771 Attn: Library	
1		National Aeronautics & Space Administration John F. Kennedy Space Center Cocoa Beach, Florida 32931 Attn: Library	
1		National Aeronautics & Space Administration Langley Research Center Langley Station Hampton, Virginia 23365 Attn: Library	
1		National Aeronautics & Space Administration Manned Spacecraft Center Houston, Texas 77001 Attn: Library	J. G. Thiobodaux, J Chief, Propulsion & Power Division

REPORT COPIES R	D	RECIPIENT	DESIGNEE
1		National Aeronautics & Space Administration George C. Marshall Space Flight Center Huntsville, Alabama 35812 Attn: Library	
	1		J. Blumrich
1		Jet Propulsion Laboratory 4800 Oak Grove Drive Pasadena, California 91103 Attn: Library	
1		Defense Documentation Center Cameron Station Building 5 5010 Duke Street Alexandria, Virginia 22314 Attn: TISIA	
1		Office of the Director of Defense Research & Engineering Washington, D.C. 20301 Attn: Office of Asst. Dir. (Chem. Technology)	
1		RTD (RTNP) Bolling Air Force Base Washington, D.C. 20332	
1		Arnold Engineering Development Center Air Force Systems Command Tullahoma, Tennessee 37389 Attn: Library	Dr. H. K. Doetsch
1		Advanced Research Projects Agency Washington, D.C. 20525 Attn: Library	D. E. Mock
1		Aeronautical Systems Division Air Force Systems Command Wright-Patterson Air Force Base, Dayton, Ohio Attn: Library	D. L. Schmidt Code ARSCNC-2

REPORT COPIES R D	RECIPIENT	DESIGNEE
1	Air Force Missile Test Center Patrick Air Force Base, Florida Attn: Library	L. J. Ullian
1	Air Force Systems Command Andrews Air Force Base Washington, D.C. 20332 Attn: Library	Capt. S. W. Bowen SCLT
1	Air Force Rocket Propulsion Laboratory (RPR) Edwards, California 93523 Attn: Library	
1	Air Force Rocket Propulsion Laboratory (RPM) Edwards, California 93523 Attn: Library	
1	Air Force FTC (FTAT-2) Edwards Air Force Base, California 93523 Attn: Library	Donald Ross
1	Air Force Office of Scientific Research Washington, D.C. 20333 Attn: Library	SREP, Dr. J. F. Ma
1	Space & Missile Systems Organization Air Force Unit Post Office Los Angeles, California 90045 Attn: Technical Data Center	
1	Office of Research Analyses (OAR) Holloman Air Force Base, New Mexico 88330 Attn: Library RRRD	
	U. S. Air Force Washington, D.C. Attn: Library	Col. C. K. Stambaugh, Code AFRST
1	Commanding Officer U. S. Army Research Office (Durham) Box CM, Duke Station Durham, North Carolina 27706 Attn: Library	

REPORT COPIES R D	RECIPIENT	DESIGNEE
1	U. S. Army Missile Command Redstone Scientific Information Center Redstone Arsenal, Alabama 35808 Attn: Document Section	Dr. W. Wharton
1	Bureau of Naval Weapons Department of the Navy Washington, D.C. Attn: Library	J. Kay, Code RTMS-41
1	Commander U. S. Naval Missile Center Point Mugu, California 93041 Attn: Technical Library	
1	Commander U. S. Naval Weapons Center China Lake, California 93557 Attn: Library	W. F. Thorm Code 4562
1	Commanding Officer Naval Research Branch Office 1030 E. Green Street Pasadena, California 91101 Attn: Library	
1	Director (Code 6T80) U. S. Naval Research Laboratory Washington, D.C. 20390 Attn: Library	H. W. Carhart J. M. Kralli
1	Picatinny Arsenal Dover, New Jersey 07801 Attn: Library	I. Forsten
1	Air Force Aero Propulsion Laboratory Research & Technology Division Air Force Systems Command United States Air Force Wright-Patterson AFB, Ohio 45433 Attn: APRP (Library)	R. Quigley C. M. Donaldson

REPORT COPIES R	D	RECIPIENT	DESIGNEE
1		Space Division Aerojet-General Corporation 9200 East Flair Drive El Monte, California 91734 Attn: Library	S. Machlawski
1	1	Ordnance Division Aerojet-General Corporation 11711 South Woodruff Avenue Downey, California 90241 Attn: Library	W. L. Arter
1		Propulsion Division Aerojet-General Corporation P.O. Box 15847 Sacramento, California 95803 Attn: Technical Library 2484-2015A	R. Stiff
1		Aerospace Corporation P.O. Box 95085 Los Angeles, California 90045 Attn: Library-Documents	
1		Air Products and Chemicals Company Allentown, Pennsylvania, 18105 Attn: P. J. DeRea	
1		ARDE, Incorporated 19 Industrial Ave., Mahwah, New Jersey, 07430	
1		ARO, Incorporated Arnold Engineering Development Center Arnold Air Force Station, Tennesee 37389 Attn: Dr. S. H. Goethert Chief Scientist	
1		Atlantic Research Corporation Shirley Highway & Edsall Road Alexandria, Virginia 22314 Attn: Security Office for Library	
1		Battelle Memorial Institute 505 King Avenue Columbus, Ohio 43201 Attn: Defense Metals Information Center	

REPORT COPIES R D	RECIPIENT	DESIGNEE
1	Bell Aerosystems Box 1, Buffalo, New York 14205 Attn: T. Rainhardt	
1	The Boeing Company Aero Space Division P.O. Box 3707 Seattle, Washington 98124 Attn: Ruth E. Peerenboom (1190)	
1	Brunswick Corporation Defense Products Division 1700 Messler Street Muskegon, Michigan 49441	
1	Western Division McDonnell Douglas Aircraft Company, Inc. 3000 Ocean Park Blvd. Santa Monica, California 90406 Attn: J. M. Toth	J. L. Waisman
1	Hercules Powder Company Chemical Propulsion Division 910 Market Street Wilmington, Delaware 19804	
1	Narmco Research & Development Co. Whittaker Corporation 131 N. Ludlow Street Dayton, Ohio 45402	
1	Plastics Technical Evaluation Center Picatinny Arsenal Dover, New Jersey 07801	
1	Rocketdyne 6633 Canoga Avenue Canoga Park, California 91304 Attn: Library, Department 596-306	
1	Rohr Corporation Department 145 Chula Vista, California 91312	

REPORT COPIES R D	RECIPIENT	DESIGNEE
1	TRW Systems 1 Space Park Redondo Beach, California 90200 Attn: Tech. Lib. Doc. Acquisitions	
1	Sandia Corporation Sandia Base Albuquerque, New Mexico 87115 Attn: H. E. Montgomery	
1	Swedlow, Incorporated 6986 Bandini Blvd., Los Angeles, California 90022	
1	Thiokol Chemical Corporation Wasatch Division P.O. Box 524, Brigham City, Utah 84302 Attn: Library Section	
1	United Aircraft Corporation United Technology Center P.O. Box 358 Sunnyvale, California 94088 Attn: Librarian	
1	Chemical Propulsion Information Agency Applied Physics Laboratory 8621 Georgia Avenue Silver Spring, Maryland 20910	
1	The Garrett Corporation 20545 Center Ridge Road Cleveland, Ohio 44116	
1	Grumman Aircraft Engineering Corp. Bethpage Long Island, New York	
1	General Dynamics/Corvair P.O. Box 1128 San Diego, California 92712 Attn: Library and Information Services (128-00)	
1	B. F. Goodrich Company Aerospace & Defense Products 500 South Main Street Akron, Ohio 44311	

REPORT COPIES R D	RECIPIENT	DESIGNEE
1	Goodyear Aerospace Corporation 1210 Massilon Rd Akron, Ohio 44306	
1	Hamilton Standard Corporation Windsor Locks, Connecticut 06096 Attn: Library	
1	ABL, Division of Hercules Powder Company Cumberland, Maryland 21502 Attn: Thomas Bates	
1	IIT Research Institute Technology Center Chicago, Illinois 60616 Attn: C. K. Hersh, Chemistry Division	
1	Martin-Marietta Company Denver, Colorado 80201 Attn: A. Feldman	
1	North American Aviation, Inc. Space & Information Systems Division 12214 Lakewood Blvd. Downey, California 90242 Attn: Technical Information Center D/096-722 (A107)	
1	U. S. Rubber Company Mishawaka, Indiana 46544	
1	General Electric Company Apollo Support Dept., P.O. Box 2500 Daytona Beach, Florida 32015 Attn: C. Day	
1	Aerojet-General Corporation Park West Building - Suite 227 20545 Center Ridge Road Cleveland, Ohio 44116 Attn: W. Snapp	
1	Marine Engineering Laboratory NSRDC ANNADIV Annapolis, Md. 21402 Attn: Karl H. Keller, Code 560	

REPORT COPIES R D	RECIPIENT	DESIGNEE
1	Brunswick Corporation Defense Products Division P.O. Box 4594 43000 Industrial Ave., Lincoln, Nebraska 68504 Attn: J. Carter	
1	Celanese Corp. Box 1000 Summit, New Jersey 07901 Attn: J. D. Lassiter	
1	Aeronutronic Division of Philco Ford Corp. Ford Road Newport Beach, California 92663 Attn: Technical Information Department	Dr. L. H. Linder